4-1-2001

Optimal shape design of steadily-loaded journal bearings using genetic algorithms

Sulaymon Eshkabilov

Optimal Shape Design of Steadily-Loaded Journal Bearings using Genetic Algorithms

by

Sulaymon L. Eshkabilov

A Thesis Submitted in Partial Fulfillment of the Requirements for the

MASTER OF SCIENCE
IN
MECHANICAL ENGINEERING

Approved by:

Dr. Stephen Boedo _____
Department of Mechanical Engineering (Thesis Advisor)

Dr. Josef S. Török _____
Department of Mechanical Engineering

Dr. Hany A. Ghoneim _____
Department of Mechanical Engineering

Dr. Mark H. Kempski _____
Department of Mechanical Engineering

Mr. William T. Scarbrough _____
Department of Mechanical Engineering

Dr. Satish G. Kandlikar _____
Department Head of Mechanical Engineering

Department of Mechanical Engineering
Rochester Institute of Technology

April 2001

PERMISSION TO REPRODUCE

Thesis Title: " Optimal Shape Design Of Steadily-Loaded Journal Bearings using Genetic Algorithms"

I, Sulaymon L. Eshkabilov, hereby grant permission to the Wallace Memorial Library of the Rochester Institute of Technology to reproduce my thesis in whole or part. Any reproduction cannot be used commercially or for profit.

April 2001

_____

(Signature)

ACKLOWLEDGEMENTS

First of all, I am grateful to GOD, that He gave me such physical and intellectual abilities.

I would love to thank to my parents for all their support, encouragement, and their great care, especially to my Mother, who is the greatest person in the world for me.

Also, I would like to thank to my lovely wife Nigora and darling daughters Anbara and Durdona, without whose support and love I would never be able to finish this work.

Finally, my very special thanks and appreciations to Professor Stephen Boedo for his priceless help, patience, and encouragement.

I would like to forward my very special gratitude to my sponsor, the UMID Foundation, Tashkent, Uzbekistan. Without their financial support and help for my education in the United States of America, I would not have been able to get my MS degree in Mechanical Engineering.

Table of Contents

Abstract

This thesis investigates the use of genetic algorithms to optimize the shape of an ungrooved fluid-film journal bearing under steady load and steady speed so that it can carry the maximum possible load while constrained to maintaining an adequate minimum film thickness. The shape of the bearing sleeve is assumed to vary only in the radial direction, and the shape is represented by linear interpolation of three film thickness design specifications along the bearing sleeve.

Each set of film thickness specifications in the design space is encoded into a binary string called a chromosome, and a set of chromosomes makes up a current generation. The bearing load is calculated for each chromosome, and the genetic algorithm creates a new generation based on these loads using elitism selection and chromosome crossover and mutation operators.

Several case studies are presented to investigate the effect of bearing geometric specifications on the resulting optimal shape. For a given bearing diameter and bearing length, a random generation of chromosomes is first constructed. Using recommended chromosome crossover and mutation probabilities, it is shown that randomly created starting sets will eventually converge to a common shape, suggesting that a global optimum may have been achieved. Additional parametric studies show that the load results are dependent upon the mutation operator to achieve global optimums. Further comparisons show that the load carried by the optimal shape bearing can be much greater than that carried by a conventional cylindrical bearing.

List of Tables

List of Figures

Nomenclature

e	- journal position (eccentricity);
h	film thickness;
h_{max}	maximal film thickness;
h_{min}	minimal film thickness;
p	film pressure;
p_i	nodal pressure;
p_{max}	maximal film pressure;
q_i	nodal net flow;
r	journal radius;
$\bar{u}$	one half of the journal angular velocity;
D	bearing diameter;
F	bearing load;
H1, H2, H3	- design variables;
$[K_p]$	- fluidity matrix;
$[K_u]$	fluidity matrix;
L	bearing length;
N_gen	number of generations;
N_chrom	number of chromosomes;
P	resultant load acting on the converging film of fluid;
P^x, P^y	load components (relative to the X, Y system axis);

P_cross - crossover probability;

P_mut - mutation probability;

Q_1, Q_2 tangential components of journal surface velocity;

R_{clr} radial clearance;

U_1, U_2 normal components of journal surface velocity;

ε - eccentricity ratio;

θ angle of rotation;

θ_m angle of maximal pressure;

ω angular velocity;

Chapter 1

Background

1.1 Introduction

Fluid-film journal bearings are used in a wide variety of applications, from automotive engines to Micro Electro-Mechanical Systems (MEMS) devices, as they can carry radial loads with minimal power loss and minimal wear. Most journal bearings are designed with cylindrical geometry, as this shape is amenable to analytical treatment and is easiest to manufacture. However, there is no evidence that the cylindrical shape is optimal in its ability to carry a maximal steady or dynamic load.

Hence, the main objective of this thesis is to find the optimal shape of a steadily loaded journal bearing so that it can carry the maximum load subject to the constraint of a specified minimum film thickness value. We intend to meet to this objective by using new applications of genetic algorithms as the optimization tool.

1.2 Historical Perspective of Genetic Algorithms

Computer scientists first started investigating genetic algorithms in the 1950s and 1960s with the concept of that evolution might be utilized as an optimization instrument for engineering problems. The idea was to create a population of nominee solutions to a selected problem by using genetic variation and natural selection operators found in nature.

Rechenberg (1965, 1973) presented *Evolutions strategies*, a method he used to optimize real-valued parameters for devices such as airfoils. The concept later was developed further by Schwefel (1975, 1977).

Also during this time, Box (1957), Friedman (1957), Bledsoe (1961), Bremermann (1962), and Reed, Toombs, and Baricelli (1967) developed evolution-inspired algorithms for their optimization problems. In addition, biologists began to use computers to simulate evolution for the purpose of modeling controlled experiments (Baricelli 1957, 1962; Fraser 1957 a,b; Martin and Cokerham 1960).

The modern viewpoint of genetic algorithms was initiated by John Holland in the 1960s, and these algorithms were subsequently developed by Holland and his students and colleagues at the University of Michigan in the 1960s and the 1970s. Holland's main goal was not to create algorithms to solve some specific problems, but to investigate the natural phenomenon of adaptation and to develop ways by which the mechanisms of natural adaptation might be imported into computer systems. Holland's 1975 book *Adaptation in Natural and Artificial Systems* introduced the genetic algorithm as a concept of natural evolution and introduced a notional structure for adaptation. Holland's genetic algorithm method is a concept of moving from one generation of "chromosomes", each chromosome encoded by a string of zeros and ones (bits), to a new generation by using genetic operators such as crossover, mutation, and inversion similar to that found in natural selection. These operations are clearly covered in the recent book, *An Introduction to Genetic Algorithms* by Melanie Mitchell (1999).

It is interesting that using genetic algorithms is similar to the biological evolution of a species in that it picks up the good qualities of parents and transfers those qualities to their children. The main reason for using genetic algorithms in any computational programming is to create, through successive generations, the most reliable and best pattern of chromosomes.

1.3 Application of Genetic Algorithms in Machine Design

Kotera *et al.* (2000) presented a design method for controlling the deflection of a micro-membrane with the aid of its thickness distribution for realizing a prescribed design in MEMS. They used as an example a micro air pump, which comprises a micro membrane actuated by an electrostatic drive. Consequently, membrane deflects and therefore, the air and electrostatic field affect the deflection. A genetic algorithm is used to find out an adequate thickness distribution and to condense a stochastic solution search.

Kotera and Shima (2000) described a method to optimize the shape of a magnetic head recording device using genetic algorithms in conjunction with the finite element method. They defined the head shape using a second order spline function, and the chromosome representing this shape was encoded from three design variables representing spline reference points and first order derivatives.

Keane (1995) proposed the concept of using genetic algorithms to control passive structural vibration through unusual geometries.

Chen *et al.* (1999) employed the genetic algorithms to optimize the designs of headstocks of precision lathes. They took into account thermal deformations generated by the heat from spindle bearings. The main goal was to reduce the overall deflection of the work piece at the cutting point. An important point of the authors was their choice of constraint, which was to make the fundamental natural frequency much larger that the working frequency to minimize dynamic deflections. The authors chose the shape dimensions, the location of the spindle bearing, the stiffness of the spindle bearings, the dimensions of the fins, and the locations of the fins as design variables.

Hajela and Lee (1995) introduced the concept of genetic algorithms as a stochastic search procedure in developing near-optimal topologies of load-bearing truss structures. Their method adjusted the ground structure by topology optimization, using a two-level genetic algorithm-based search.

Chapman *et al.* (1994) applied genetic algorithms to problems of topology design and gave some overview of the genetic algorithm operators and its representations. A discretized design representation and methods for mapping genetic algorithm "chromosomes" into this design representation was detailed. The author addressed in general the optimization of cantilevered plate structures and described research methods for optimizing finely-discretized design domains. In addition, the author described several examples of genetic algorithm-based structural topology optimization problems and some tests of genetic algorithm's ability to find families of best fit designs.

1.4 Review of Bearing Optimization

The main purpose of this section is to review the various methods employed in the shape optimization of journal bearings and related machine components.

Montusiewicz and Osyczka (1997) presented a general model of a spindle system with hydraulic bearings. They found the design shape by dividing the whole system into subsystems and then model each subsystem to get the global response. To solve the problem, a four-stage multicriterion optimization strategy was utilized. Based on this strategy, a computer aided optimum design software package for spindle systems for grinding and lathe machine tools was developed. The software was supported by computer graphics. Designing of a grinding machine spindle system was presented as an example.

Wang *et al.* (2000) presented the idea of an engineering approach for optimizing the performance of fluid-film lubricated bearings. The paper discussed standard optimization schemes such as unconstrained nonlinear programming, lattice search and simplex methods to improve the merit of fluid-film bearings with two or more design variables. Application to elliptical bearings showed that high eccentricity ratio and two large pressure zones for high-speed stability could be attained by maximizing film pressures in the upper and lower lobes. The authors used an automatic mesh generation technique to make the numerical optimization as a flexible design tool.

Robert (1990) showed that the gap profile of a two-dimensional self-acting gas bearing could be determined so as to maximize the static stiffness of the bearing system. Three fundamental profiles were obtained according to the stiffness mode considered: normal, pitch, or roll. The optimization process took place within the framework of compressible lubrication theory.

Elsharkawy and Guedouar (2000) presented a solution to an inverse problem for the elastohydrodynamic lubrication of one-layered journal bearings. Eccentricity ratio, viscosity of the lubricant, pressure viscosity coefficient, and lubricant bulk modulus were the parameters to be estimated from a given pressure distribution. A least-squares optimization technique was used to solve the proposed inverse problem. Results were presented only for infinite-width journal bearings.

Haraldsson *et al.* (1997) showed that journal bearings with water as a lubricating fluid and a rubber layer in the bearing housing could be considered for shape optimization. Their goal was to vary the shape of the bearing housing in order to lower the high maximum pressure and hence improve the durability life of the layer material. For their optimization process, a design element technique is utilized applying NURBS for geometric modeling of the journal bearing shape.

Kicinski and Haller (1994), using a complex thermoelastohydrodynamic model, presented various models to assess the external fixation of a bushing in its supports, and they investigated other models that considered deformation of the fixation itself. In addition, the authors showed that the static and dynamic properties of the bearing in a simple rotor-bearing

system were dependent on the way in which the bushing was supported. The authors also concluded that they obtained broader possibilities to improve system properties by optimization of the fixation and clamping methods of the bushing in the bearing supports.

Hashimoto (1997) introduced an optimum design method for high-speed, short journal bearings, based on quadratic programming. Bearing radial clearance, bearing slenderness ratio, and the viscosity of lubricant were treated as design variables, and the characteristics of these optimized design variables were examined under both laminar and turbulent flow conditions.

Robert (1995) proposed the idea of a new class of sliders numerically designed for maximum stiffness. The desired gap profile was based on the method of an iterative approach coupled with a finite element solution of the pressure distribution. The canonical example of a plain square slider is provided as an example.

1.5 Present Research Work

To the author's best knowledge, there are apparently no published shape optimization methods for fluid-film bearings utilizing genetic algorithms. The main concept and goal of the work in this thesis work is to employ genetic algorithms to maximize the load carried by a steadily loaded fluid- film journal bearing subject to realistic geometric shape specifications and constraints.

The genetic algorithm will be implemented in a FORTRAN computer program using a finite element based lubrication module especially suited to model arbitrary sleeve geometry.

Chapter 2

Problem Formulation

The objective of this chapter is to explain theoretically the lubrication of the fluid-film journal bearings in some detail, describe the problem statement of the research, and present the genetic algorithm implementation.

2.1 Lubrication of cylindrical fluid-film bearings

Whenever one body slides upon another, frictional forces are generated. Such forces, in general, must be considered in design calculations since it has been estimated that between one-third and one-half of all the energy produced in the world is consumed in overcoming various kinds of friction. In fluid-film bearings, a thin layer of lubricant separates the moving parts and assists in reducing friction. The book *Mechanical Analysis and Design* (Burr, 1982) gives a clear theoretical explanation of lubrication of the journal bearings and is summarized as follows.

Most journal bearings are comprised of a cylindrical journal that interacts with a cylindrical sleeve through a thin lubricant film, as shown in Fig. 2.1.1. A small lateral shift of the journal, combined with journal and/or sleeve rotation, creates a converging oil film which generates film pressure and hence, the means to support an external radial load. The journal position (eccentricity) e is measured from the bearing center O_b to the shaft center O_j (Fig. 2.1.1). The largest value that the eccentricity can attain is the radial

clearance R_{clr}, or one-half the difference in journal and sleeve diameters. It is more convenient to utilize an *eccentricity ratio* ε defined as

$$\varepsilon = \frac{e}{R_{clr}}$$

The eccentricity ratio is zero when journal and sleeve are concentric, and the eccentricity ratio attains a maximum value of 1 when the journal contacts the bearing sleeve. The film thickness h varies between

$$h_{max} = R_{clr}(1 + \varepsilon)$$

and

$$h_{min} = R_{clr}(1 - \varepsilon)$$

This expression is obtained from the geometry of the given Fig. 2.1.1, where the journal radius is r, the sleeve radius is $r + R_{clr}$, and θ is measured counterclockwise from the position of h_{max}. For typical production-level bearings, the radial clearance is of the order of one thousandth of the diameter; thus, to a high approximation,

$$OO_j = OO_b + e\cos\theta$$

or

$$h + r = r + R_{clr} + e\cos\theta$$

$$h = R_{clr} + e\cos\theta$$

or finally

$$h = R_{clr}(1 + \varepsilon\cos\theta) \qquad (2.1)$$

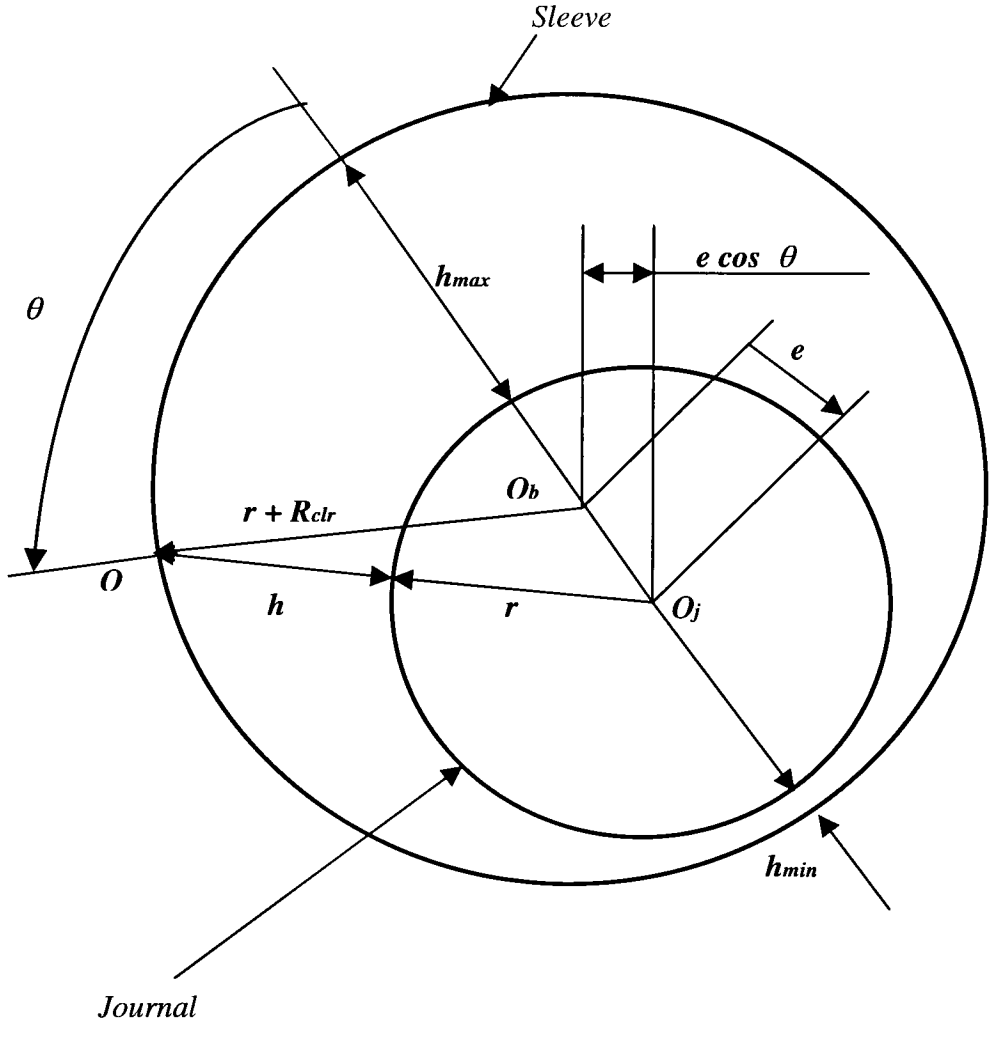

Figure 2.1.1 Relationship between film thickness and eccentricity in a hydrodynamic cylindrical journal bearing.

In the analysis that follows, we assume that the journal and sleeve rotate at constant angular velocities. In addition, we assume that a steady radial load is applied to the journal, causing the journal to rotate at a fixed static eccentricity position. If the origin of coordinates is taken at any position O on the surface of the bearing (Fig. 2.1.2), the X-axis is tangent and the Z-axis is parallel to the axis of rotation. When the bearing sleeve rotates, its surface velocity is U_1 along the X-axis. The surface of the shaft has a velocity Q_2 making with the X-axis an angle whose tangent is $\frac{\partial}{\partial x}h$ and whose cosine is approximately 1. Hence the normal and tangential components of the journal surface velocity are to a high approximation

$$V_2 = U_2\left(\frac{\partial}{\partial x}h\right) \qquad U_2 = Q_2$$

Assuming that the normal and axial surface velocities of the sleeve are zero, with zero axial journal velocity results, in a special form of the Reynolds equation (Burr, 1982)

$$\frac{\left[\left(\frac{\partial}{\partial x}\frac{h^3\left(\frac{\partial}{\partial x}p\right)}{\mu}\right)+\left(\frac{\partial}{\partial z}\frac{h^3\left(\frac{\partial}{\partial z}p\right)}{\mu}\right)\right]}{6} = (U_1 - U_2)\left(\frac{\partial}{\partial x}h\right) + 2V_2$$

$$= (U_1 + U_2)\left(\frac{\partial}{\partial x}h\right) = U\left(\frac{\partial}{\partial x}h\right) \qquad (2.2)$$

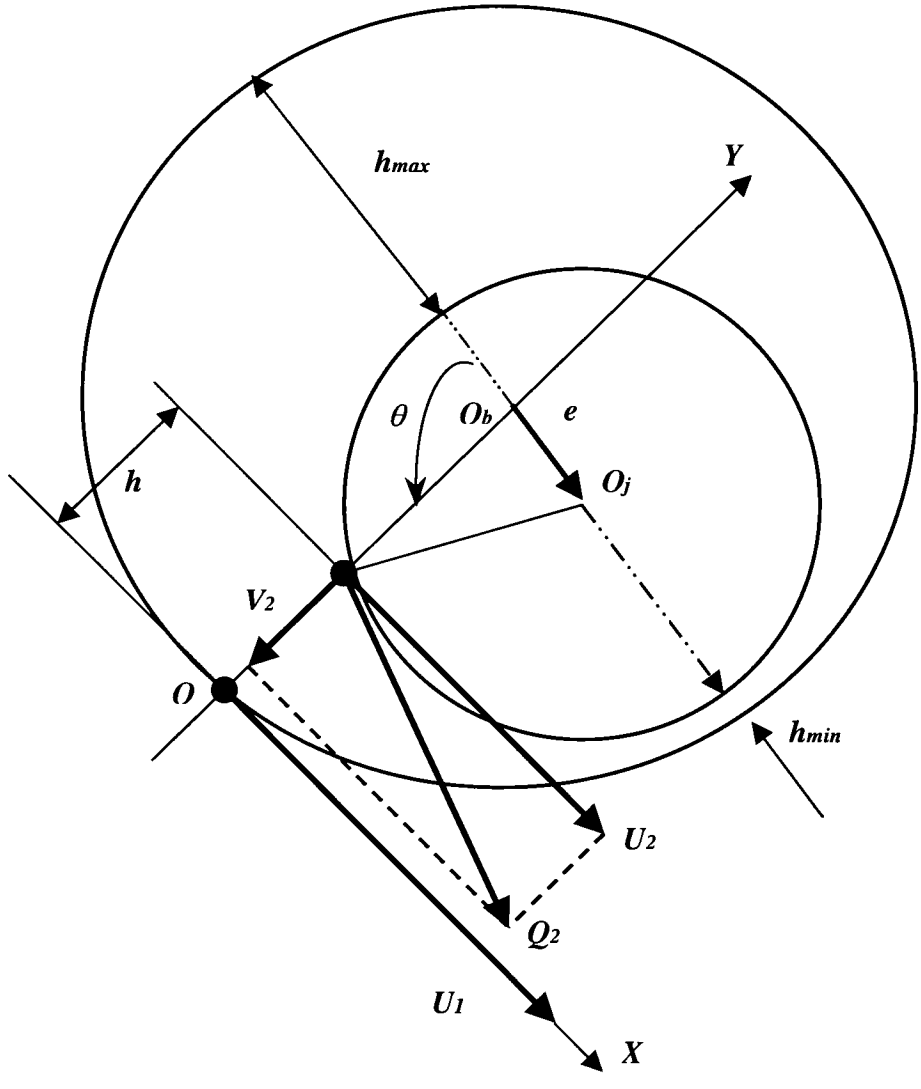

Figure 2.1.2. Surface velocity components in a journal bearing.

where $U = U_1 + U_2$. The same result is obtained if the origin of coordinates is taken on the journal surface with X tangent to it.

It has been found from experiments (e.g. Davies, 1964) that negative pressures cannot be sustained in a lubricant film; thus, the film ruptures or cavitates. The pressure in this cavitated region generally lies between zero and atmospheric (absolute) values. Thus, to a high approximation, one way to address cavitation mathematically is to set negative pressures to zero where they are encountered in the pressure solution.

Assuming cylindrical film thickness of the form in equation 2.1, a closed-form analytic solution of equation 2.2 along with consideration of cavitation does not exist. Various approximations have been suggested (Booker, 1965), depending on the application.

In the 1800s, journal bearing length to diameter ratios were generally large. Hence, Reynolds in 1886 supposed an infinite length approximation for the bearing, assuming zero endwise flow and thus making $\frac{\partial}{\partial z} p = 0$. Together with μ constant, this simplifies equation 2.2 to the following expression (Burr, 1982)

$$\frac{\partial}{\partial x} h^3 \left(\frac{\partial}{\partial x} p \right) = 6 \mu U \left(\frac{\partial}{\partial x} h \right) \qquad (2.3)$$

Reynolds obtained a series solution to equation 2.3 which was limited to small eccentricity ratios. Later Sommerfeld found a suitable integral substitution that enabled him to get a solution of equation 2.3 in closed form. The result was

$$p = \frac{\mu U r \left[\dfrac{6\varepsilon \sin\theta (2 + \varepsilon \cos\theta)}{(2+\varepsilon^2)(1+\varepsilon\cos\theta)^2} \right]}{R_{clr}^{\ 2}} \qquad (2.4)$$

Together with experimentally determined end-leakage factors, equation 2.4 has been broadly utilized to correct for finite bearing lengths. It will be called the Sommerfeld solution or the long-bearing solution.

As discussed by Burr (1982), modern bearings are generally a lot shorter than those used in the 1800s, with length-to-diameter ratios often less than 1. This makes the flow in the Z direction and the end leakage a much larger portion than the circumferential flow. Michell in 1929 and Cardullo in 1930 proposed that the $\frac{\partial}{\partial z} p$ form of equation (2.2) be kept and that the $\frac{\partial}{\partial x} p$ term be dropped. Ocvirk in 1952 by neglecting the parabolic, pressure-induced circumferential flow, obtained Reynolds equation in the same form as proposed by Michell and Cardullo, but with greater justification. This form is expressed

$$\frac{\partial}{\partial z} h^3 \left(\frac{\partial}{\partial z} p \right) = 6\,\mu\, U \left(\frac{\partial}{\partial x} h \right) \qquad (2.5)$$

If there is no flexure or misalignment of the shaft and bearing, h and $\frac{\partial}{\partial x}h$ are independent of z and equation (2.5) may be readily integrated twice to give

$$p = \frac{3\,\mu\, U\left(\frac{\partial}{\partial x}h\right)z^2}{h^3} + \frac{C_1 z}{h^3} + C_2$$

From boundary conditions $\frac{\partial}{\partial z}p = 0$ at $z = 0$ and $p = 0$ at $z = \frac{l}{2}$ and $z = -\frac{l}{2}$, we obtain

$$p = -\frac{3\,\mu\, U\left(\frac{l^2}{4} - z^2\right)\left(\frac{\partial}{\partial x}h\right)}{h^3} \qquad (2.6)$$

Substitution into equation (2.6) the slope $\frac{\partial}{\partial x}h = \frac{\frac{\partial}{\partial \theta}h}{r}$ and $\frac{\partial}{\partial x}h = -\frac{R_{clr}\,\varepsilon \sin\theta}{r}$ from equation (2.1) gives

$$p = \frac{3\mu U\left(\frac{l^2}{4} - z^2\right)\varepsilon \sin\theta}{(1+\varepsilon\cos\theta)^3 r R_{clr}^{\ 2}} \qquad (2.7)$$

Equation (2.7) shows that pressures will be distributed radially and axially as shown in Fig. 2.1.3.a and Fig. 2.1.3.b, with the axial distribution being parabolic. The peak pressure occurs in the central plane $z = 0$ at an angle

$$\theta_m = \cos^{-1}\left(\frac{1-\sqrt{1+24\varepsilon^2}}{4\varepsilon}\right) \qquad (2.8)$$

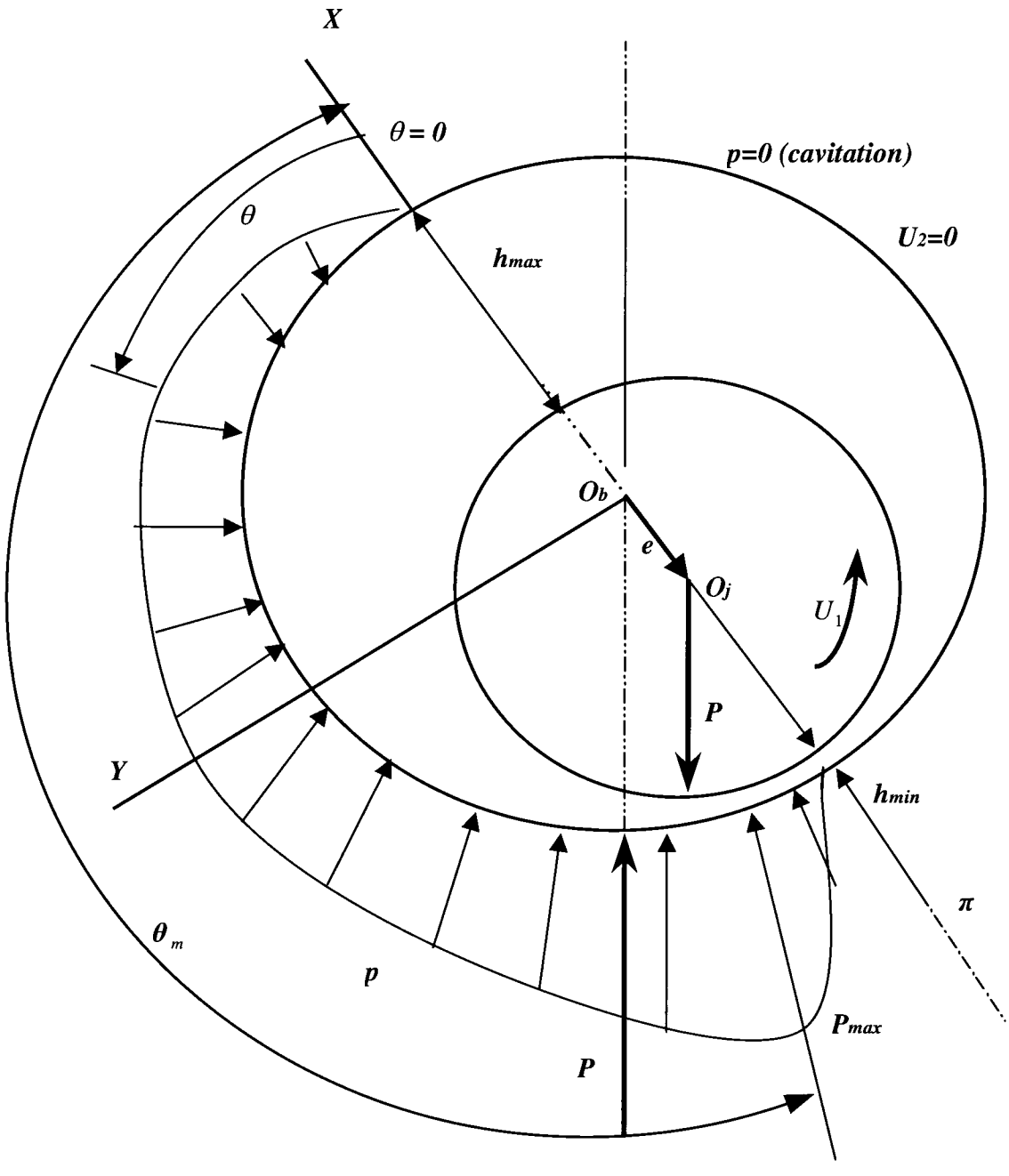

Figure 2.1.3.a. Radial pressure distribution p and resultant load P acting on converging film of fluid in a steadily loaded journal bearing.

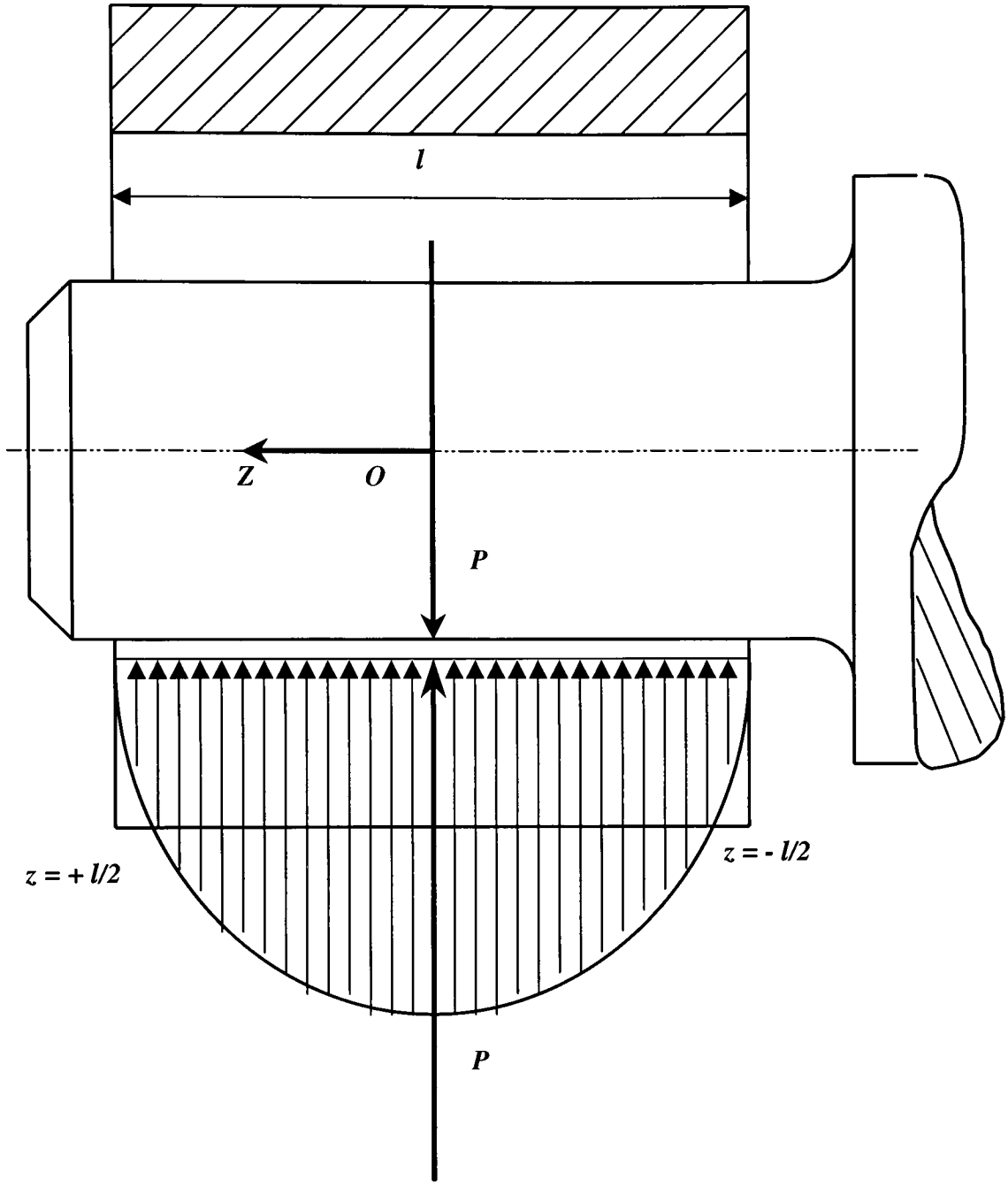

Figure 2.1.3.b. Axial pressure distribution p and resultant load P acting on the converging film of fluid in a steadily loaded journal bearing.

and the value of maximum film pressure $p_{\max}$ may be found by substituting θ_m into equation (2.6), namely

$$p_{\max} = \frac{3\mu U\left(\frac{l^2}{4} - z^2\right)\varepsilon \sin\theta}{(1+\varepsilon\cos\theta_m)^3 r{R_{clr}}^2} \qquad (2.9)$$

Given pressure distribution (2.7), load components P^X and P^Y (relative to the X,Y system axis of Figure 2.1.3a) carried by the bearing can be found from integration:

$$P^X = -\int_{-\frac{l}{2}}^{+\frac{l}{2}}\int_0^{\theta_c} pr\cos\theta d\theta dz$$

$$P^Y = -\int_{-\frac{l}{2}}^{+\frac{l}{2}}\int_0^{\theta_c} pr\sin\theta d\theta dz$$

where θ_c is the positive extent of the pressure region.

2.2 Lubrication of finite-length journal bearings with non-cylindrical sleeve geometry.

With non-cylindrical sleeve geometry, numerical methods are the only resort to find the pressure distribution from the Reynolds equation. Among the many numerical techniques, the finite element method of solution allows great flexibility in representing lubricant films with feed grooves and oil holes. The application of the finite element to lubrication is discussed more in detail in Booker and Huebner (1972) and is summarized as follows.

Figure 2.2.1 shows a lubricant film represented as a system of finite elements interconnected at a discrete set of nodes. At each node, nodal net flow q_i and nodal pressure p_i form a set of complementary unknowns. In other words, at each node, either the nodal net flow q_i is specified, leaving the pressure pi as an unknown, or the nodal pressure p_i is specified, leaving the net flow q_i to be determined. Nodal net flows are usually set to zero in the bearing interior regions, and nodal pressure is usually specified on the boundary or in cavitated regions.

For steadily loaded journal bearings, the film pressure and net flow at each of n nodes can be computed from the following system of equations (Booker and Huebner, 1972)

$$\begin{Bmatrix} q_1 \\ q_2 \\ q_3 \\ \vdots \\ q_n \end{Bmatrix} = [\mathbf{K_p}] \begin{Bmatrix} p_1 \\ p_2 \\ p_3 \\ \vdots \\ p_n \end{Bmatrix} + [\mathbf{K_u}] \begin{Bmatrix} u_1 = \bar{u} \\ u_2 = \bar{u} \\ u_3 = \bar{u} \\ \vdots \\ u_n = \bar{u} \end{Bmatrix}$$

n x 1 n x n n x 1 n x n n x 1

where fluidity matrices $[K_p]$ and $[K_u]$ depend on specified nodal film thickness values, and where $\bar{u}$ is one-half of the journal surface velocity.

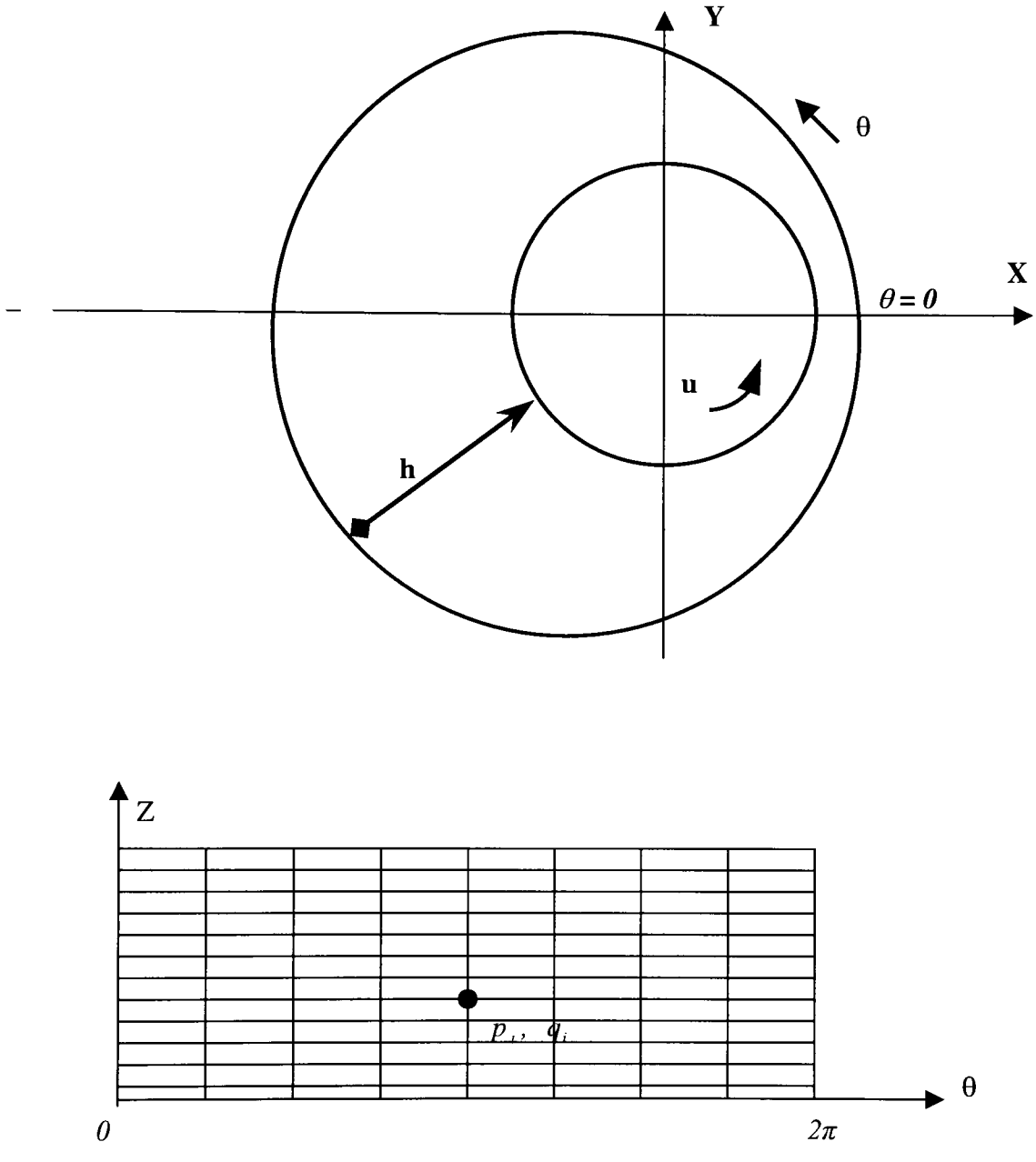

Lubricant film attached to sleeve (unwrapped view)

Figure 2.2.1. Finite element meshing scheme for non-cylindrical journal bearings.

2.3 Problem Statement

The task of this thesis is to find the optimal bearing sleeve shape of a steadily loaded journal bearing under steady journal rotation. The objective function to be maximized is defined as the bearing load subject to the constraint that the minimum film thickness is equal to 1 micron.

This 1 micron target value is based on numerical studies (Wang, *et al.* 1997) which suggest that asperity contacts for typical bearing materials can be ignored when the film thickness to composite roughness ratio is greater than 3. Most bearing materials today can be manufactured to have roughness values around 0.25 micron; hence, the reason for choosing the 1 micron target is a conservative value.

Fig. 2.3.1 shows a fluid-film bearing where film thickness of 1 micron is specified at bearing angle $\theta = 0$ (measured from the X axis), and thicknesses H1, H2, and H3 are specified at bearing angles $\theta = \pi/2$, π, and $3\pi/2$ respectively. The following limits for the values of H1, H2, and H3 are specified as follows:

$$1\ \mu m \leq H1 \leq 127\ \mu m$$

$$1\ \mu m \leq H2 \leq 127\ \mu m$$

$$1\ \mu m \leq H3 \leq 127\ \mu m.$$

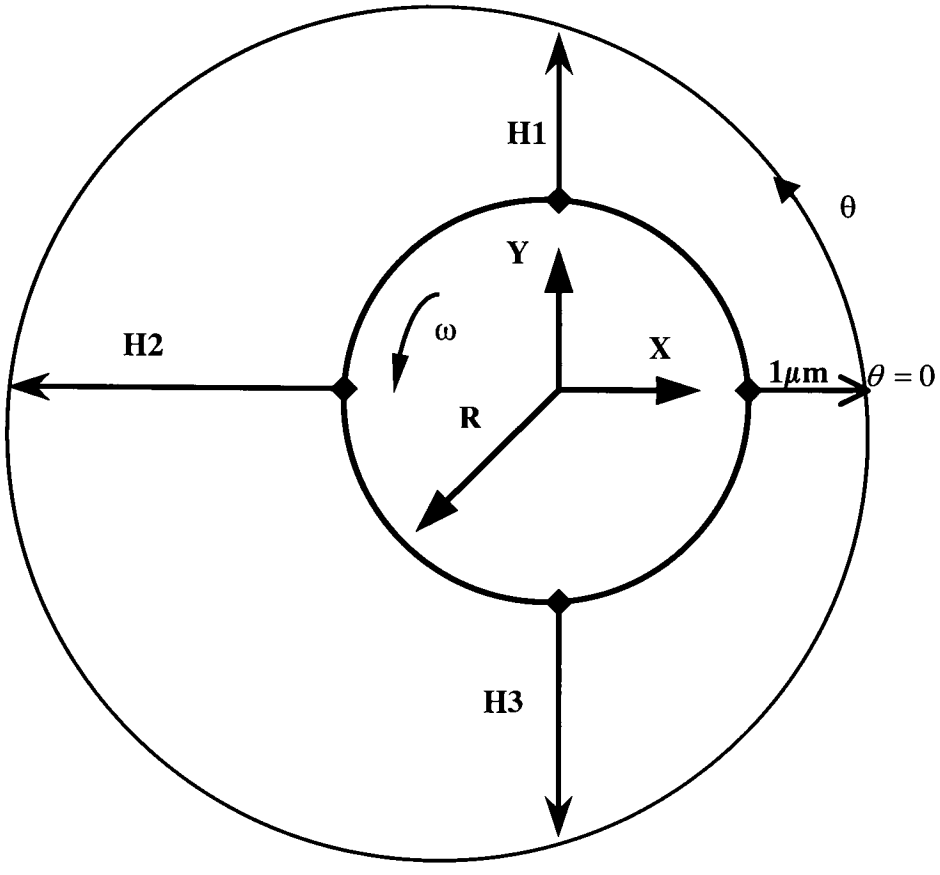

Figure 2.3.1. Steadily loaded journal bearing with design variables H1, H2, and H3.

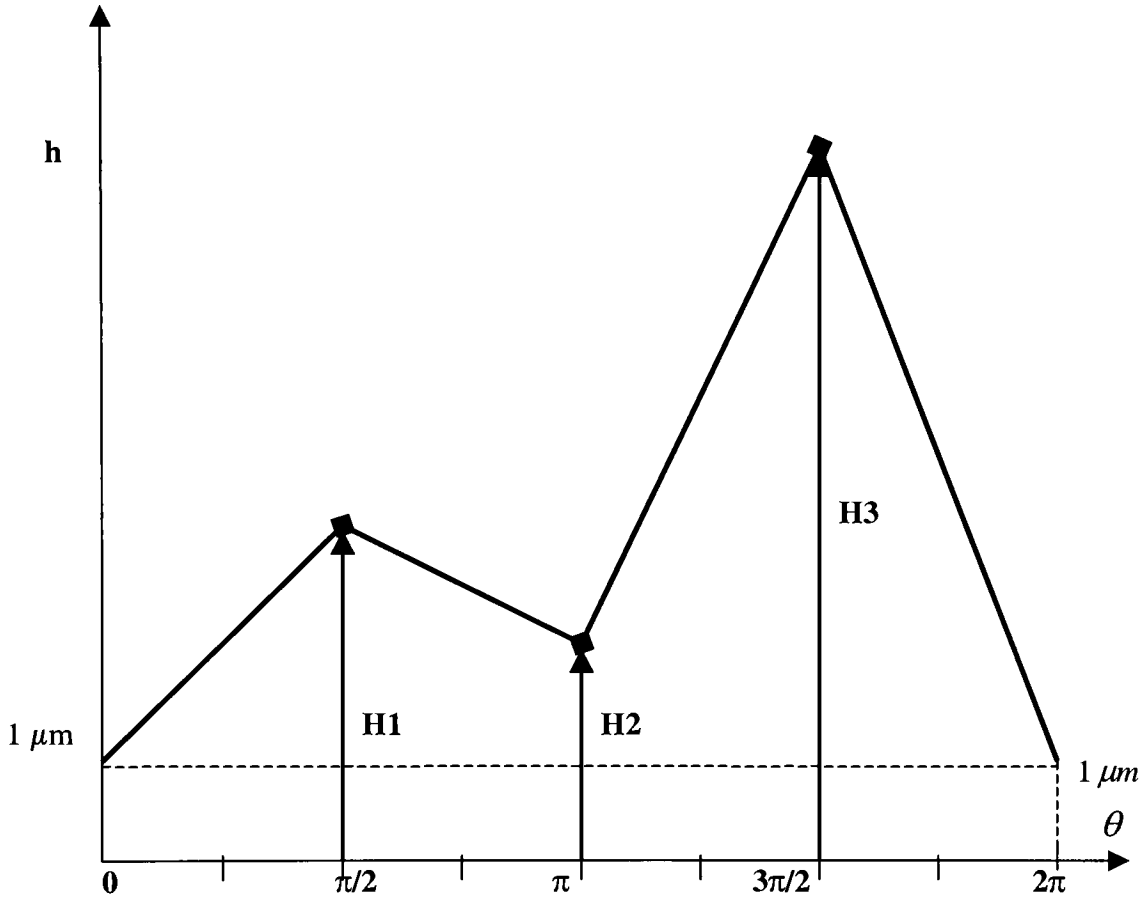

Figure 2.3.2. Interpolated film thickness based on design variables.

Hence, given values of H1, H2, and H3, the film thickness around the bearing can be found by linear interpolation as shown in Figure 2.3.2. The film thickness is assumed not to vary in the axial direction.

2.4 Genetic Algorithms

The method of solution for this optimization problem will be using genetic algorithms, and in this section, we will introduce the genetic algorithms, how they operate and their important key features.

The term *chromosome* generally refers to a contestant solution to a problem, often encoded as a bit string, in genetic algorithms. The *genes* can be either single bits or short blocks of contiguous bits that encode a particular element of the contestant solution. Another term, an *allele,* is a bit in the string, which for our purposes can be either 0 or 1. However, note that genetic algorithms in general are not limited to binary values.

Following the method proposed by Chapman (1994), the three design variables, H1, H2, and H3 representing film thickness are encoded as one chromosome, which for our case consists of 21 bits. Each design variable is represented as a seven bit string of binary numbers representing the range of 0 – 127 μm in 1 micron increments.

2.4.1. Genetic Algorithm Operators

The simplest form of the genetic algorithm involves three types of operators--selection, crossover, and mutation.

Selection: This operator chooses chromosomes in the population for the future reproduction. The fitter the chromosome, the more times it is likely to be chosen to reproduce (Melanie, 1999).

Elitism: The operator preserves some number of the best individuals at each generation. It is very likely that if such best individuals are not chosen for reproduction, they can be lost or destroyed by crossover and mutation operators (Melanie, 1999).

Crossover: This operator randomly picks a locus and exchanges the subsequences before and after that locus between two chromosomes to create two offspring (Melanie, 1999). For instance, the strings 1001111001 and 1111000011 can be crossed over after the second locus in each to produce the two new generations 1011000011 and 1101111001. The operator of crossover works very similarly to biological recombination between two single-chromosome (haploid) organisms.

This operator is shown more clearly in detail in the following example, (Hillis; 1992), and it is for numerically encoded chromosomes looks like the following:

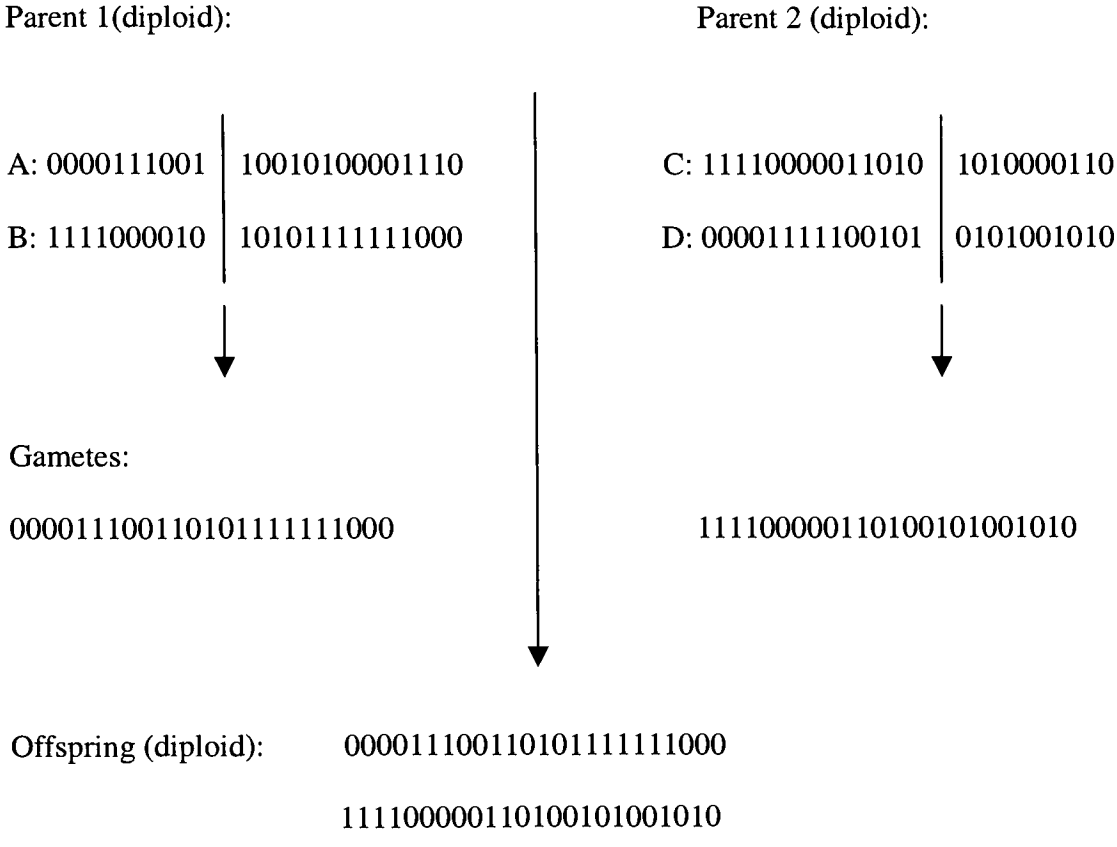

Figure 2.4.1. An illustration of diploid recombination, (Hillis, 1992).

Fig.2.4.1 shows an illustration of diploid recombination (Hillis, 1992), an individual's genotype consisted of 13 pairs of chromosomes (for clarity only one pair of chromosomes for each parent is shown in Figure 2.4.1). A crossover point was selected at random for each pair of chromosomes or diploid. The codons before the crossover point in the first chromosome and the codons after the crossover point in the second chromosome formed a gamete. Each codon is representative of an integer number between 0 and 15, and gives a position in a 16-element list. Figure 2.4.1 shows that parents of the gamete from parent 1 plus the gamete from parent 2 creates an offspring diploid (chromosome pair). In general, the 13 gametes from one parent were paired with the 13 gametes from the other parent to make a new individual. (Again for the clarity point of view, only one gamete pairing is shown.)

The rate of crossover operator defines the probability of performing this operator. The rate has independent values, which are different for the different size of the population; for the population size of 20-30 it is typical to pick the crossover rate between the range 0.75-0.95 (Melanie, 1999) and for a population size of 50-100 individuals, it is the best to pick the crossover rate ~ 0.6 per pair of parents. Hence, crossover rate does not apparently depend on the problem itself.

Mutation: This operator randomly flips some of the bits in a chromosome. For instance, the string:

1 0 1 0 1 0 1 0 1 1 **1 1**

can be mutated to the following:

1 0 1 0 1 0 1 0 1 1 **0 0**

In the past, the crossover operator alone played a major tool in computation and innovation of genetic algorithms, and mutation played a secondary role. However, in solving very complex problems, the mutation operator in genetic algorithms is now considered one of the key instruments of modern genetic algorithms. Similar to crossover, mutation also has a rate, which differs depending on the population size. For the population size of 50 – 100, mutation rate is typically recommended be 0.001 per bit, and for the population size of 20-30, it is considered best practice to choose the mutation rate in the range of 0.005 - 0.01 (Melanie, 1999).

2.5 Implementation of the genetic algorithm for bearing shape optimization.

The FORTRAN computer program OPTJBG 1.3 (Boedo, 2000, see Appendix I) employs a genetic algorithm to optimize the sleeve shape of a steadily loaded journal bearing. The program works to perform sequences of the operations as noted in this section with pseudocode presented in the Appendix I. The OPTJBG program initially creates a fixed number of randomly generated chromosomes, each 21 binary digits long. Each chromosome represents binary values of design variables H1, H2, and H3. Figure 2.5.1 shows the encoding scheme for a sample randomly generated chromosome.

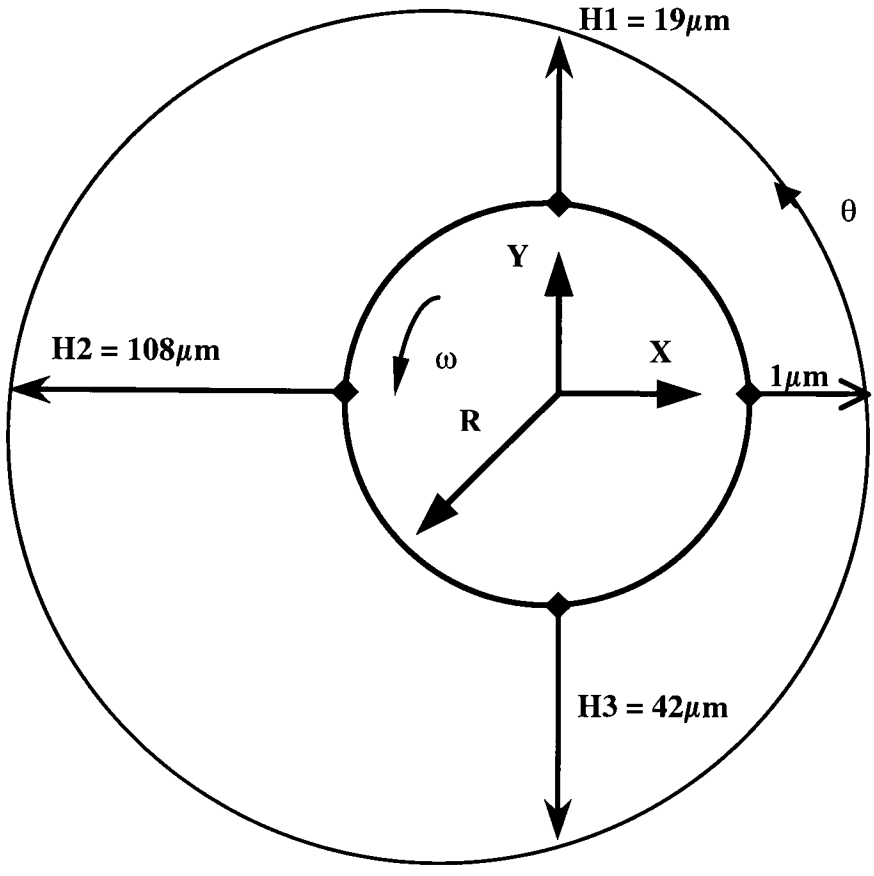

0 1 0 1 0 0 1	1 1 0 1 0 1 1	0 0 1 0 0 1 0
(H3-1) *μm*	(H2-1) *μm*	(H1-1) *μm*

Figure 2.5.1 Encoding scheme for design variables.

The bearing film is represented by a set of two-dimensional finite elements connected at a discrete set of nodes attached to the sleeve surface, as shown in Figure 2.2.1 for a given set of values H1, H2, H3 in the design space, the film thickness distribution at each node is found by linear interpolation as shown in Figure 2.3.2. For boundary conditions, the nodal pressure at the bearing ends and the nodal net flows in the bearing interior are set to zero.

Given film thickness distribution, bearing dimensions, journal speed, and boundary conditions, either the unknown film pressure or the unknown flow at each node in Section 2.2 is found using the CUIMPD version 1.1 subroutine (Boedo and Booker, 2000). The bearing load (journal to sleeve) is subsequently found by integration of nodal pressures.

For each chromosome, the bearing loads are recorded. The chromosomes are then sorted into decreasing load magnitudes as shown in Figure. 2.5.2. This set of chromosomes and loads represents the *k*-th generation.

In OPTJBG, to create the k+1 generation of chromosomes, chromosomes 1 and 2 (the best and runner-up load bearing designs) are simply carried over to the next generation (elitism), while crossover/mutation operators act on succeeding pairs of chromosomes, as shown in Figures 2.5.3 and 2.5.4. This process is repeated for a specified number of generations, whereupon the best design at the end is declared optimal. Our current selection criterion is based solely on the number of generations typically 500 to 1000 as recommended by Chapman (1994).

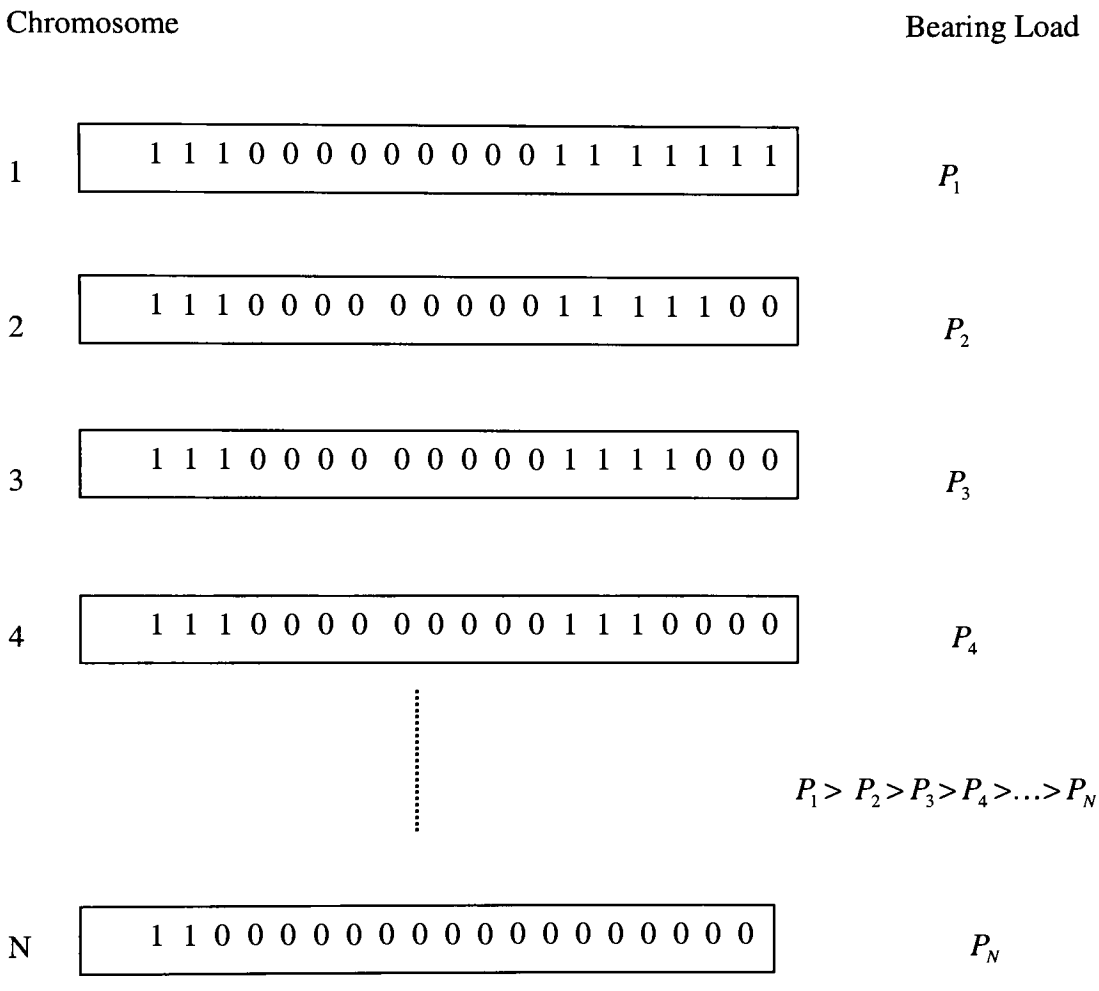

Figure 2.5.2 Ordering of the k-th generation prior to recombination.

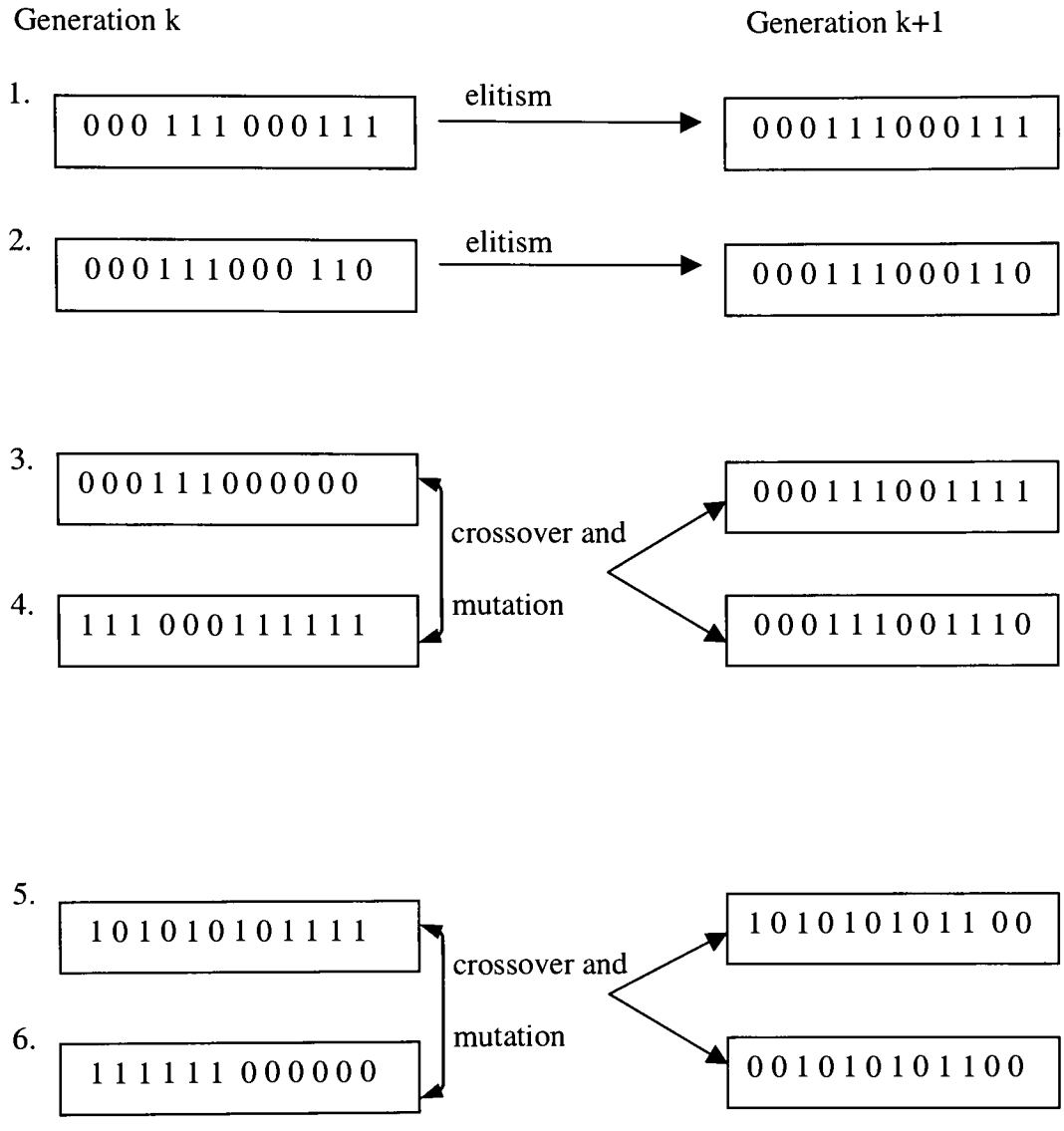

Figure 2.5.3 Creation of a new generation.

a) Crossover:

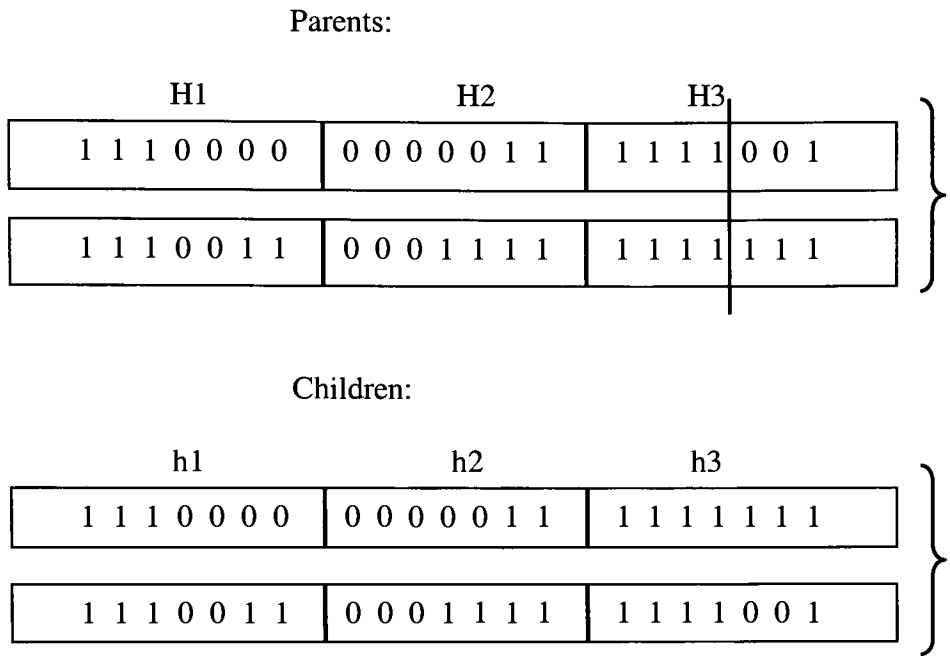

b) Mutation:

Before mutation:

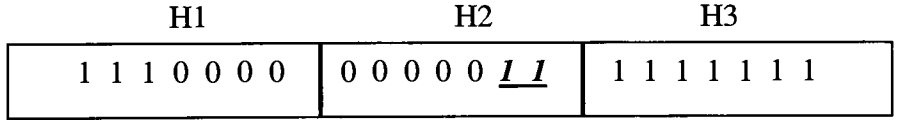

After mutation:

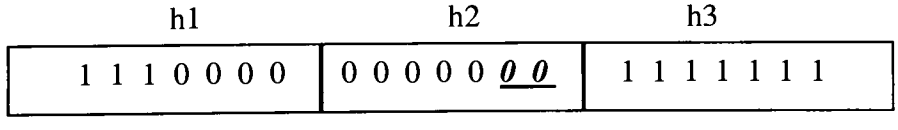

Figure 2.5.4 Crossover and mutation operators.

Chapter 3

Application

3.1 Introduction

Four case studies were performed. Each case study represents a particular bearing length and diameter configuration, and the goal is to achieve an optimal shape of the form shown in Figure 3.1.1. Table 1 lists bearing specifications and genetic algorithm parameters.

Given bearing specifications in Table 1, each case study started with an initial set (first generation) of *N_chrom* chromosomes. This set represented design variables H1, H2, H3 and was randomly generated using a random number generator (Matsumoto and Nishimura, 1997) and a seed value (sv) taken from a set of randomly generated integers (Abramonitz and Stegun, 1965). This initial set of chromosomes was allowed to evolve to 1000 generations using crossover and mutation probabilities listed in Table 1.

For each generation, the maximum load among the *N_chrom* chromosomes was recorded. The design variables that make up this best chromosome, along with maximal film pressure power loss, were also recorded for each generation.

The process was repeated with two different randomly generated sets of *N_chrom* chromosomes, and all three subcases were plotted and tabulated for comparison.

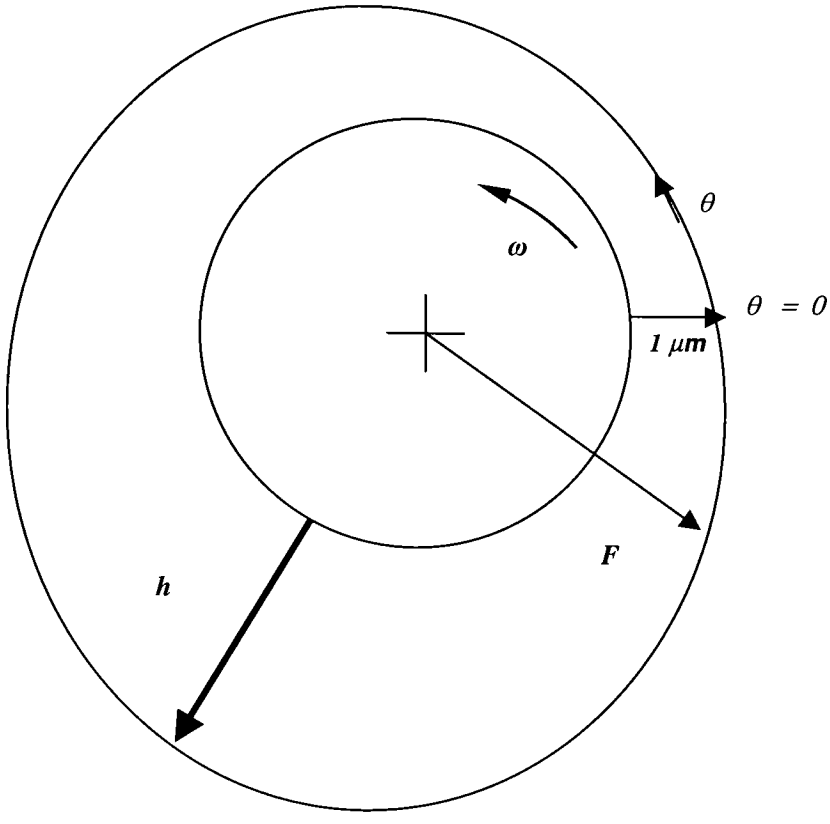

Figure 3.1.1 Bearing geometry

Table 1. Case studies

	Case # 1	Case # 2	Case # 3	Case # 4
Bearing Diameter, D (mm)	5	10	20	40
Bearing Length, L (mm)	5	10	10	10
Viscosity, m (mPa-s)	5	5	5	5
Cavitation Pressure, (Pa)	0	0	0	0
Ambient pressure, (Pa)	0	0	0	0
Journal angular velocity, ω (rad/s)	104.72	104.72	104.72	104.72
Chromosomes per generation, N_chrom	10,20,40	10,20,40	20	20
Number of generations, N_gen	1000	1000	1000	1000
Crossover probablity, P_{cross}	0.95	0.95	0.95	0.65, 0.78, 0.95
Mutation Probablity, P_{mut}	0.01	0.01	0.01	0, 0.01, 0.001

3.2 Case Study 1

This case study represents a bearing with diameter D = 5 mm, bearing length L = 5 mm, and journal angular velocity ω = 104.720 rad/s (Table 1). Three subcases are studied by specifying the number of chromosomes per generation in sets of 10, 20, and 40, along with crossover probability of 0.95 and mutation probability of 0.01.

With *N_chrom* =10, Figure 3.2.1 shows a plot of load evolutions for each of three randomly selected sets. Figure 3.2.2 shows the plot of the resulting power loss with three randomly selected sets. Figure 3.2.3 shows the maximum film pressure of the bearing. Figure 3.2.4 a, b, c shows the resulting film thickness with three randomly selected seed values. All these plots show that even after 1000 generations, there are still three distinctly different solutions were found, suggesting that only local optimums were achieved.

With *N_chrom* =20, Figure 3.2.5 shows a plot of load evolutions for each of three randomly selected sets. Figure 3.2.6 shows the plot of power loss with three randomly selected sets. Figure 3.2.7 shows the maximum film pressure of the bearing. Figure 3.2.8 a, b, c shows the film thickness with three randomly selected seed values. After 1000 generation, the evolutions are approaching a common value, suggesting that a global optimum has been achieved.

With *N_chrom* = 40, Figure 3.2.9 shows a plot of load evolutions for each of three randomly selected sets. Figure 3.2.10 shows the plot of power loss with three randomly selected sets.

Figure 3.2.11 shows the maximum film pressure of the bearing. Figure 3.2.12 a, b, c shows the film thickness with three randomly selected seed values. The final results are very similar to *N_chrom* = 20. *N_chrom* = 40 gave somewhat better final convergence at *N_gen* = 1000. There is a difference between these subcases, but this difference is approximately ± 5 %. However, the computation time is more than twice as long with chromosome size of 40 than with chromosome size of 20. Running this case took more than 8 hours for computation.

3.3 Case Study 2

This case study represents a bearing with diameter D = 5 mm, bearing length L = 10 mm, and journal angular velocity ω = 104.720 rad/s (Table 1). As in case 1, three subcases are studied by specifying the number of chromosomes in sets of 10, 20, and 40, along with crossover probability of 0.95 and mutation probability of 0.01.

With *N_chrom* = 10, Figure 3.3.1 shows a plot of load evolutions for each of three randomly selected sets. Figure 3.3.2 shows the plot of power loss with three randomly selected sets. Figure 3.3.3 shows the maximum film pressure of the bearing. Figure 3.3.4 a, b, c shows the film thickness with three randomly selected seed values. All these plots show that even after 1000 generations, still three distinctly different solutions were found, again suggesting that local optimums were achieved.

With *N_chrom* = 20, Figure 3.3.5 shows a plot of load evolutions for each of three randomly selected sets. Figure 3.3.6 shows the plot of power loss with three randomly selected sets. Figure 3.3.7 shows the maximum film pressure of the bearing. Figure 3.3.8 a, b, c shows the film thickness with three randomly selected seed values. After 1000 generations, the evolutions are approaching a common value, as with that found in case 1.

With *N_chrom* = 40, Figure 3.3.9 shows a plot of load evolutions for each of three randomly selected sets. Figure 3.3.10 shows the plot of power loss with three randomly selected sets. Figure 3.3.11 shows the maximal film pressure of the bearing. Figure 3.3.12 a, b, c shows the film thickness with three randomly selected seed values. As in case 1, the final results are very similar to *N_chrom* = 20, differing only by about 5 %. Hence, based on this and the previous case study, it appears that using 20 chromosomes per generation with 1000 generations is sufficient for further computations.

3.4 Case Study 3

This case study represents a bearing with diameter D = 10 mm, bearing length L = 20 mm, and journal angular velocity ω = 104.720 rad/s (Table 1). This case differs from previous cases studied in that only a chromosome size of 20, crossover probability of 0.95 and mutation probability of 0.01 will be used.

Figure 3.4.1 shows a plot of load evolutions for each of three randomly selected sets. Figure 3.4.2 shows the plot of power loss with three randomly selected sets. Figure 3.4.3 shows the

maximum film pressure of the bearing. Figure 3.4.4 a, b, c shows the film thickness with three randomly selected seed values.

This study showed that the chromosome size of 20 with 1000 generations gives convergence trends similar to Case Study # 2. Another interesting fact with this case is that by decreasing the ratio of bearing length to diameter L/D, global optimal solutions in load evolutions, maximal film pressure and power loss can be simultaneously attained, which was not obtained in Case 1 or 2, with L/D =1.

3.5 Case Study 4

This case study represents a bearing with diameter D = 40 mm, bearing length L = 10 mm, and journal angular velocity ω = 104.720 rad/s (Table 1). This case is studied with only chromosome size of 20, but with different crossover probability values (0.65, 0.78, 0.95) and mutation probability values (0, 0.001, 0.01) to investigate the sensitivity of the probability values of crossover and mutation operators. Crossover probability values are selected from the minimum, average and maximum values suggested for the population size of 20-35 as suggested by Melanie (1999).

Figure 3.5.1 shows a plot of load evolutions for each of three randomly selected sets with crossover probability of 0.95 and mutation probability of 0.01. Figure 3.5.2 shows the plot of power loss with three randomly selected sets crossover probability of 0.95 and mutation probability of 0.01. Figure 3.5.3 shows the maximum film pressure of the bearing crossover

probability of 0.95 and mutation probability of 0.01. Figure 3.5.4 a, b, c shows the film thickness with three randomly selected seed values after 1000 generations.

This case study also showed that the chromosome size of 20 with 1000 generations gives convergence trends similar to the previous case studies.

Figure 3.5.5 shows a plot of load evolutions for each of three randomly selected sets with crossover probability of 0.65 and mutation probability of 0.01. Figure 3.5.6 shows the plot of power loss with three randomly selected sets crossover probability of 0.65 and mutation probability of 0.01. Figure 3.5.7 shows the maximal film pressure of the bearing crossover probability of 0.65 and mutation probability of 0.01. Figure 3.5.8 shows a plot of load evolutions for each of three randomly selected sets with crossover probability of 0.78 and mutation probability of 0.01.

Figure 3.5.9 shows the plot of power loss with three randomly selected sets crossover probability of 0.78 and mutation probability of 0.01. Figure 3.5.10 shows the maximum film pressure of the bearing crossover probability of 0.78 and mutation probability of 0.01.

Figure 3.5.11 shows a plot of load evolutions for each of three randomly selected sets with crossover probability of 0.95 and mutation probability of 0 (without mutation). Figure 3.5.12 shows the plot of power loss with three randomly selected sets crossover probability of 0.95 and mutation probability of 0 (without mutation). Figure 3.5.13 shows the maximal film

pressure of the bearing crossover probability of 0.95 and mutation probability of 0 (without mutation).

Figure 3.5.14 shows a plot of load evolutions for each of three randomly selected sets with crossover probability of 0.95 and mutation probability of 0.001. Figure 3.5.15 shows the plot of power loss with three randomly selected sets crossover probability of 0.95 and mutation probability of 0.001. Figure 3.5.16 shows the maximal film pressure of the bearing crossover probability of 0.95 and mutation probability of 0.001.

All these plots show that the acceptable values of crossover probability and mutation probability are 0.95 and 0.01 respectively, along with chromosome size of 20.

3.6 Comparison with cylindrical bearings

Finally, comparison with conventional cylindrical bearing designs needs to be investigated. Using the CUIMPD module, a cylindrical finite element mesh was constructed As Figure 3.6.1 shows, the film thickness at $\theta = 0$ is fixed to 1 micron, and the film thickness h_{max} at $\theta =$ 180 is varied from 1 to 128 microns. For each case study, plots of specified h_{max} value, a circular bearing sleeve is constructed and bearing load F is computed. F vs. film thickness h_{max} were drawn, as shown in Figure 3.6.2 (Case 1), Figure 3.6.3 (Case 2), Figure 3.6.4 (Case 3), and Figure 3.6.2 (Case 4). The maximum values of F from each case study were tabulated in Table 2.

The comparison of results in Table 2 show that the investigated optimization technique gives approximately 10 % improvement in a bearing maximal load with bearing size of D = 5 mm and L = 5 mm Case 1, nearly 50 % improvement in a bearing with dimensions of D = 10 mm and L = 10 mm Case 2, approximately 7.1 % improvement in a bearing with dimensions of D = 20 mm and L = 10 mm Case 3, and approximately 5 % improvement in a bearing with dimensions of D = 40 mm and L = 10 mm Case 4.

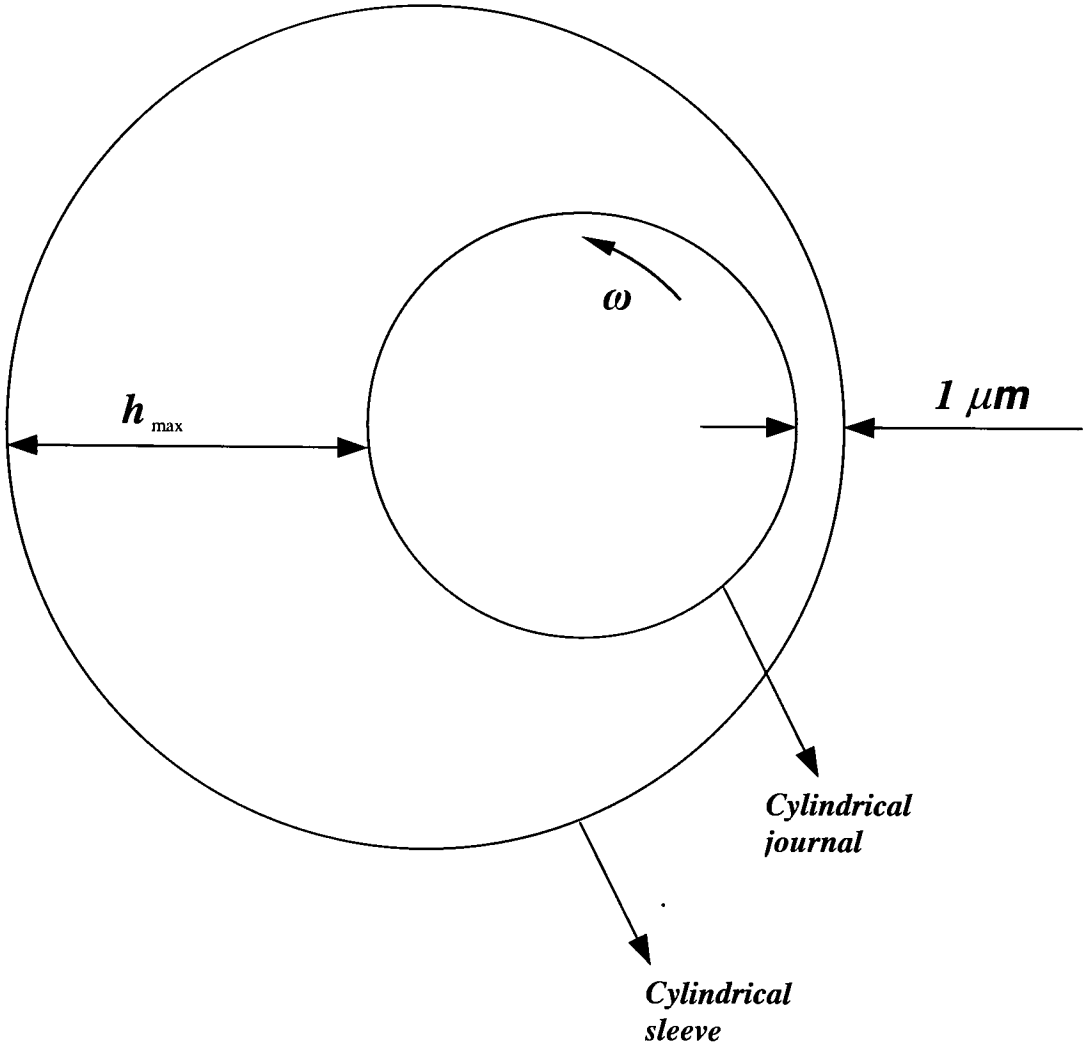

Figure 3.6.1 Cylindrical bearing geometry.

Table 2. Comparison of optimal bearings with best cylindrical bearing

N_chrom = 20, P_mut = 0.01
P_cross =0.95

Case #	Maximum Optimal Load, F (N)	Best Cylindrical bearing, Fcyl (N)	Fmax / Fcyl
CASE # 1	21.704	19.958	1.08751914
CASE # 2	443.566	297.975	1.488602913
CASE # 3	903.028	843.2	1.070953866
CASE # 4	2126.579	2045.745	1.039513475

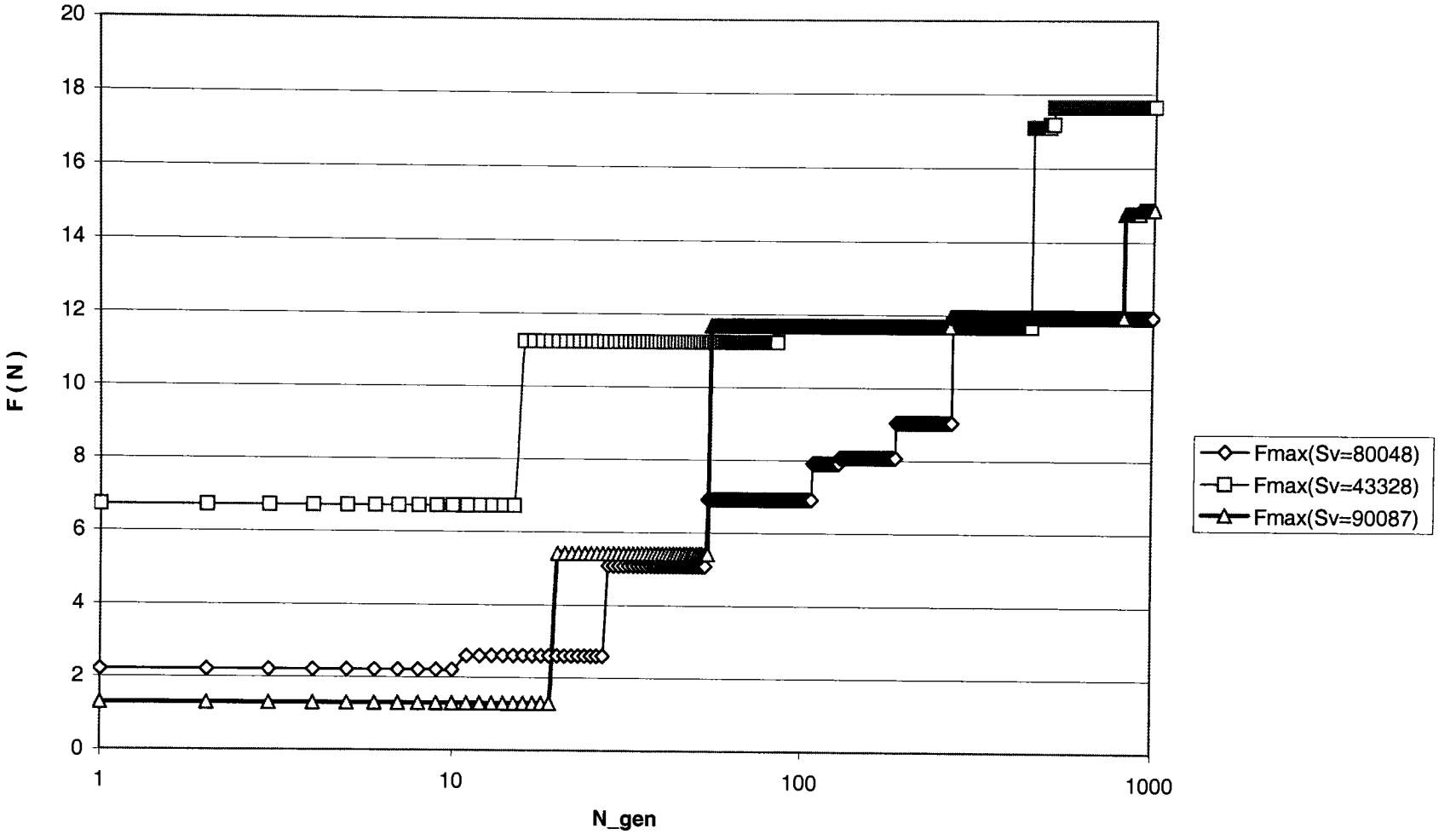

Figure 3.2.1. Bearing load evolutions for each of three randomly selected sets (D=5.0mm, N_chrom=10).
CASE # 1.

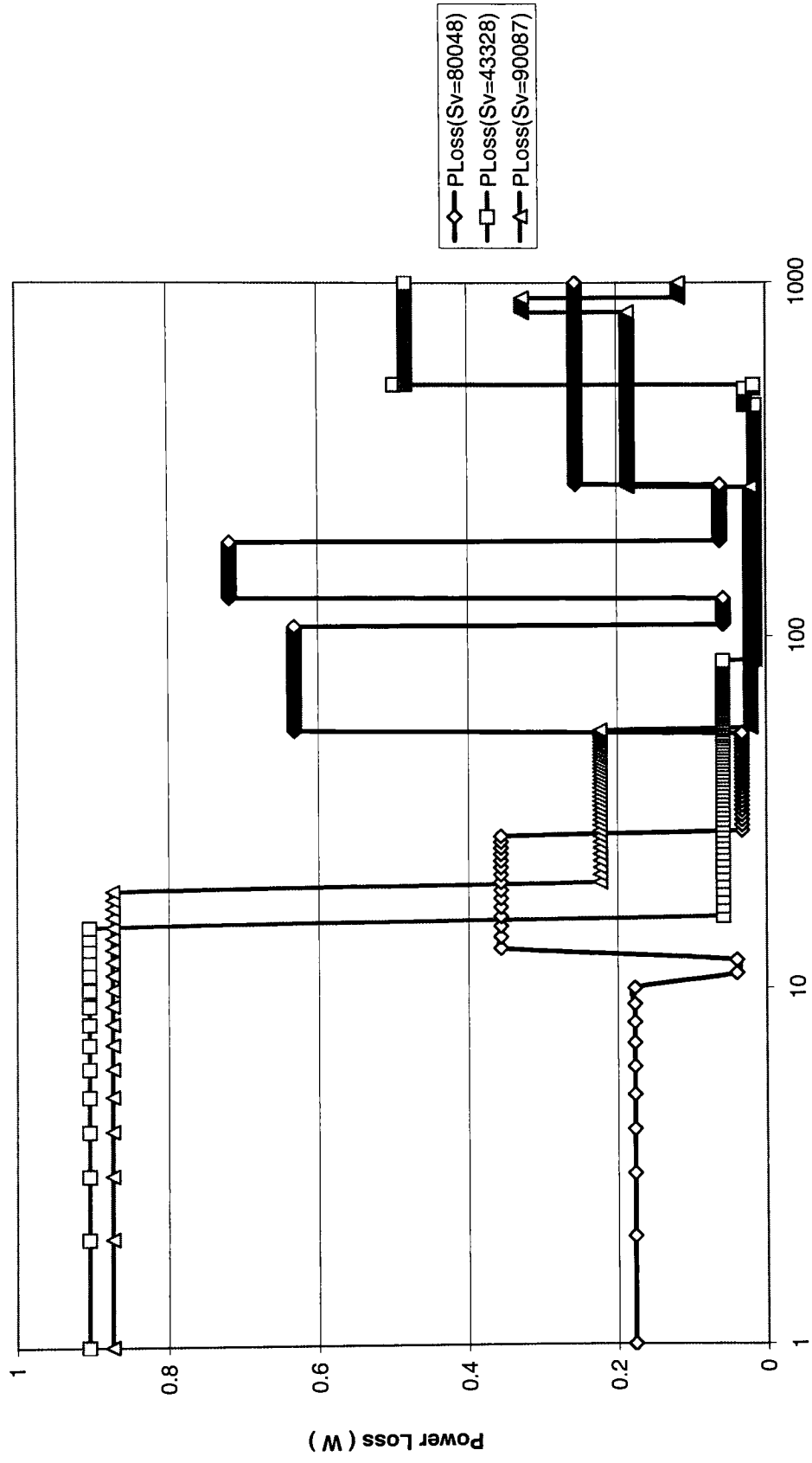

Figure 3.2.2. Plot of Power Loss with three randomly selected sets (D=5.0, N_chrom=10) CASE # 1.

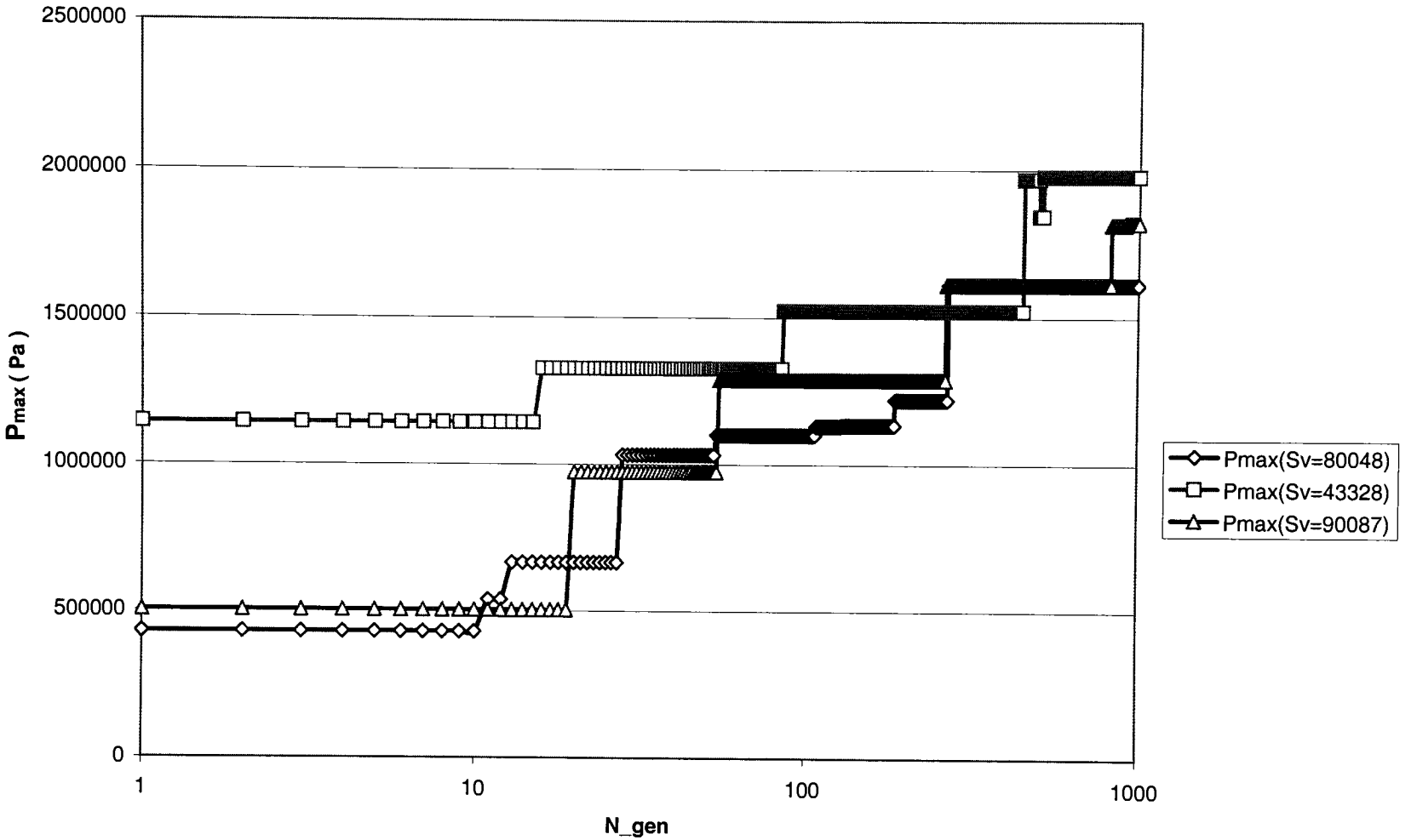

Figure 3.2.3. Plot of Pmax with three randomly selected sets (D=5.0mm, N_chrom=10)
CASE # 1.

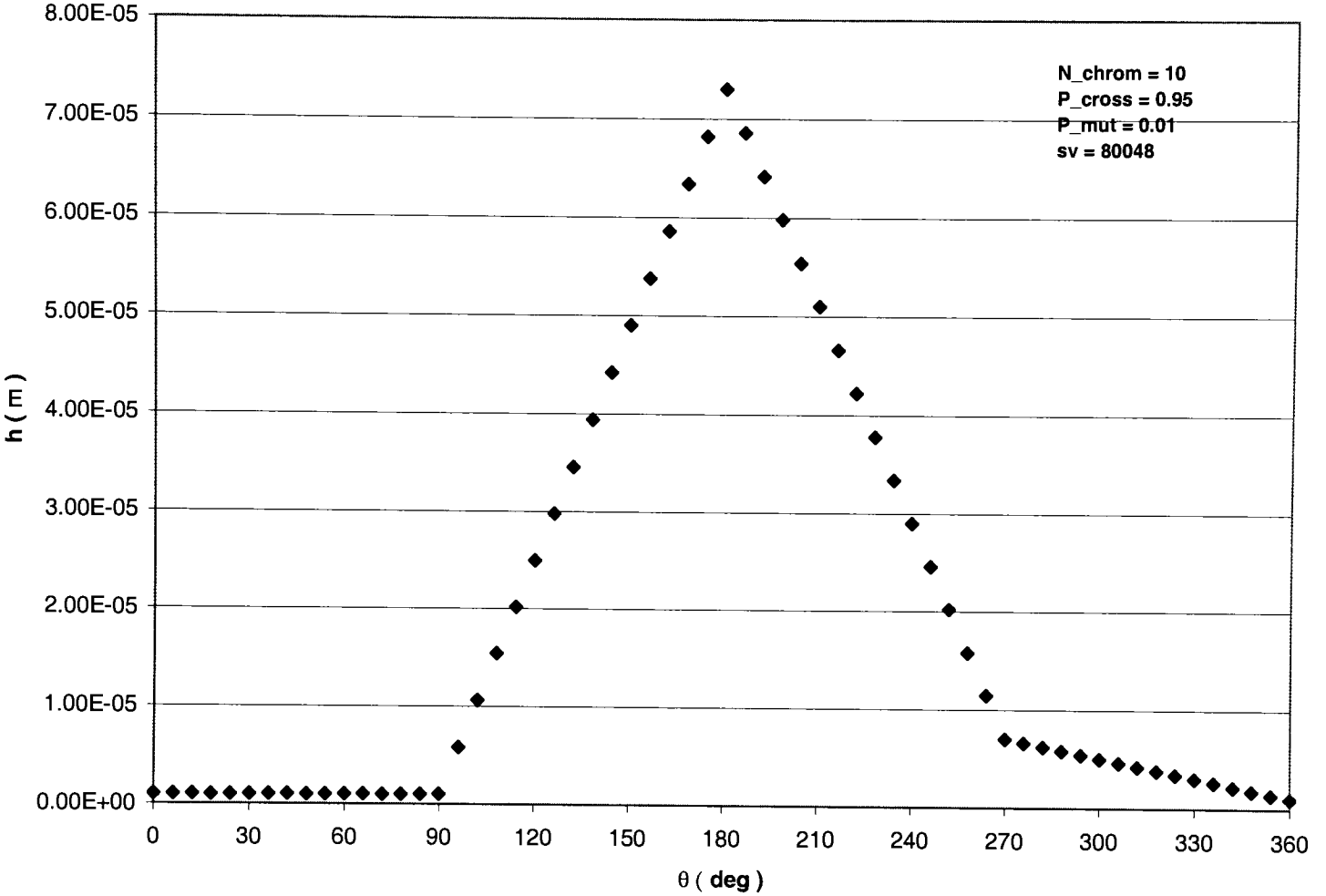

Figure 3.2.4, a. Film thickness distribution with first random set of chromosomes (sv=80048) after 1000 generations
C a s e # 1, N_chrom= 10.

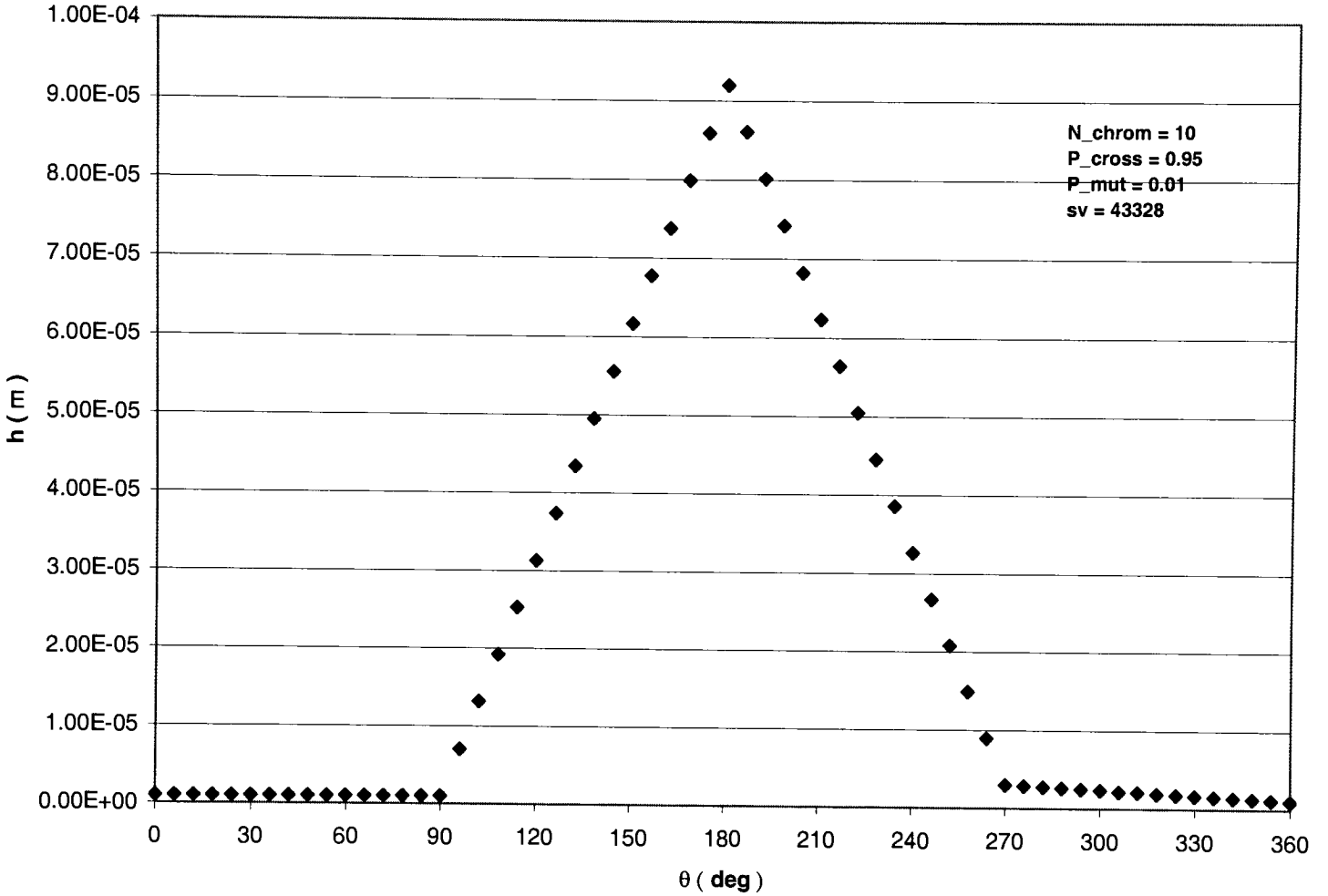

Figure 3.2.4, b. Film thickness distribution with second random set of chromosomes (sv=43328) after 1000 generations
C a s e # 1, N_chrom= 10.

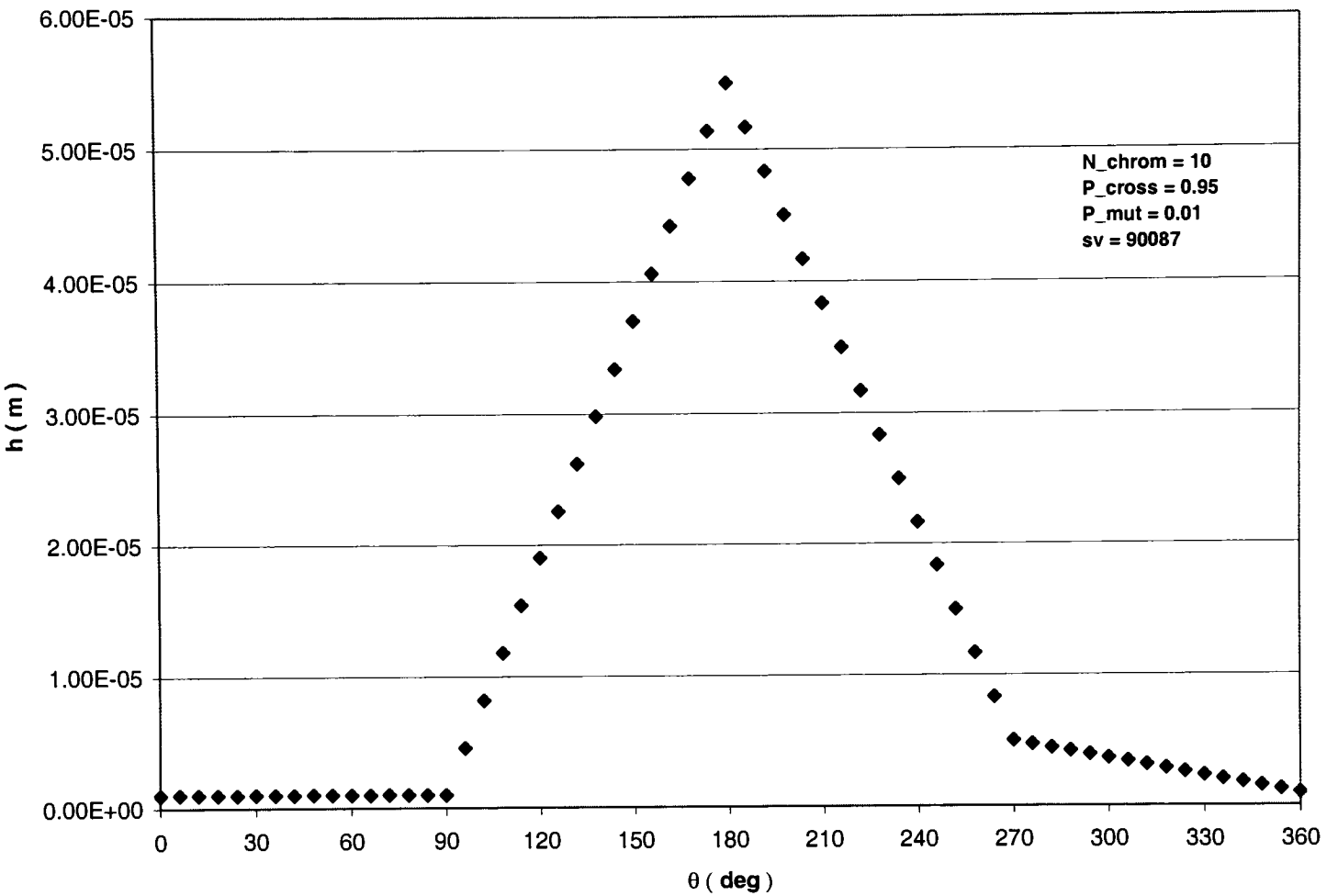

Figure 3.2.4, c. Film thickness distribution with first random set of chromosomes (sv=90087) after 1000 generations
C a s e # 1, N_chrom= 10.

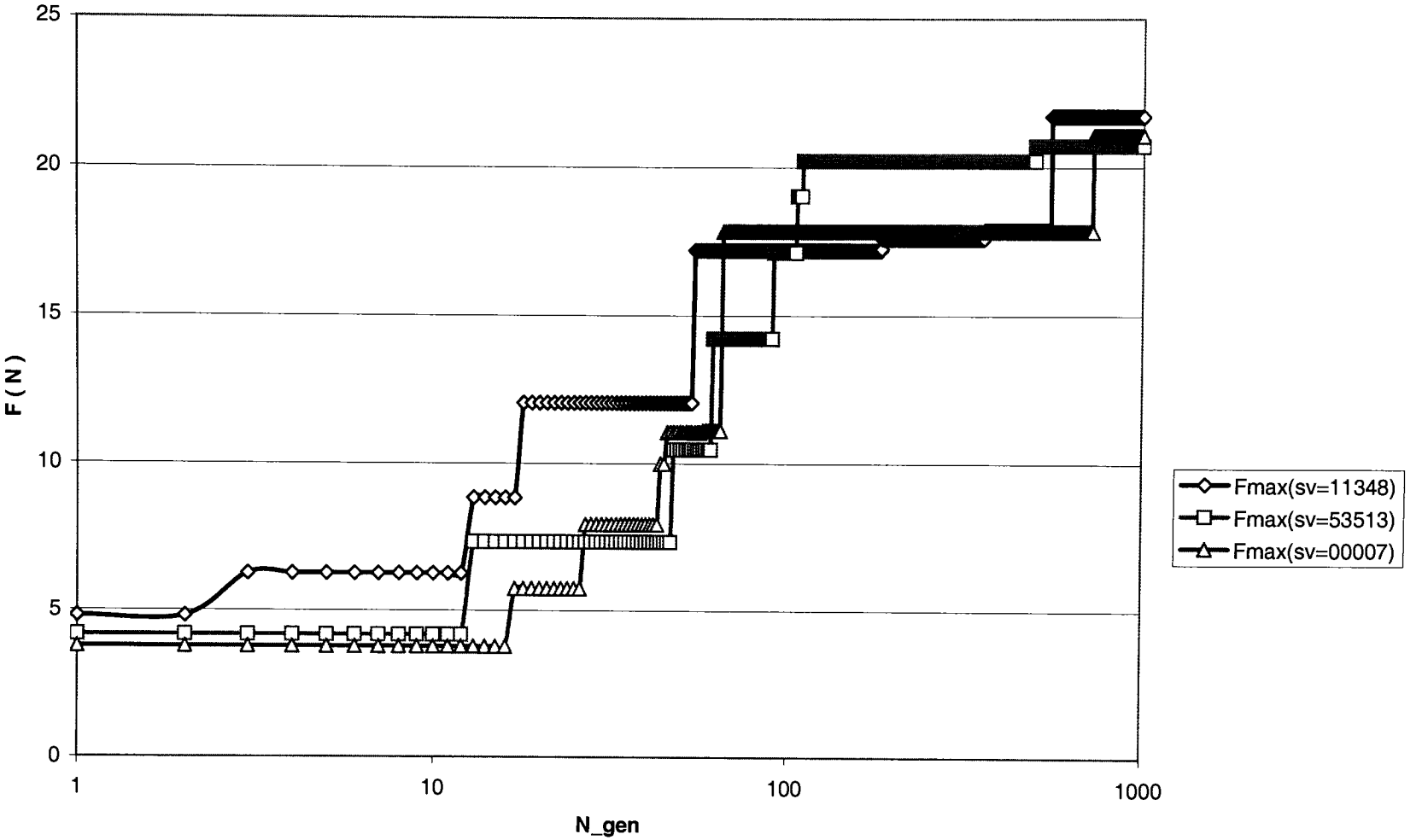

Figure 3.2.5. Bearing load evolutions for each of three randomly selected sets (D=5.0mm, N_chrom=20)
Case # 1.

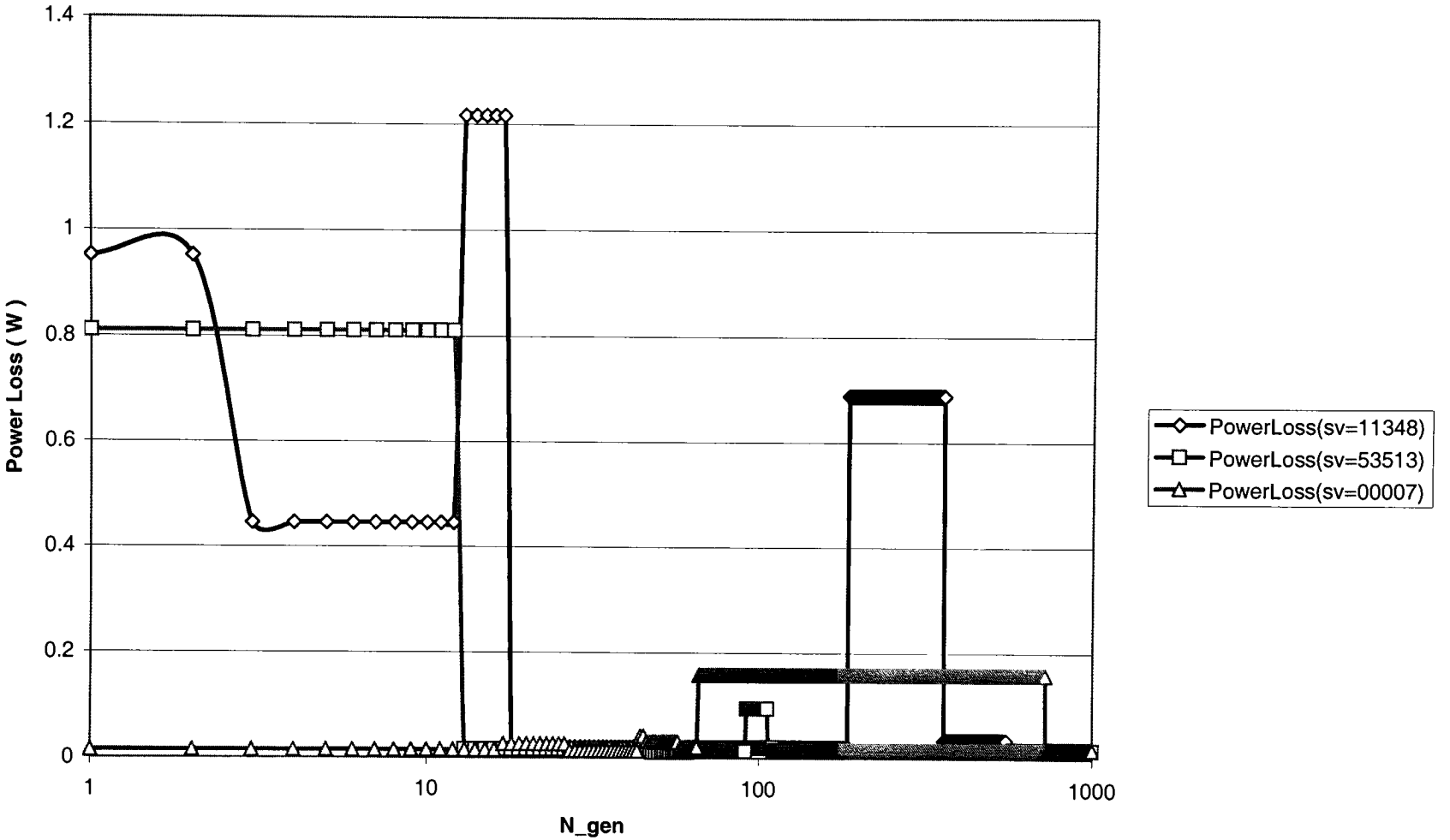

Figure 3.2.6. Plot of Power Loss with three randomly selected sets (D=5.0mm, N_chrom=20) Case # 1.

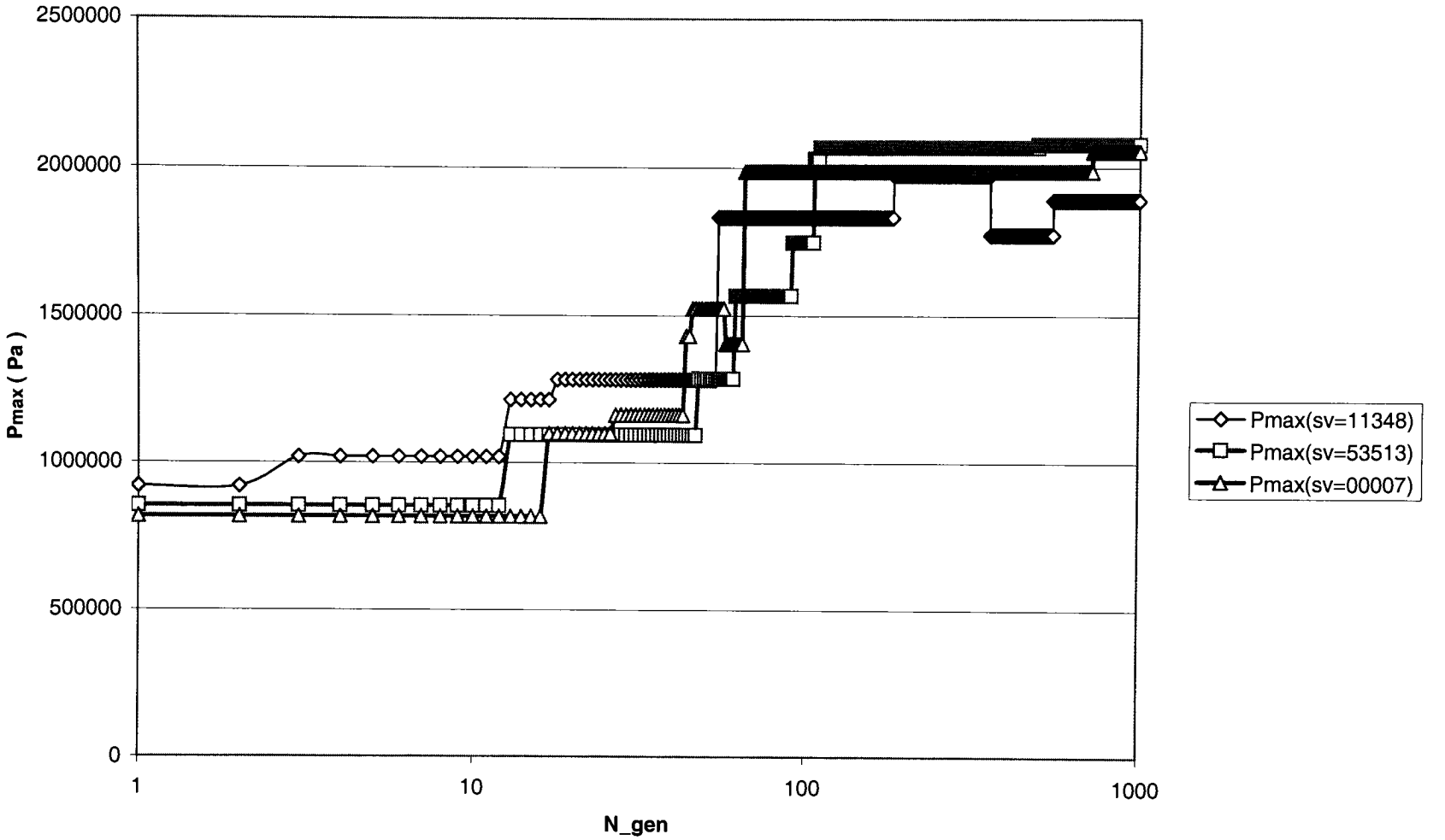

Figure 3.2.7. Plot of P_{max} with three random sets (D=5.0mm, N_chrom=20) Case # 1.

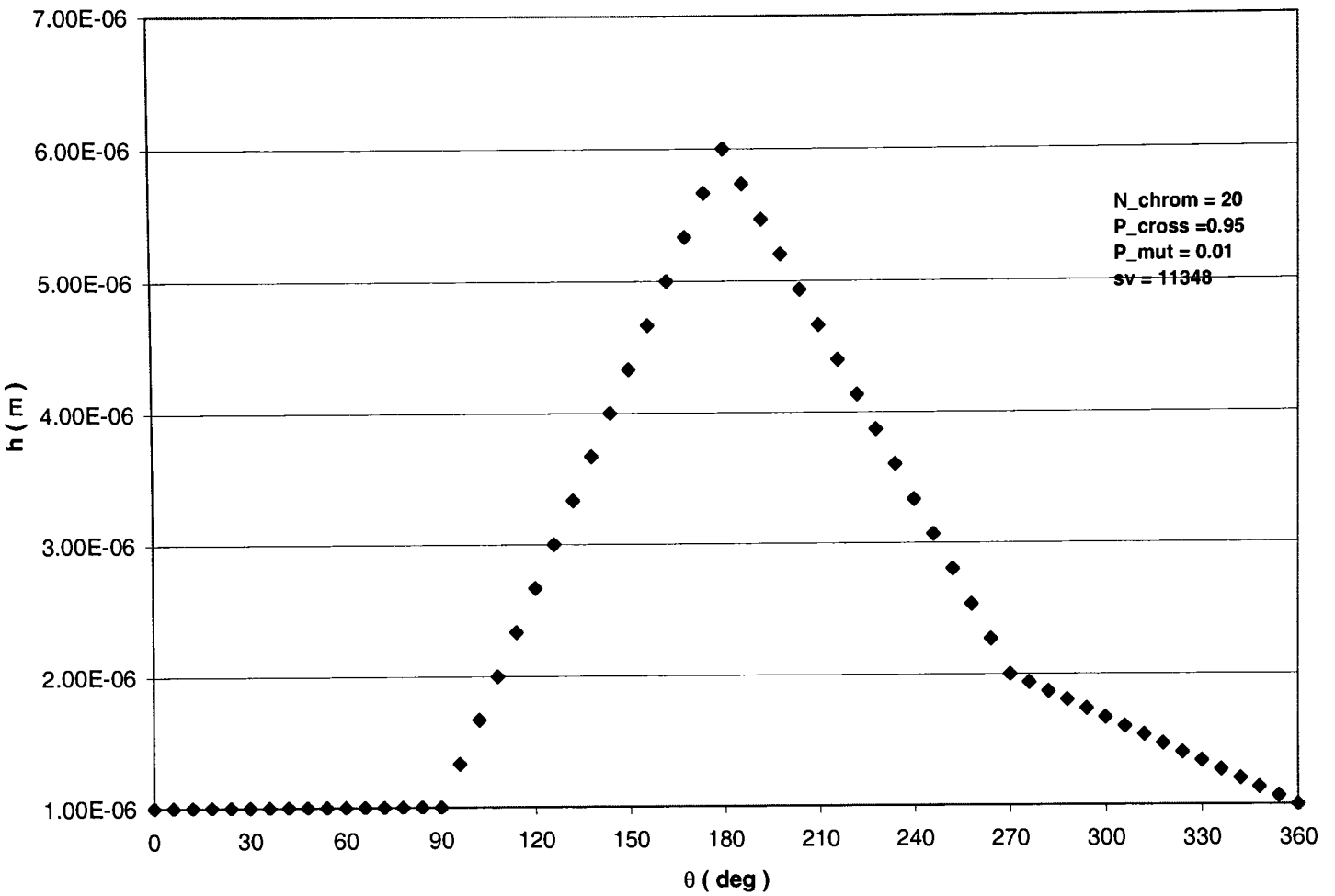

Figure 3.2.8, a. Film thickness distribution with first random set of chromosomes (sv = 11348) after 1000 generations
Case #1. N_chrom = 20.

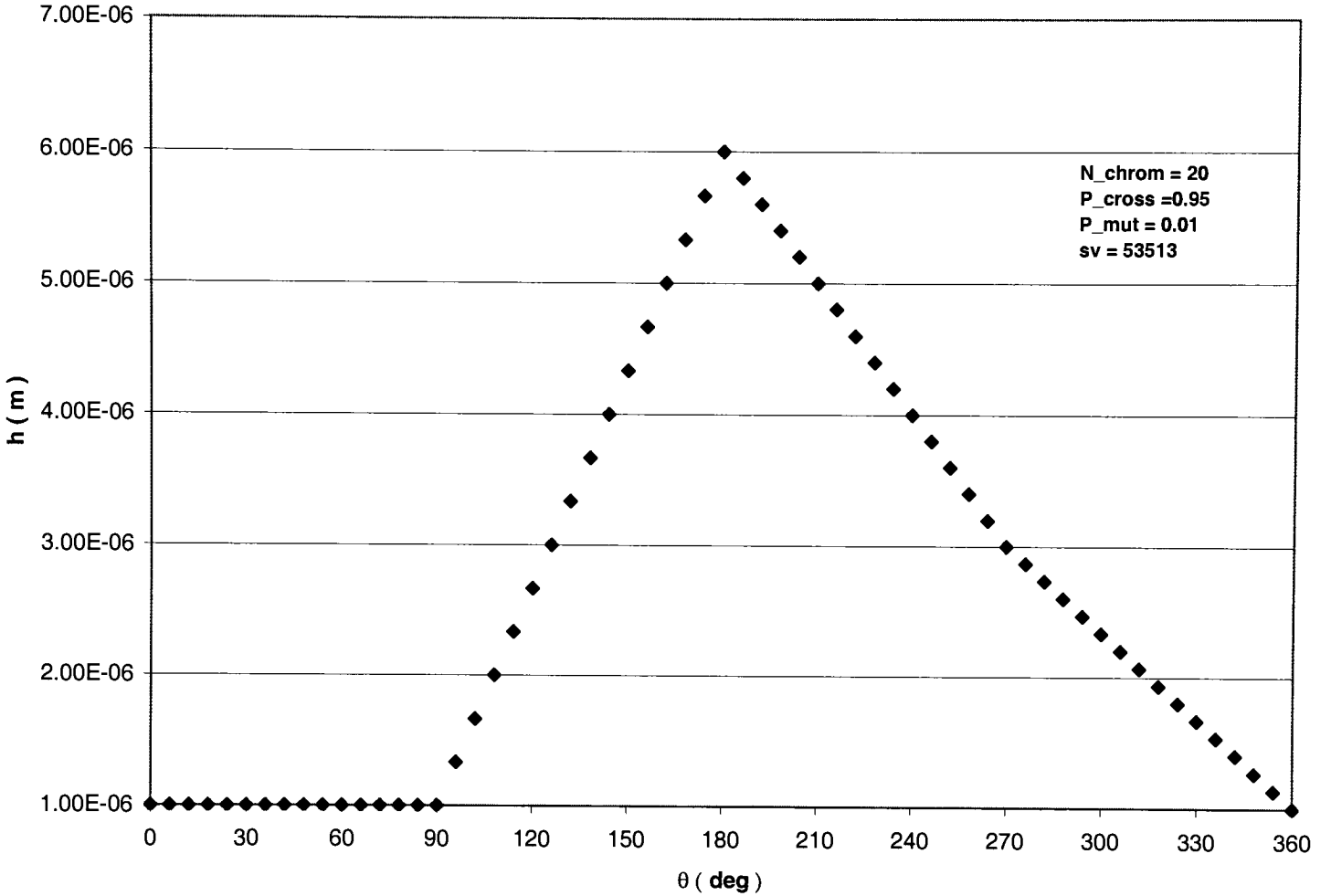

Figure 3.2.8, b. Film thickness distribution with second random set of chromosomes (sv = 53513) after 1000 generations
Case #1. N_chrom = 20.

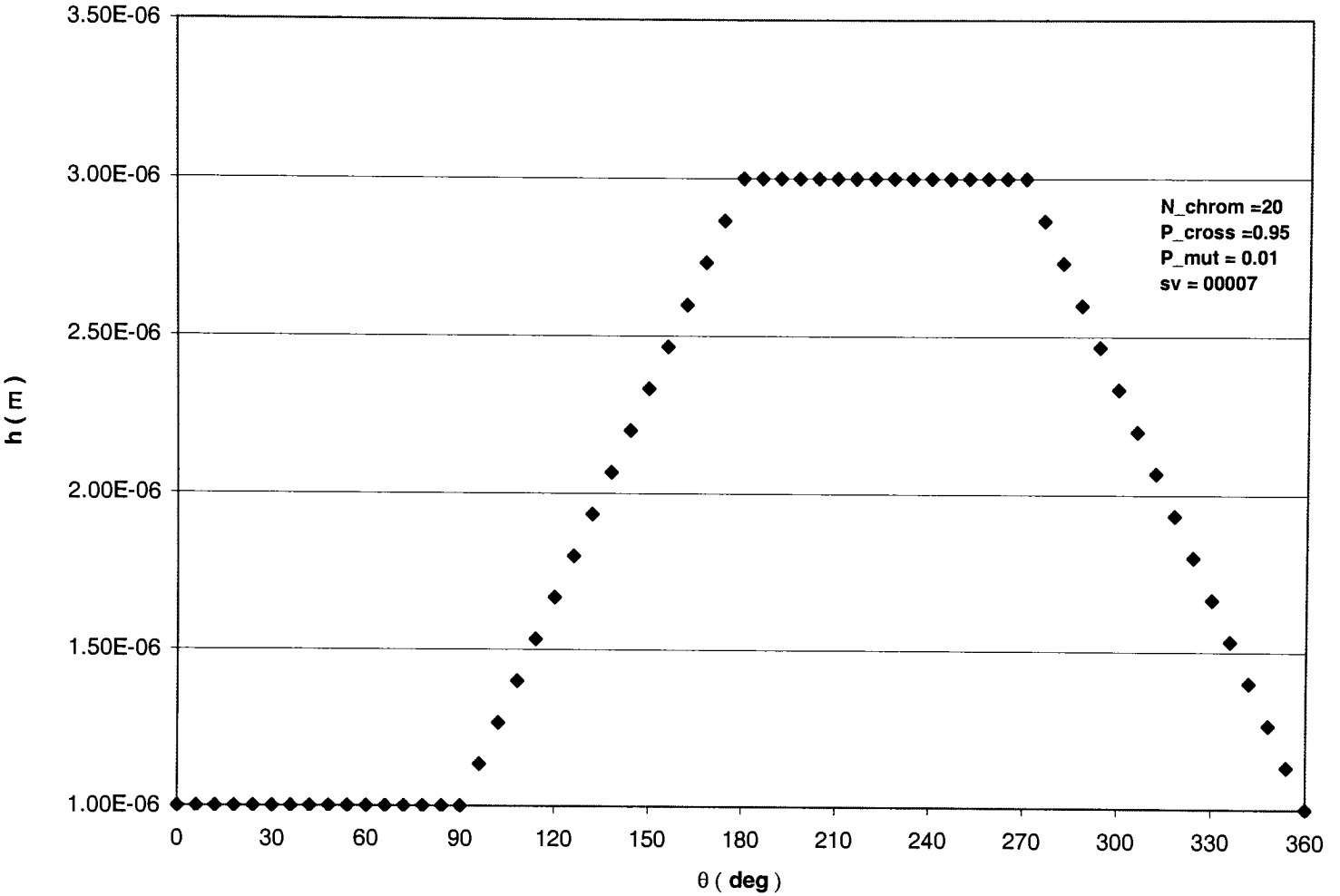

Figure 3.2.8, c. Film thickness distribution with third random set of chromosomes (sv = 00007) after 1000 generations
Case #1. N_chrom = 20.

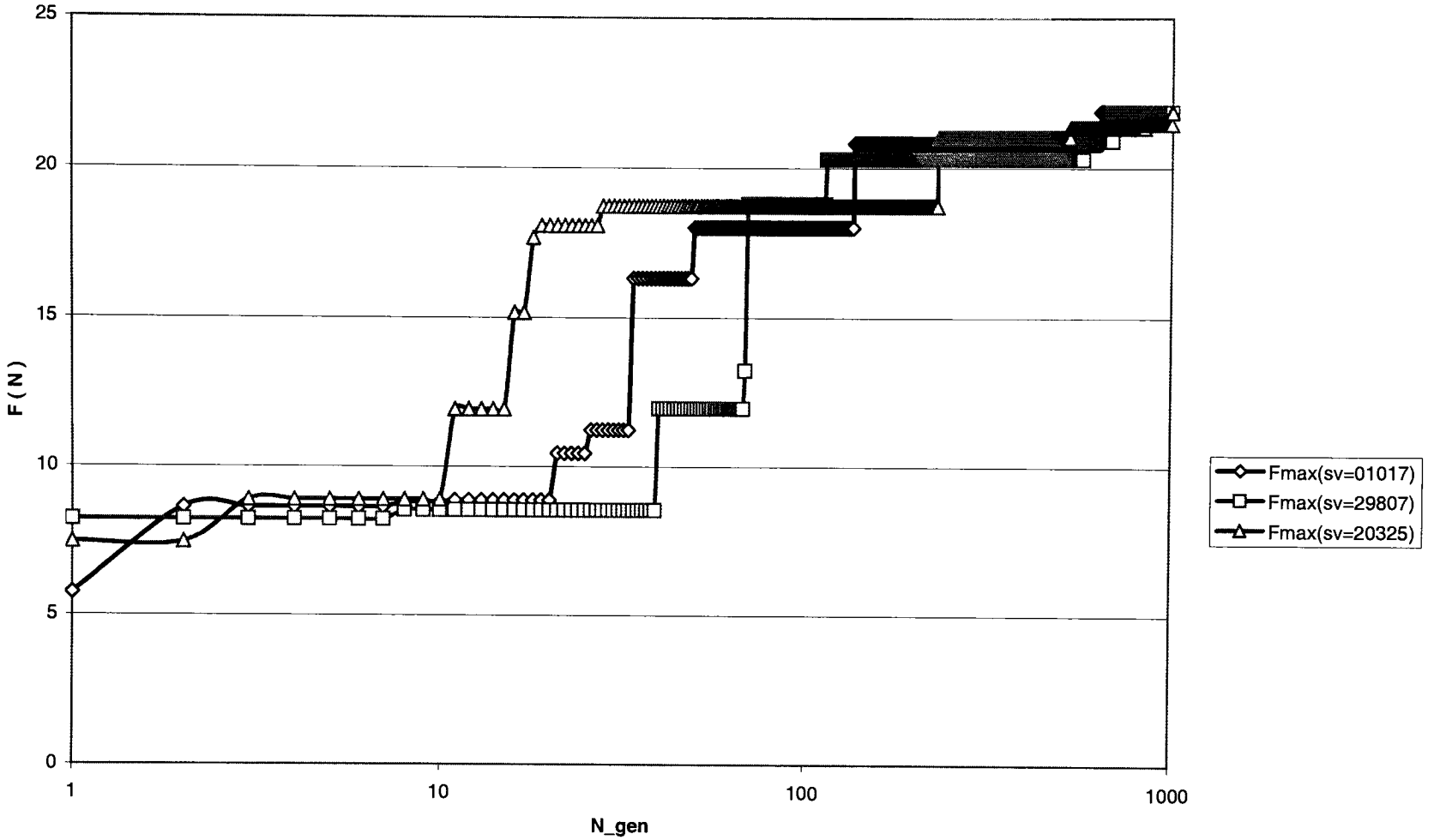

Figure 3.2.9. Bearing load evolutions for each of three randomly selected sets (D=5.0mm, N_chrom=40)
Case # 1

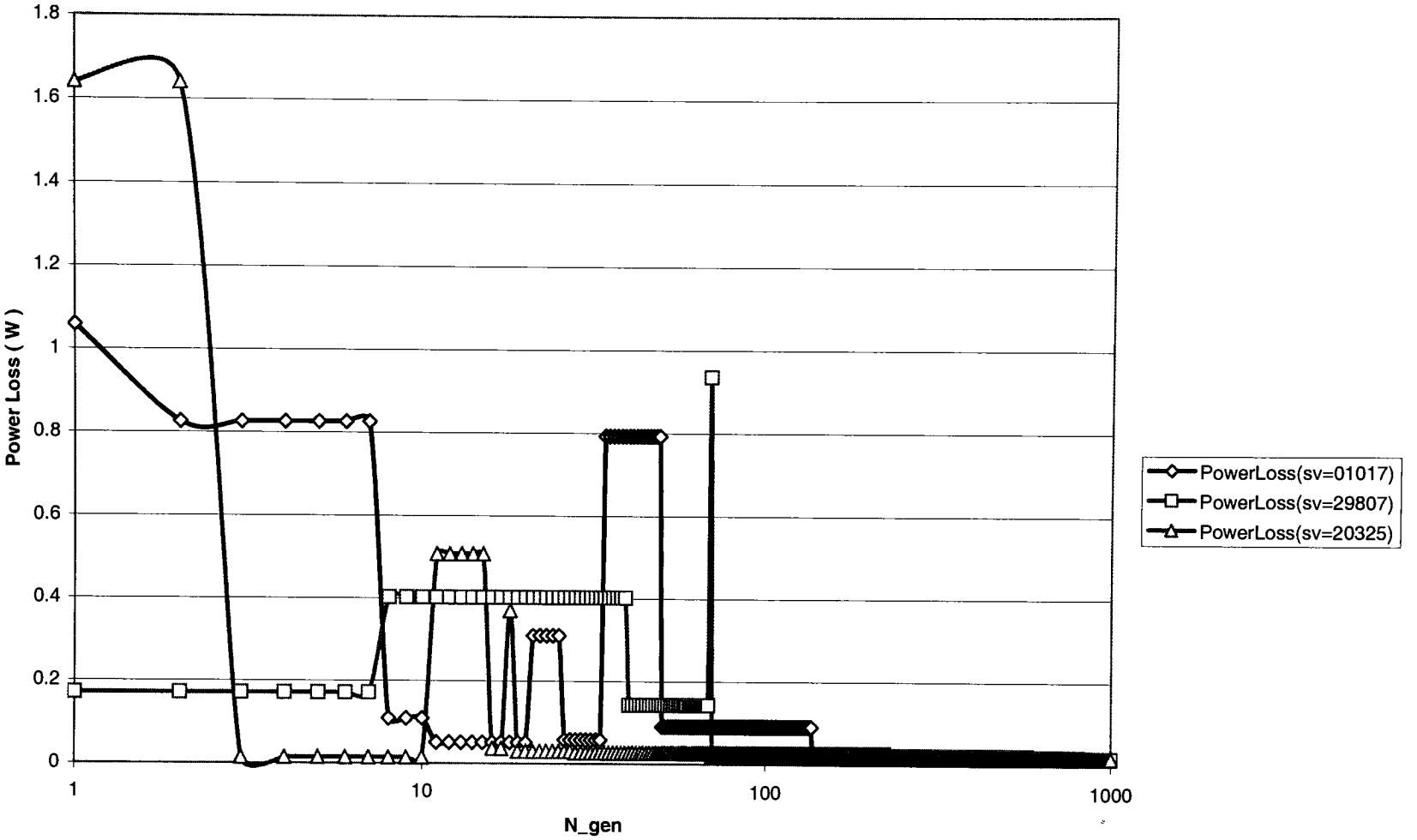

Figure 3.2.10. Plot of Power Loss with three randomly selected sets (D=5.0mm, N_chrom=40)
Case # 1

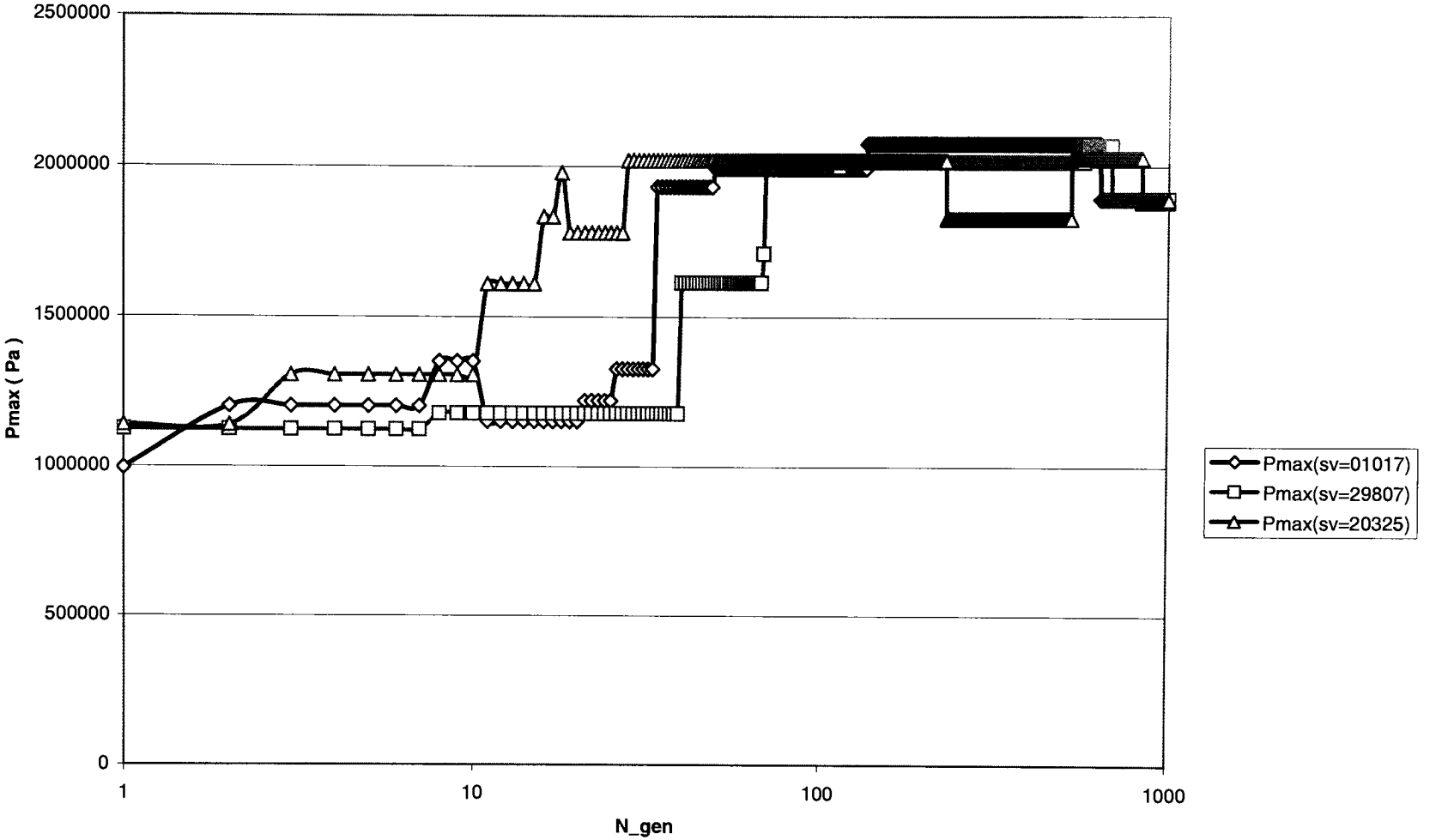

Figure 3.2.11. Plot of Pmax with three randomly selected sets (D=5.0mm, N_chrom=40) Case # 1.

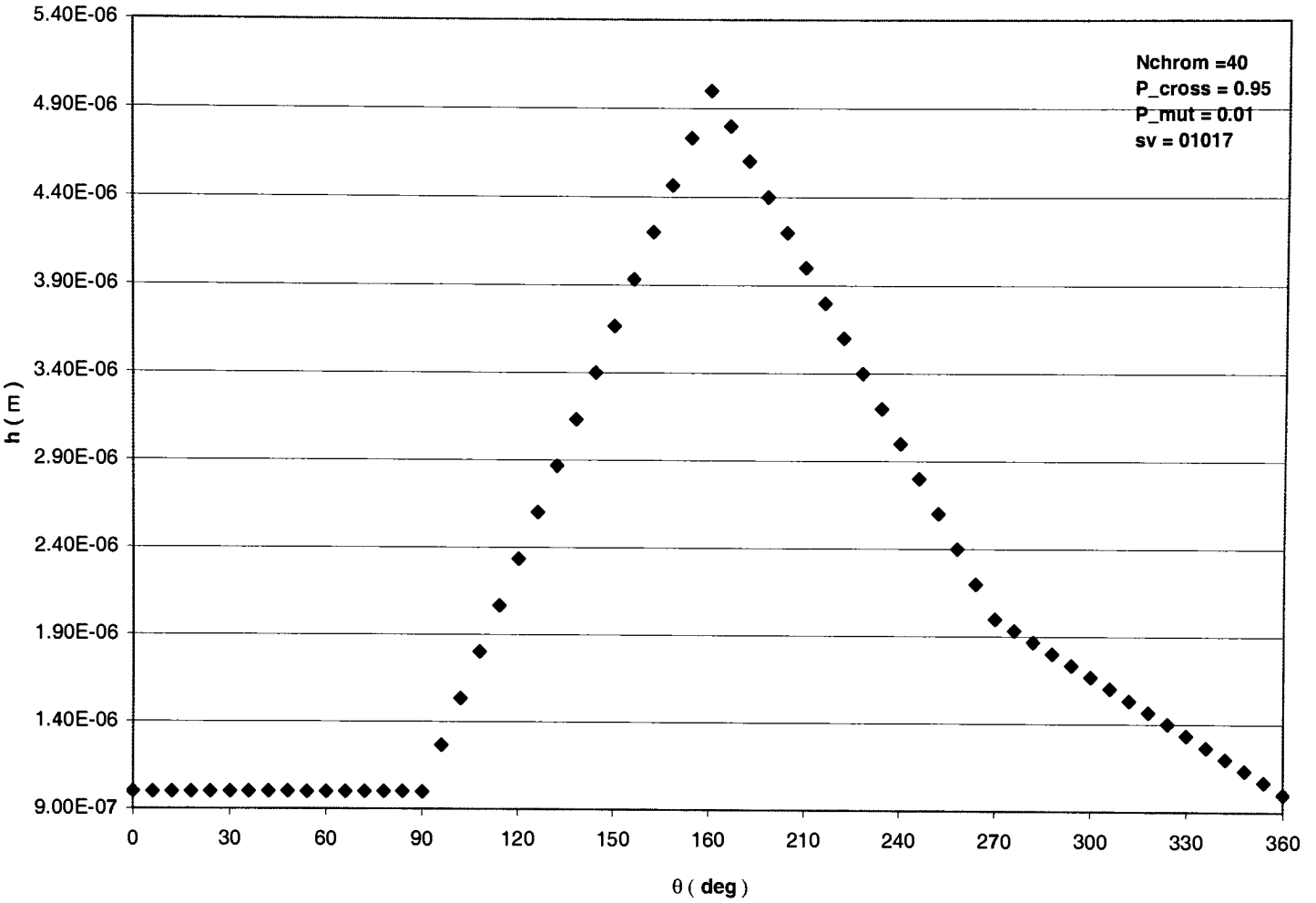

Figure 3.2.12, a. Film thickness distribution with first random set of chromosomes (sv=01017) after 1000 geenrations
Case # 1. N_chrom = 40

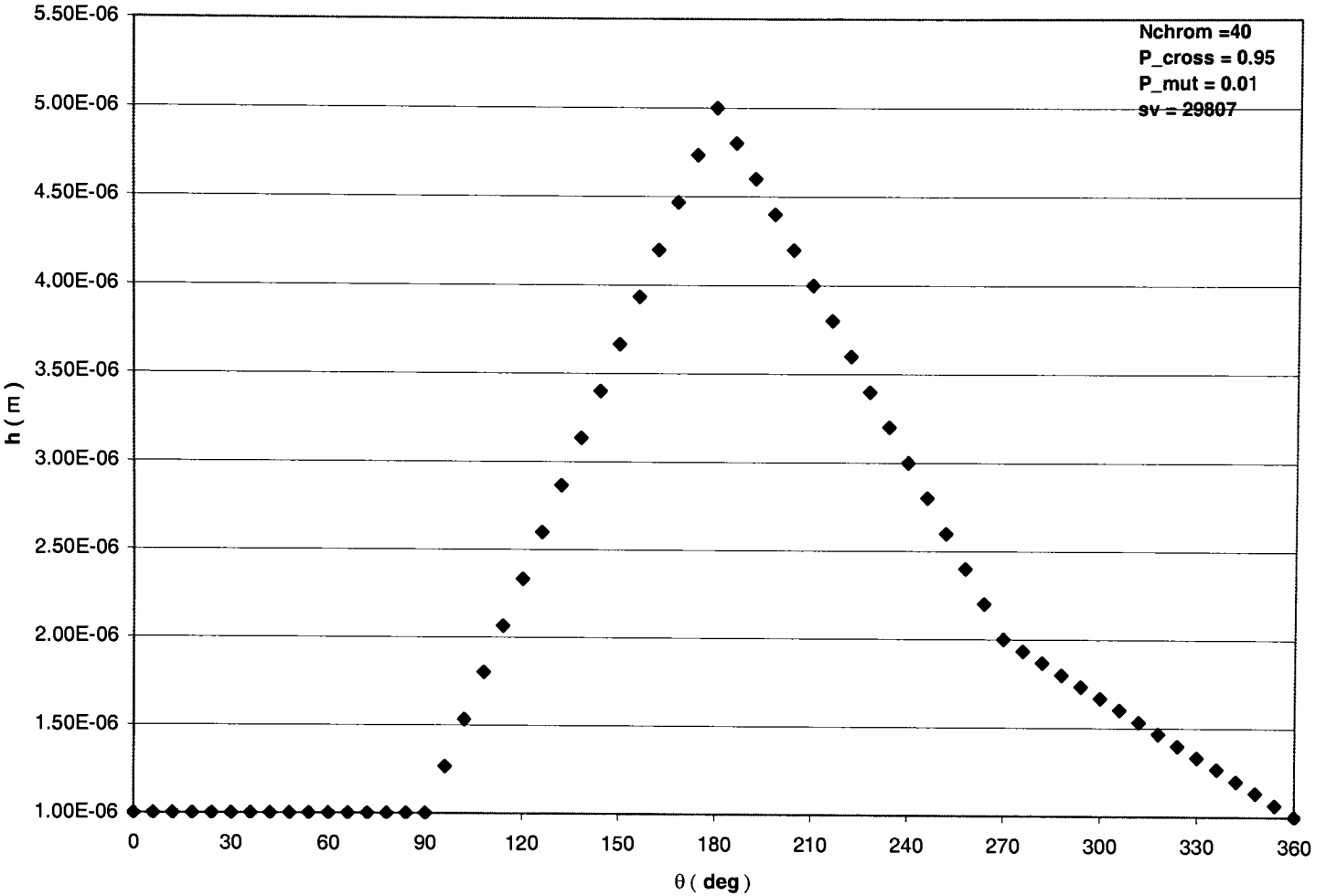

Figure 3.2.12, b. Film thickness distribution with second random set of chromosomes (sv=29807) after 1000 geenrations
Case # 1. N_chrom = 40

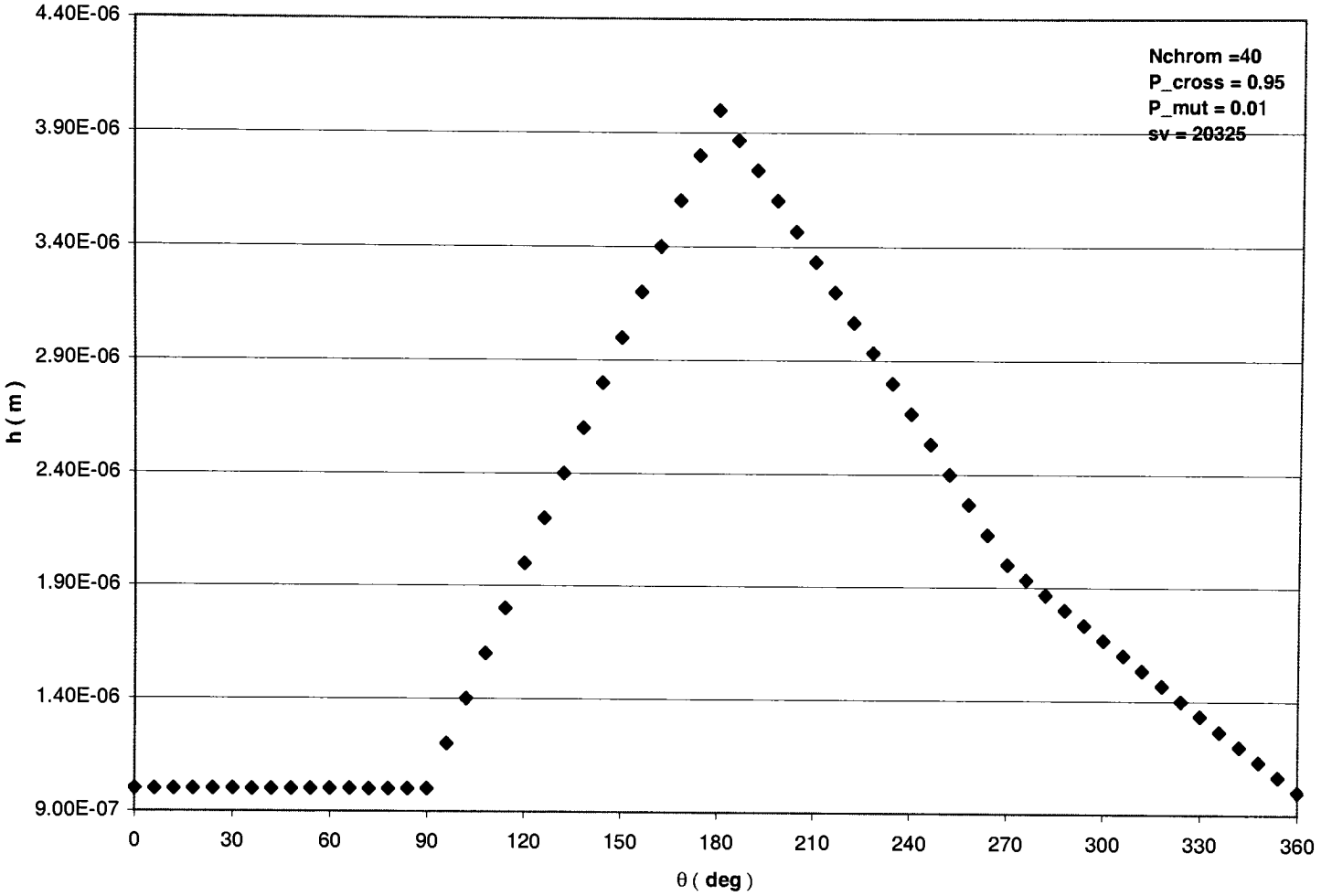

Figure 3.2.12, c. Film thickness distribution with third random set of chromosomes (sv=20325) after 1000 geenrations
Case # 1. N_chrom = 40

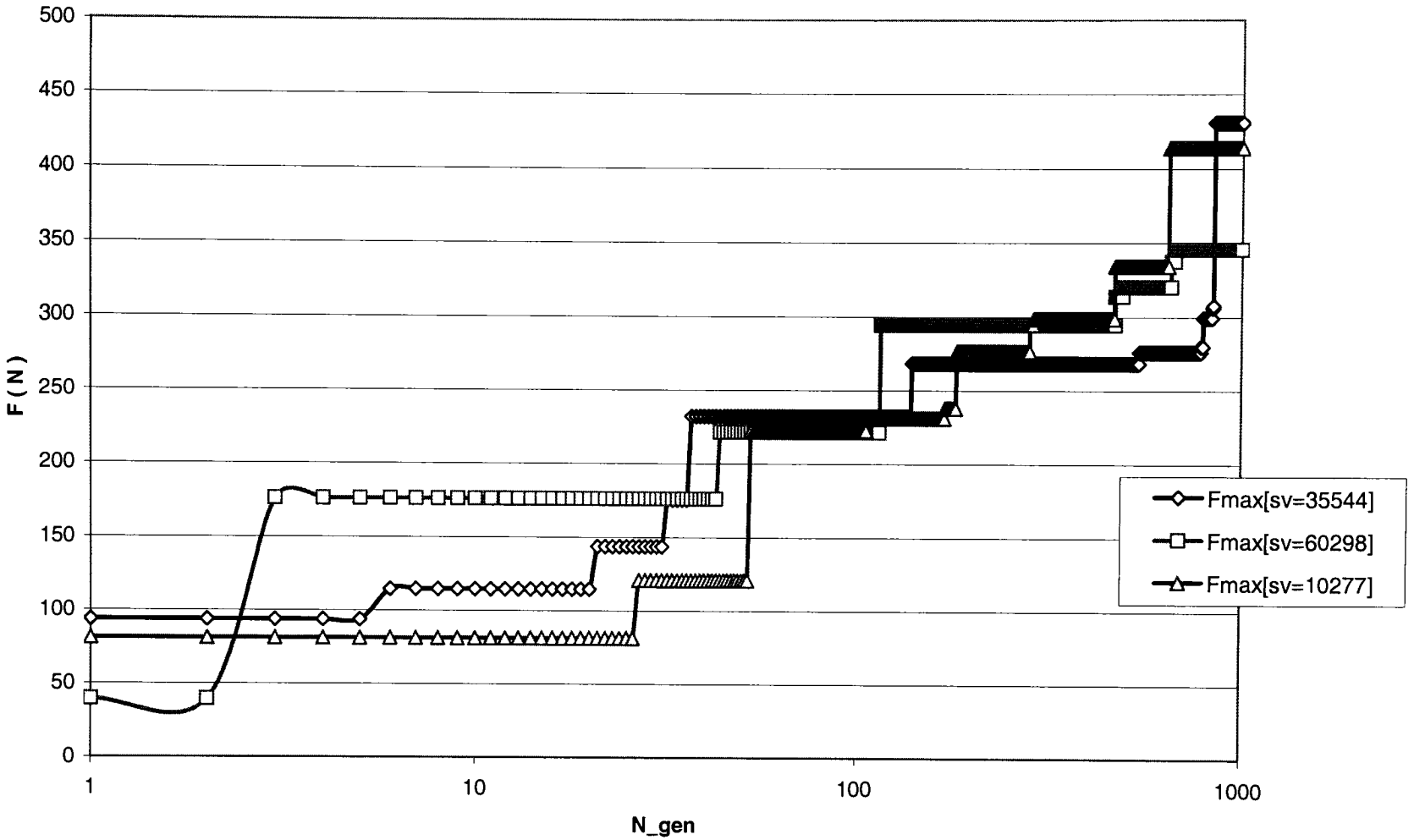

Figure 3.3.1. Bearing load evolutions for each of three randomly selected sets (D=10.0mm, N_chrom=10)
CASE # 2.

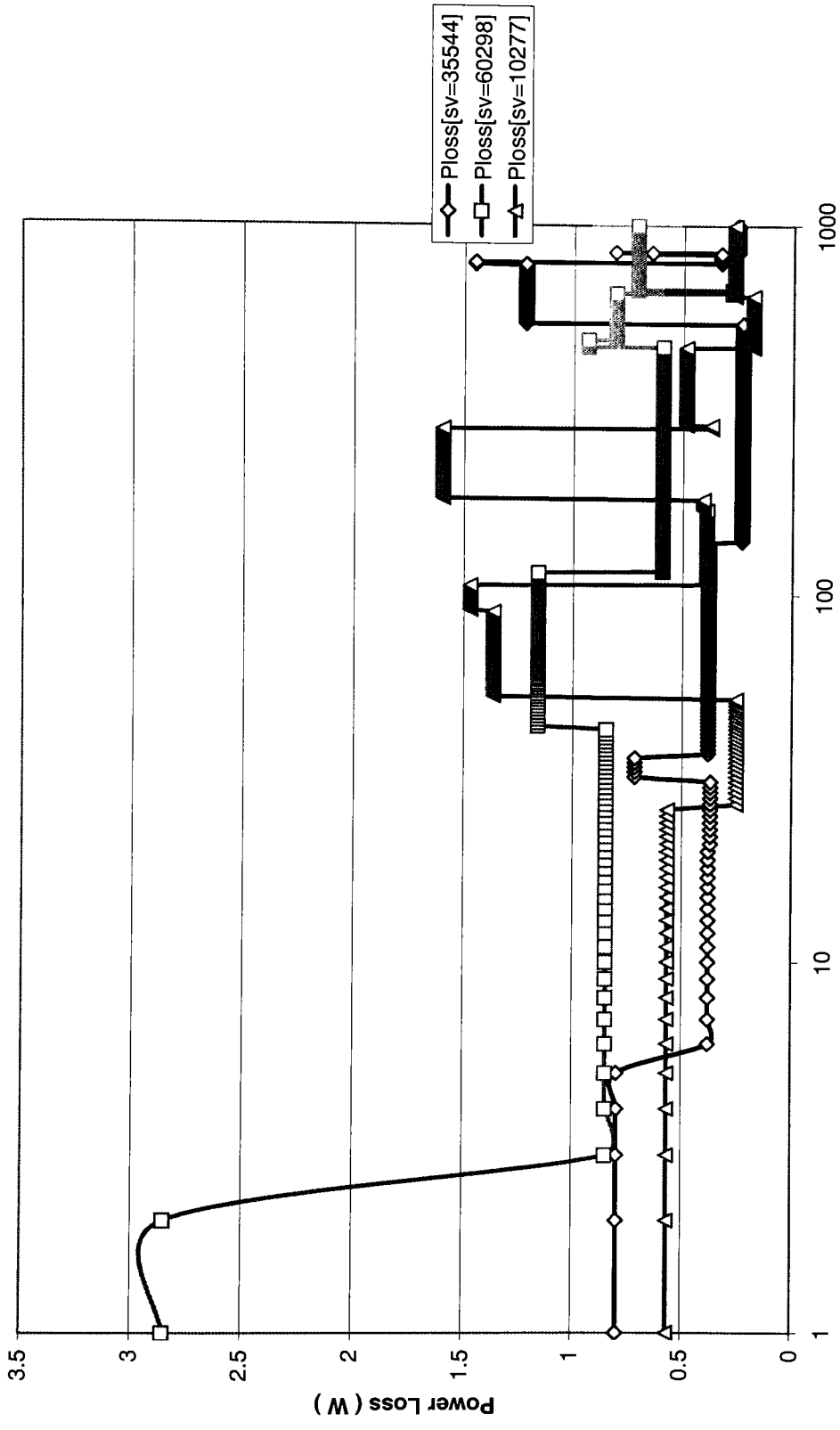

Figure 3.3.2. Plot of Power Loss with three randomly selected sets (D=10.0mm, N_chrom=10) CASE # 2.

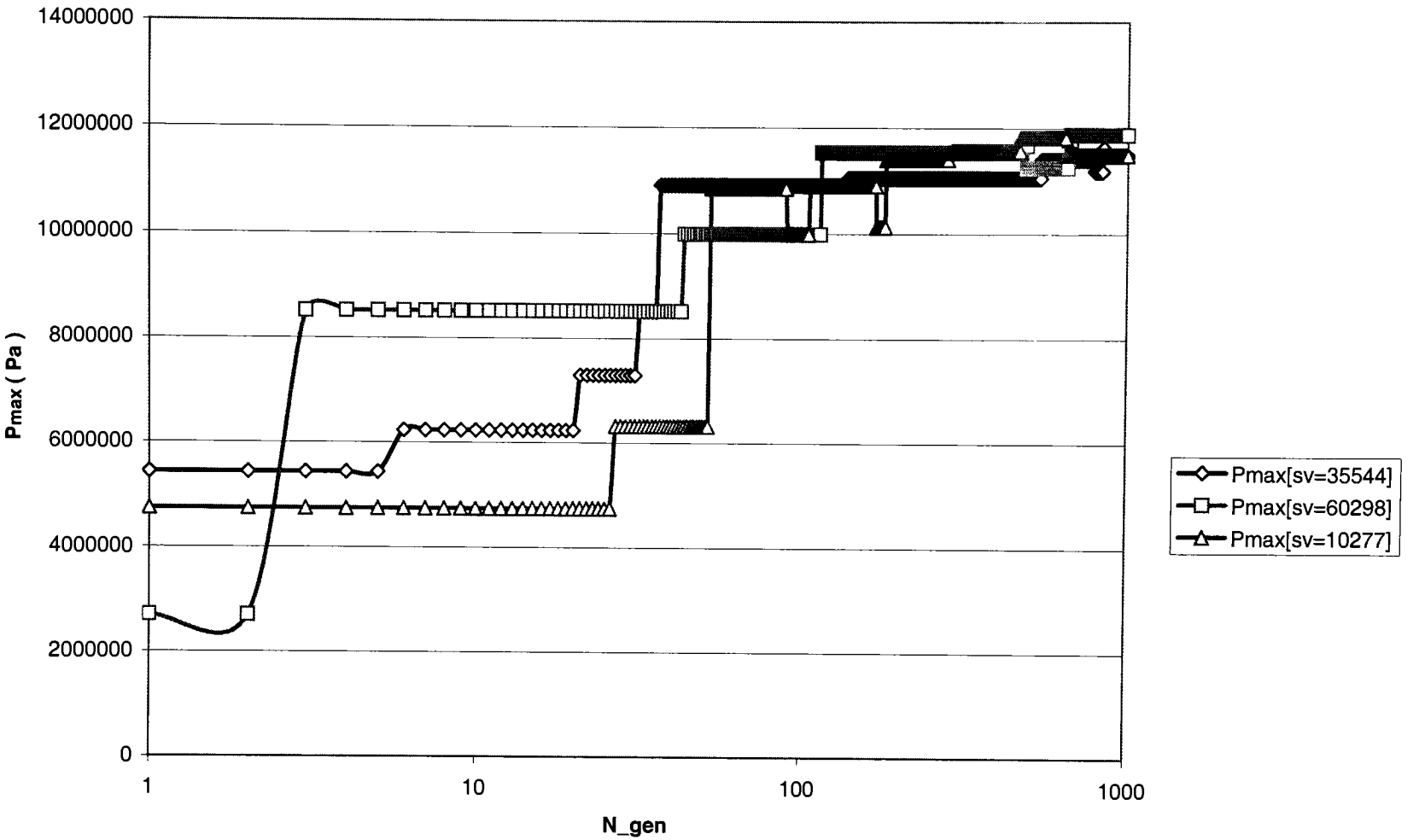

Figure 3.3.3. Plot of P_{max} with three randomly selected sets (D=10.0mm, N_chrom=10) CASE # 2.

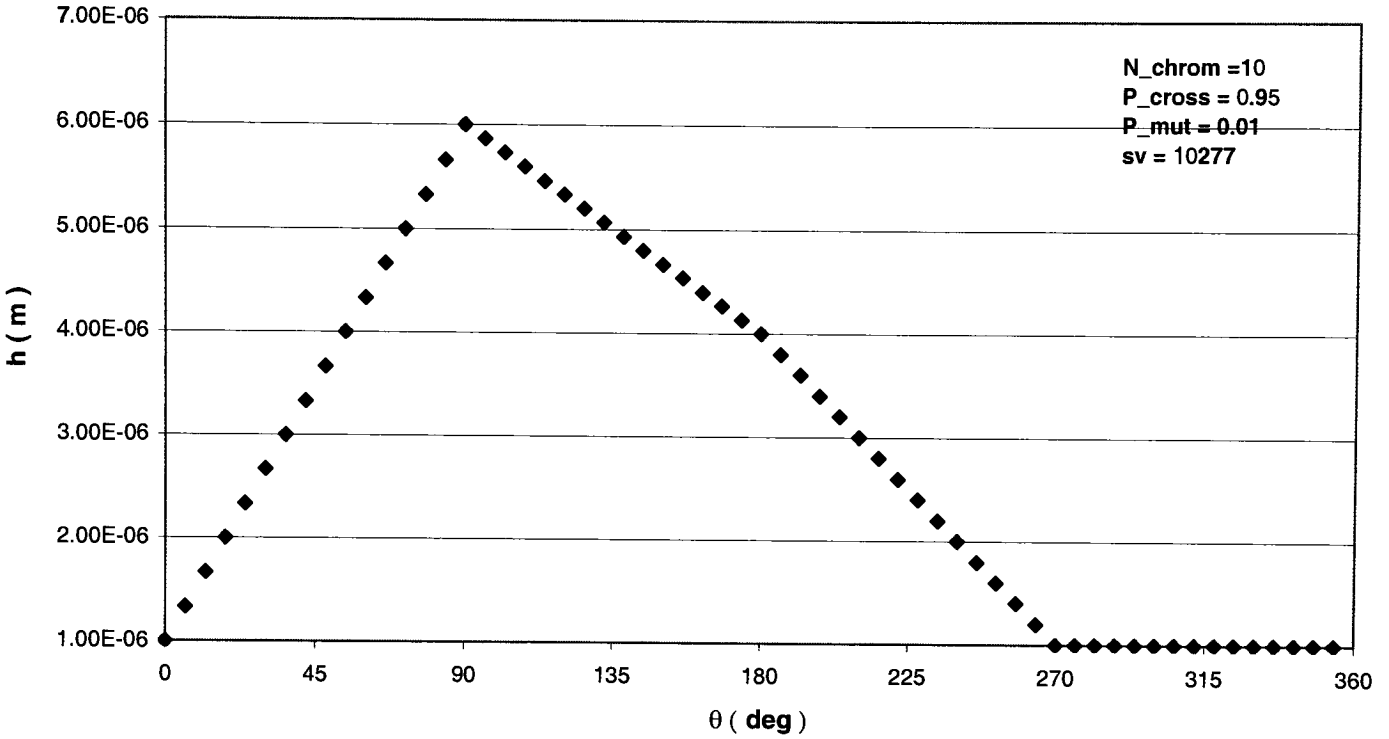

Figure 3.3.4, a. Film thickness distribution with third random set of chrmosomes (sv=10277) after 1000 generations
Case # 2. N_chrom=10

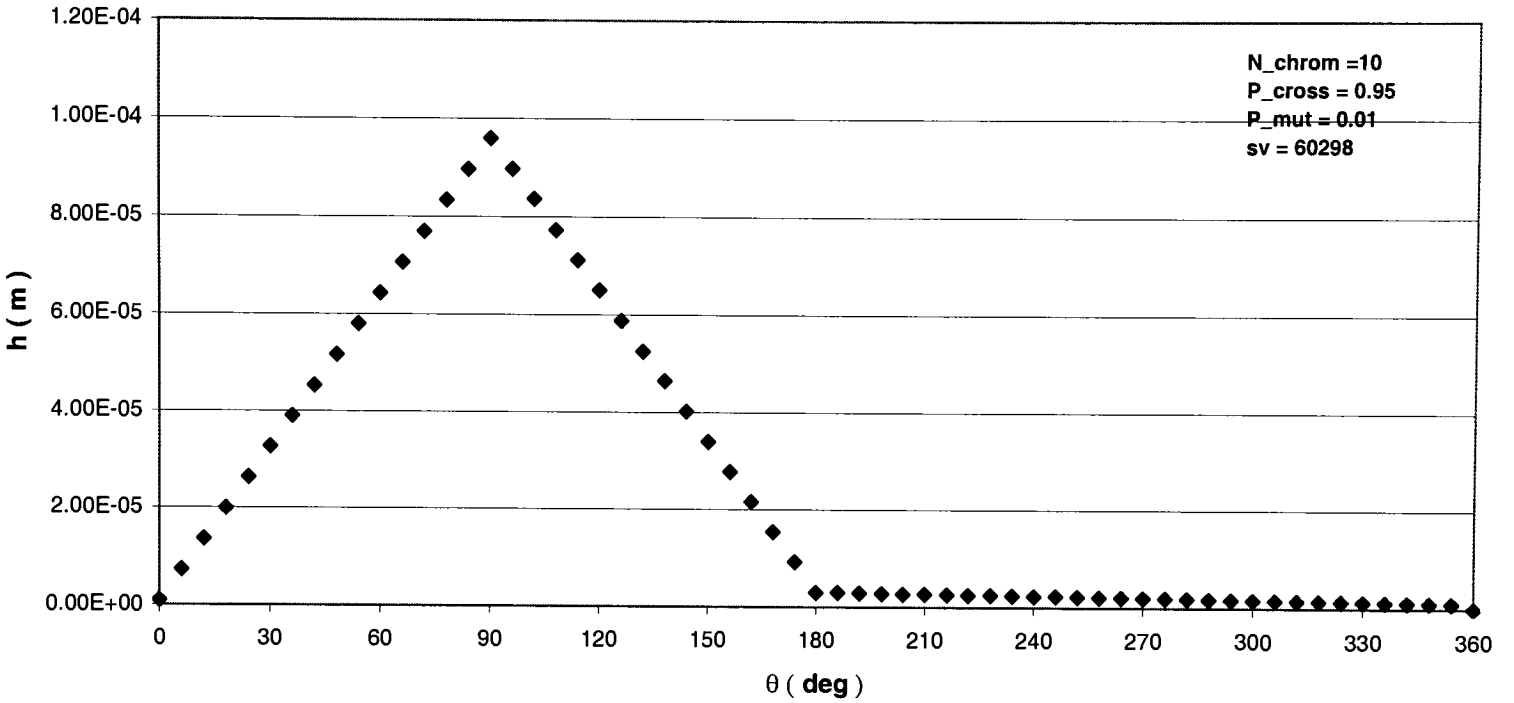

Figure 3.3.4, b. Film thickness distribution with second random set of chrmosomes (sv=60298) after 1000 generations
Case # 2. N_chrom=10

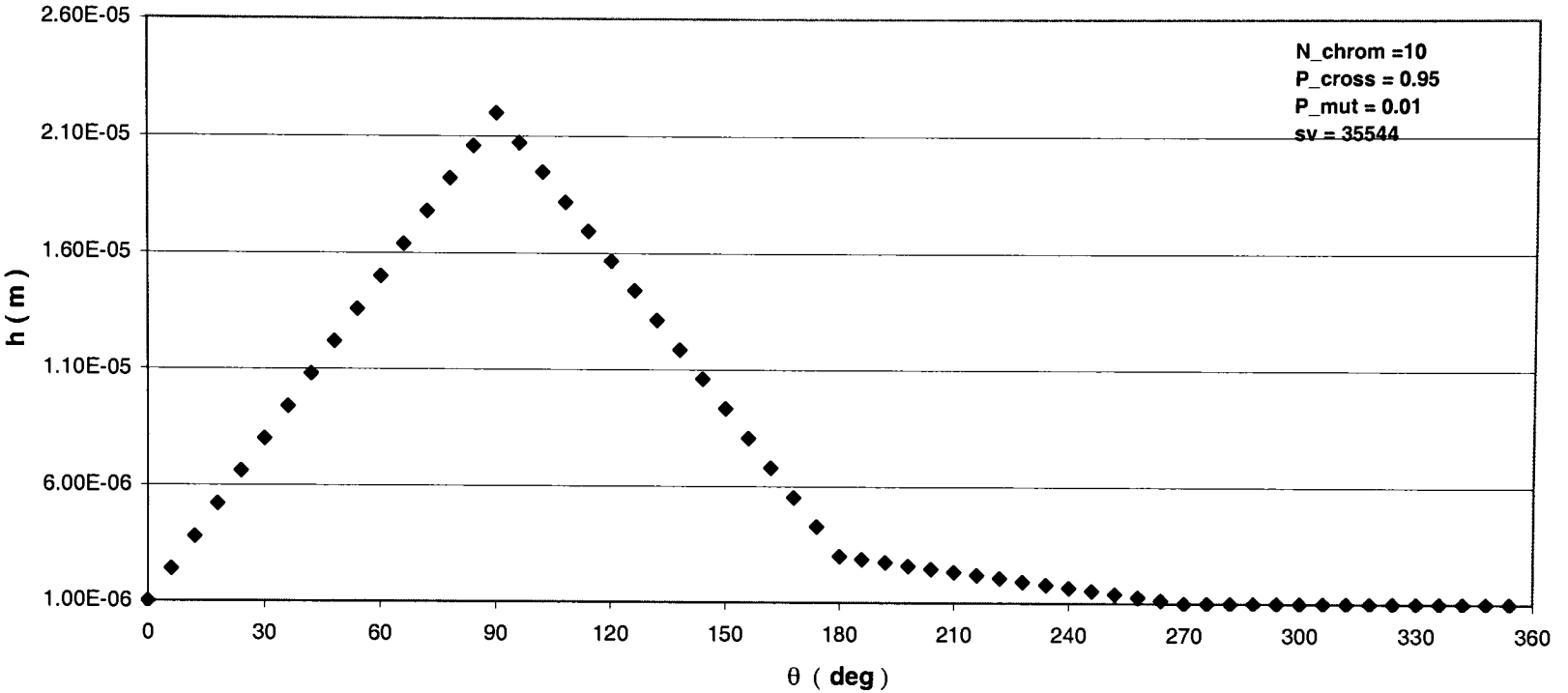

Figure 3.3.4, c. Film thickness distribution with first random set of chrmosomes (sv=35544) after 1000 generations
Case # 2. N_chrom=10

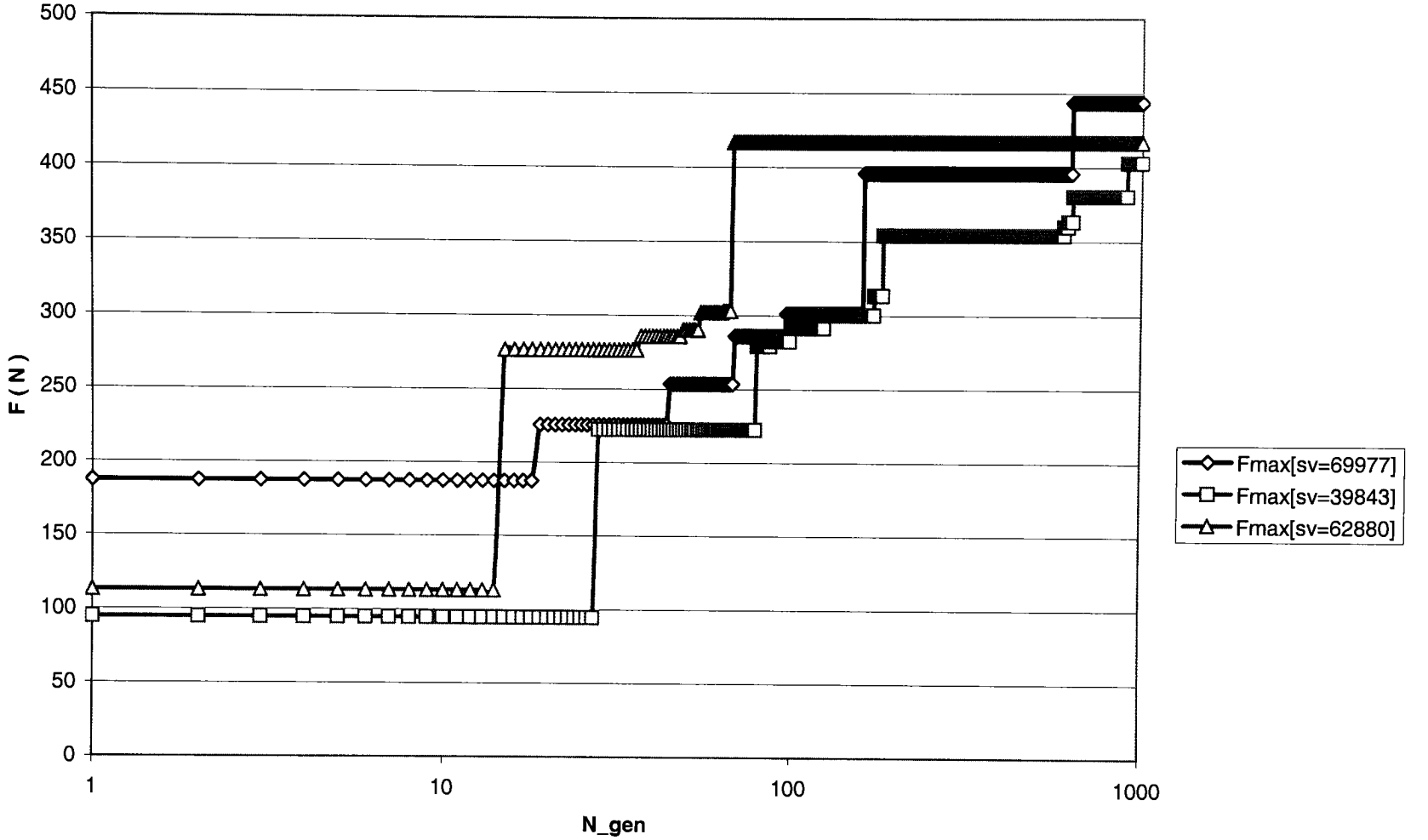

Figure 3.3.5. Bearing load evolutions for each of three randomly selected sets (D=10.0mm, Nchrom=20)
CASE # 2.

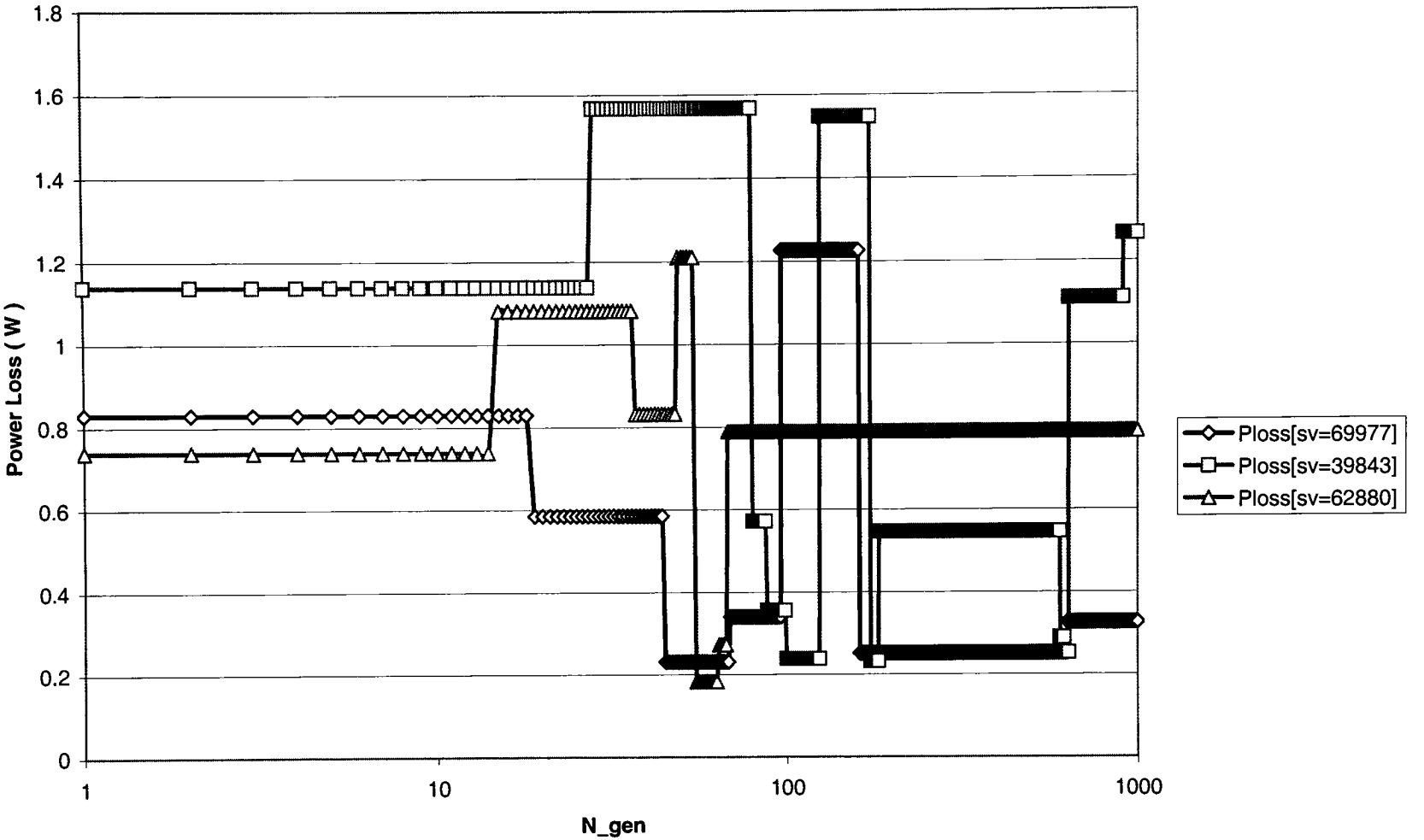

Figure 3.3.6. Plot of Power Loss with three randomly selected sets (D=10.0mm, Nchrom=20) CASE # 2.

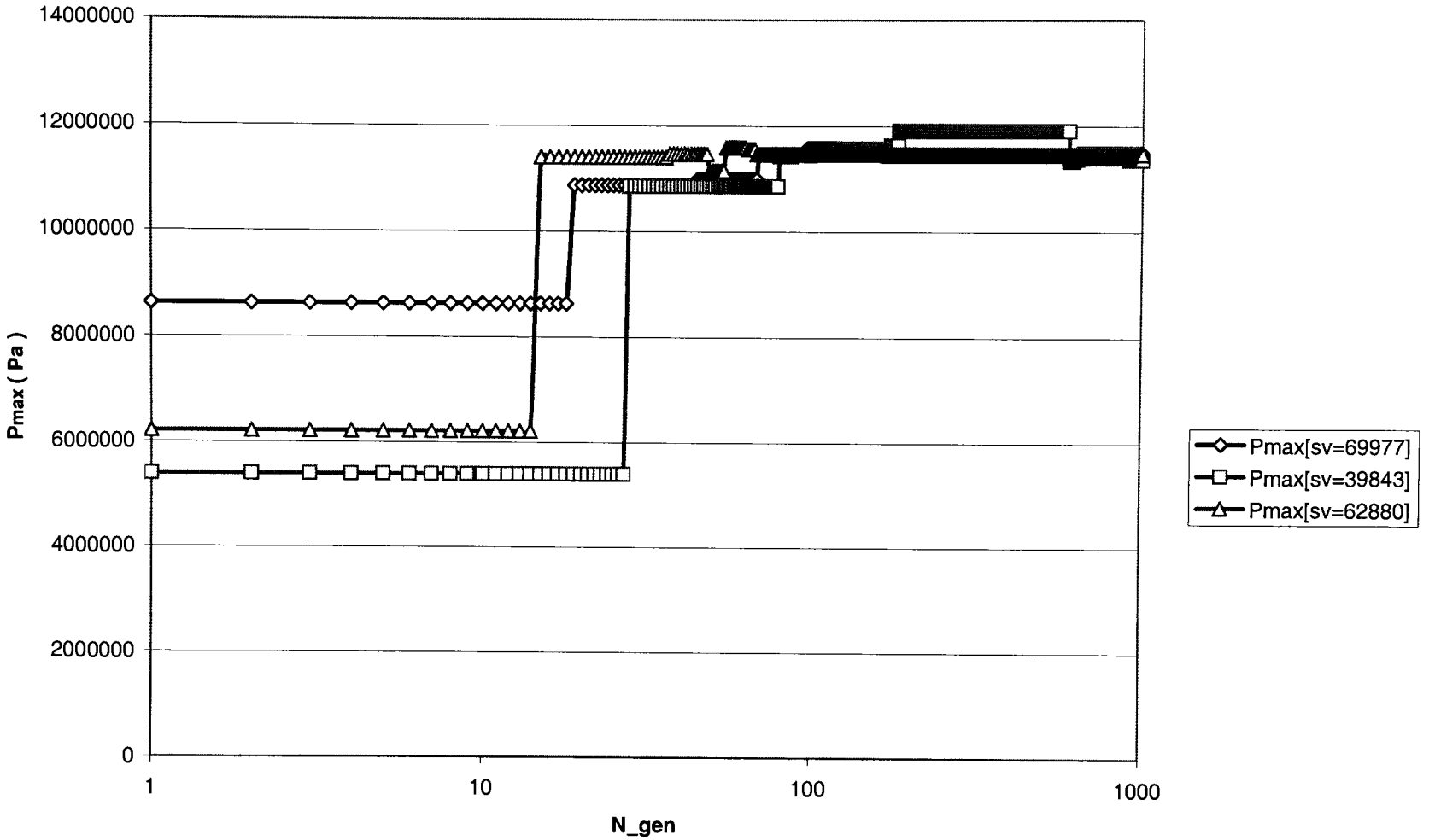

Figure 3.3.7. Plot of P_{max} wih three randomly selected sets (D=10.0mm, Nchrom=20) CASE # 2.

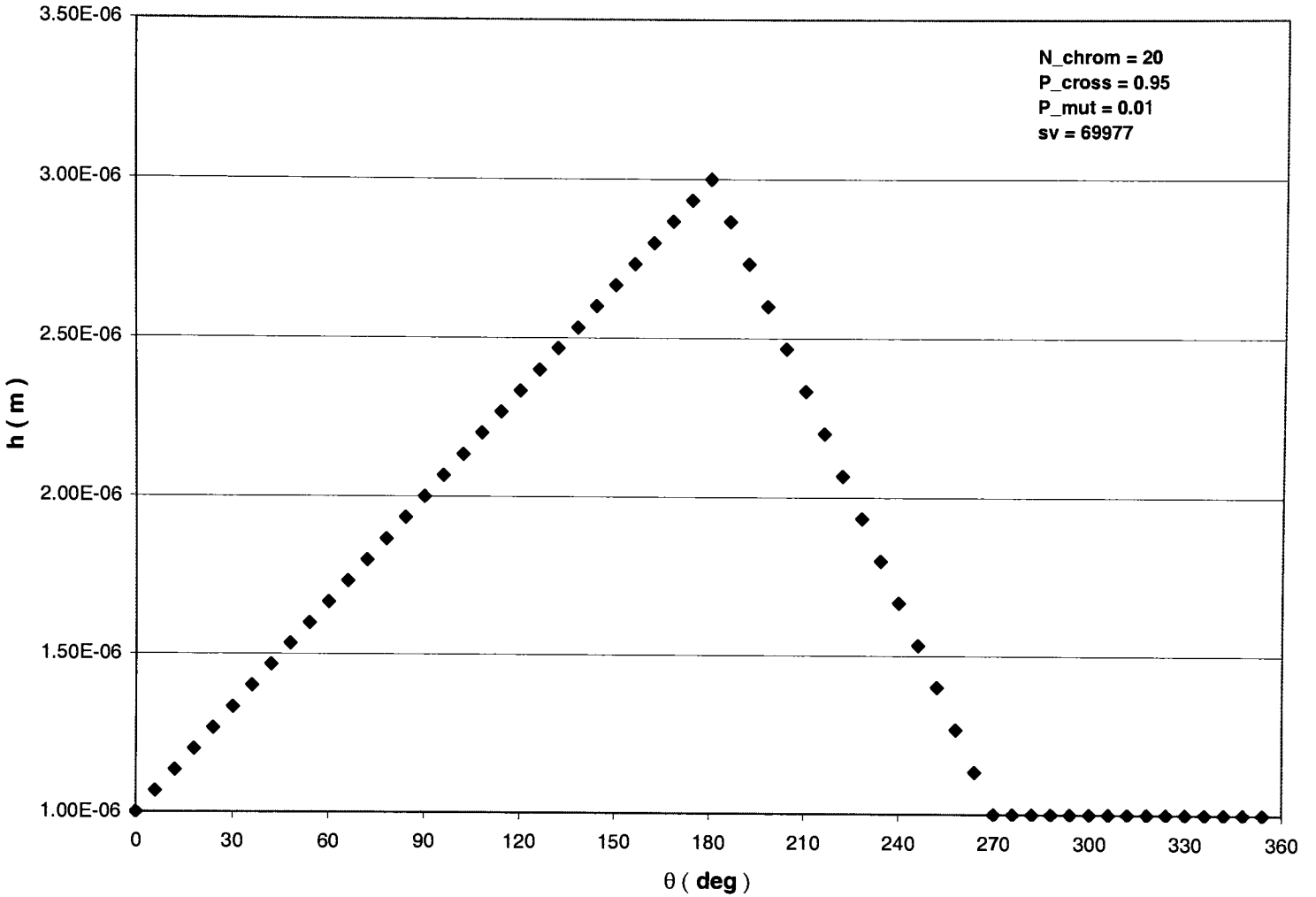

Figure 3.3.8, a. Film thickness distribution with first random set of chromosomes (sv = 69977)after 1000 generations
Case # 2. N_chrom = 20

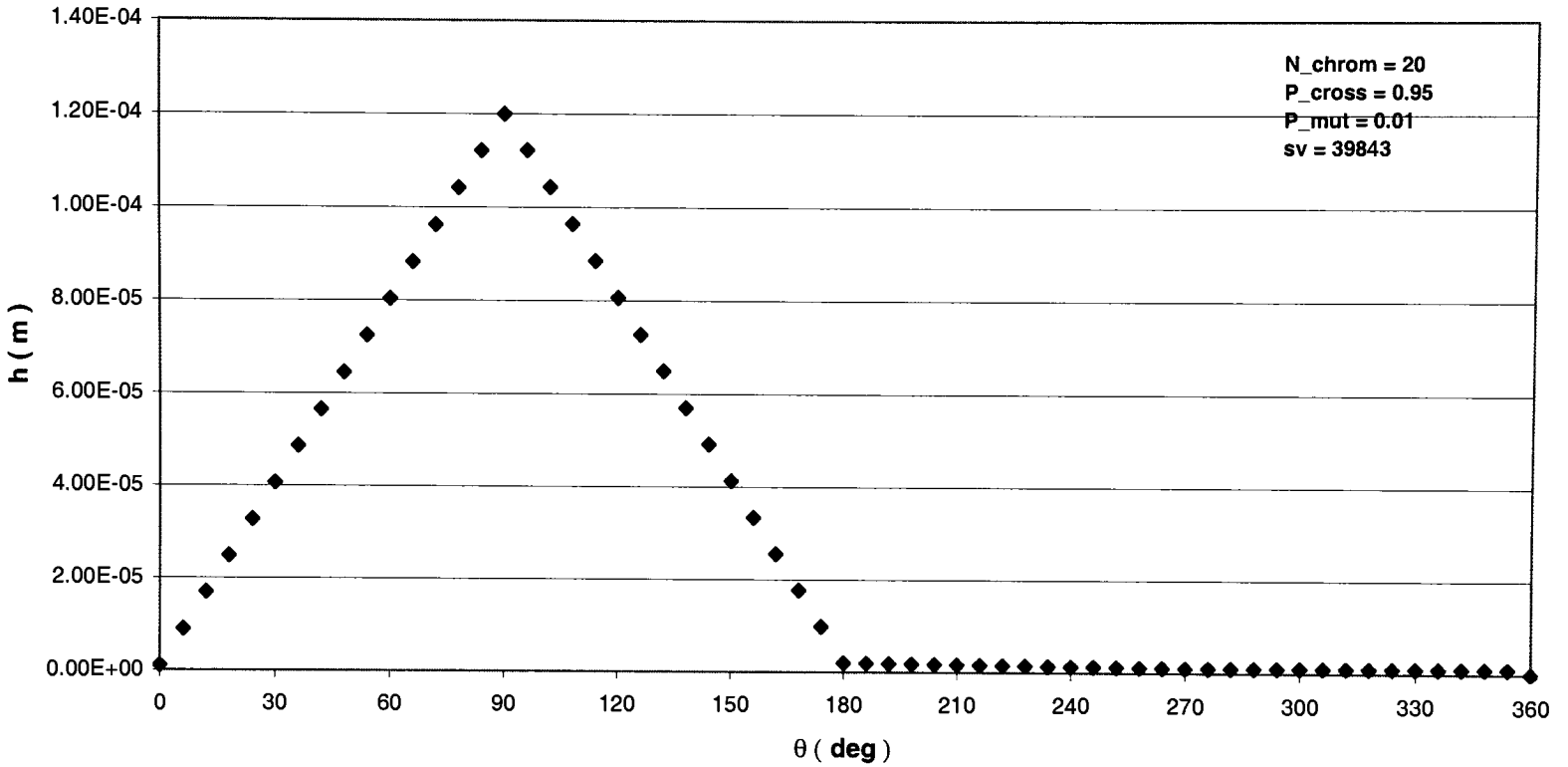

Figure 3.3.8, b. Film thickness distribution with first random set of chromosomes (sv = 39843)after 1000 generations
Case # 2. N_chrom = 20

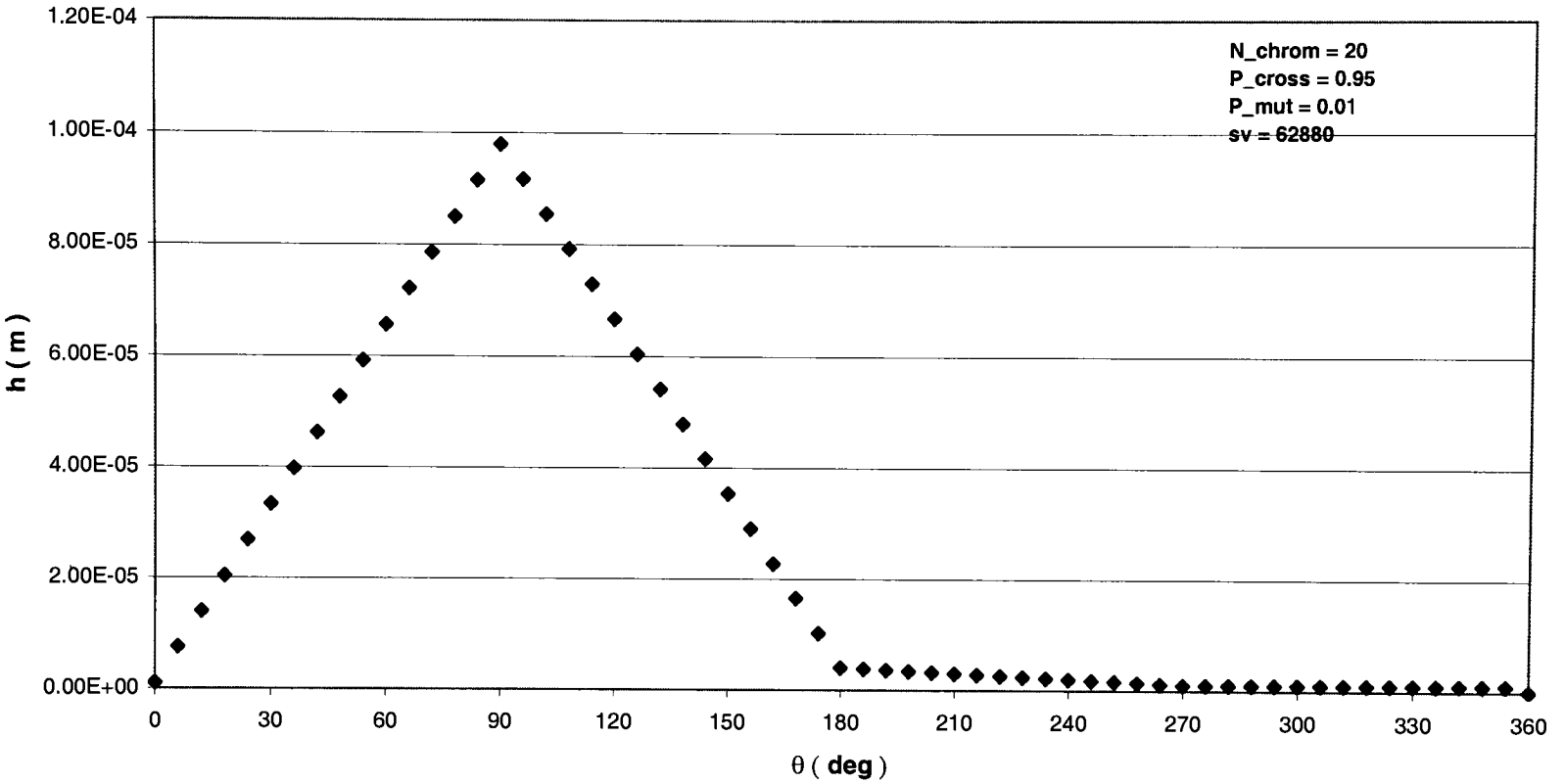

Figure 3.3.8, c. Film thickness distribution with first random set of chromosomes (sv = 62880) after 1000 generations
Case # 2. N_chrom = 20

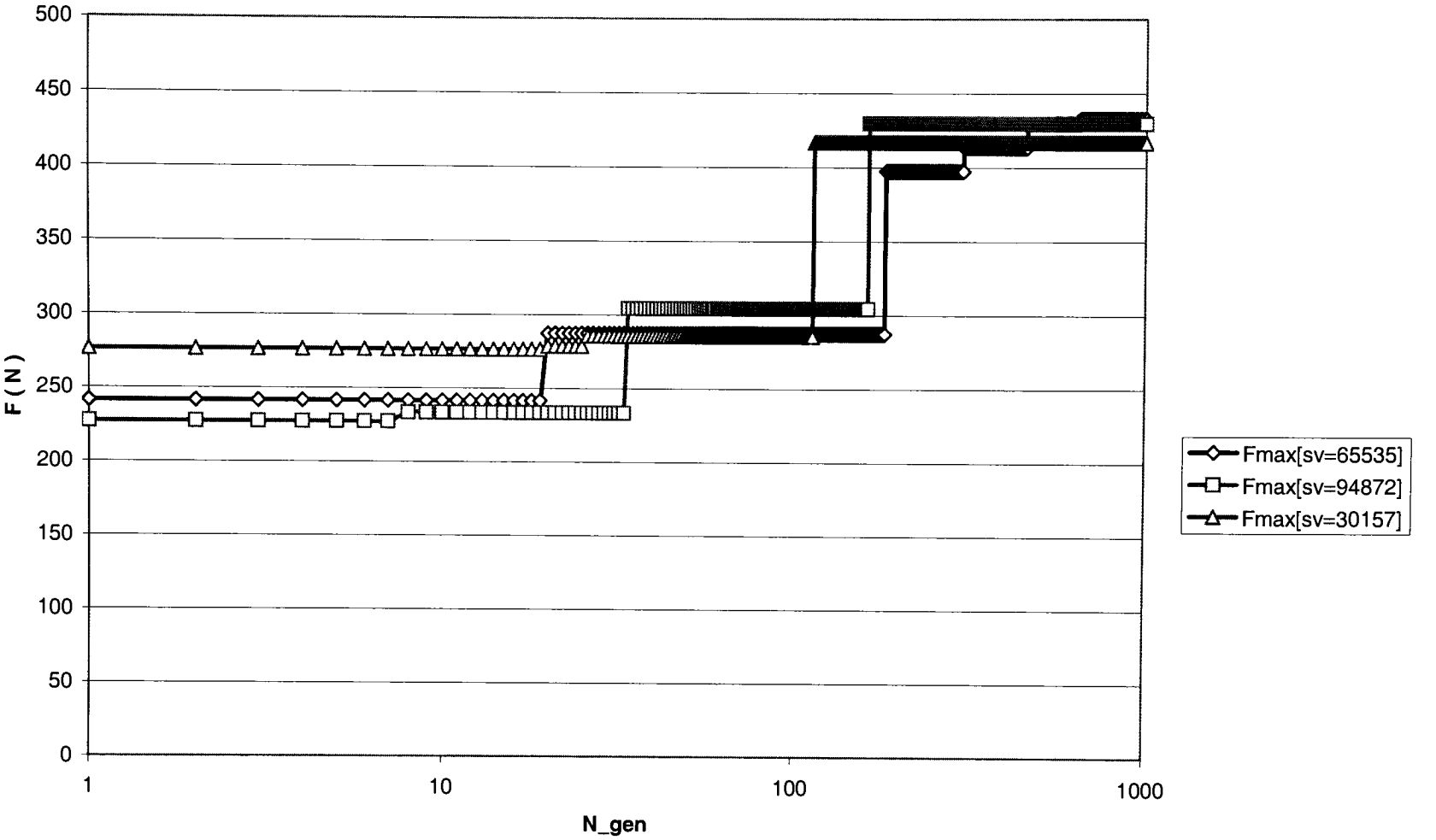

Figure 3.3.9. Bearing load evolutions for each of three randomly selected sets (D=10.0mm, N_chrom=40)
C A S E # 2.

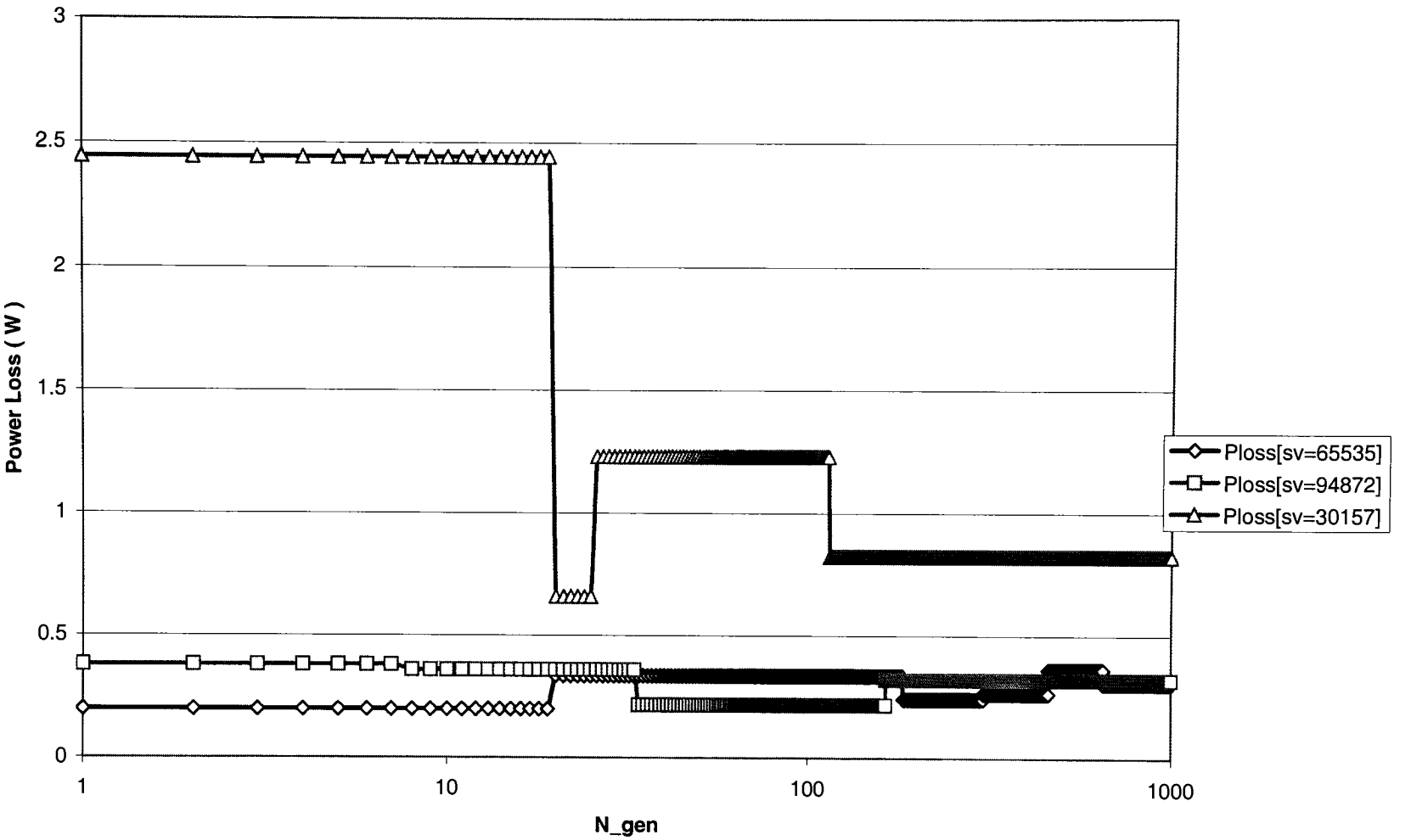

Figure 3.3.10. Plot of Power Loss with three randomly selected sets (D=10.0mm, N_chrom=40)
C A S E # 2.

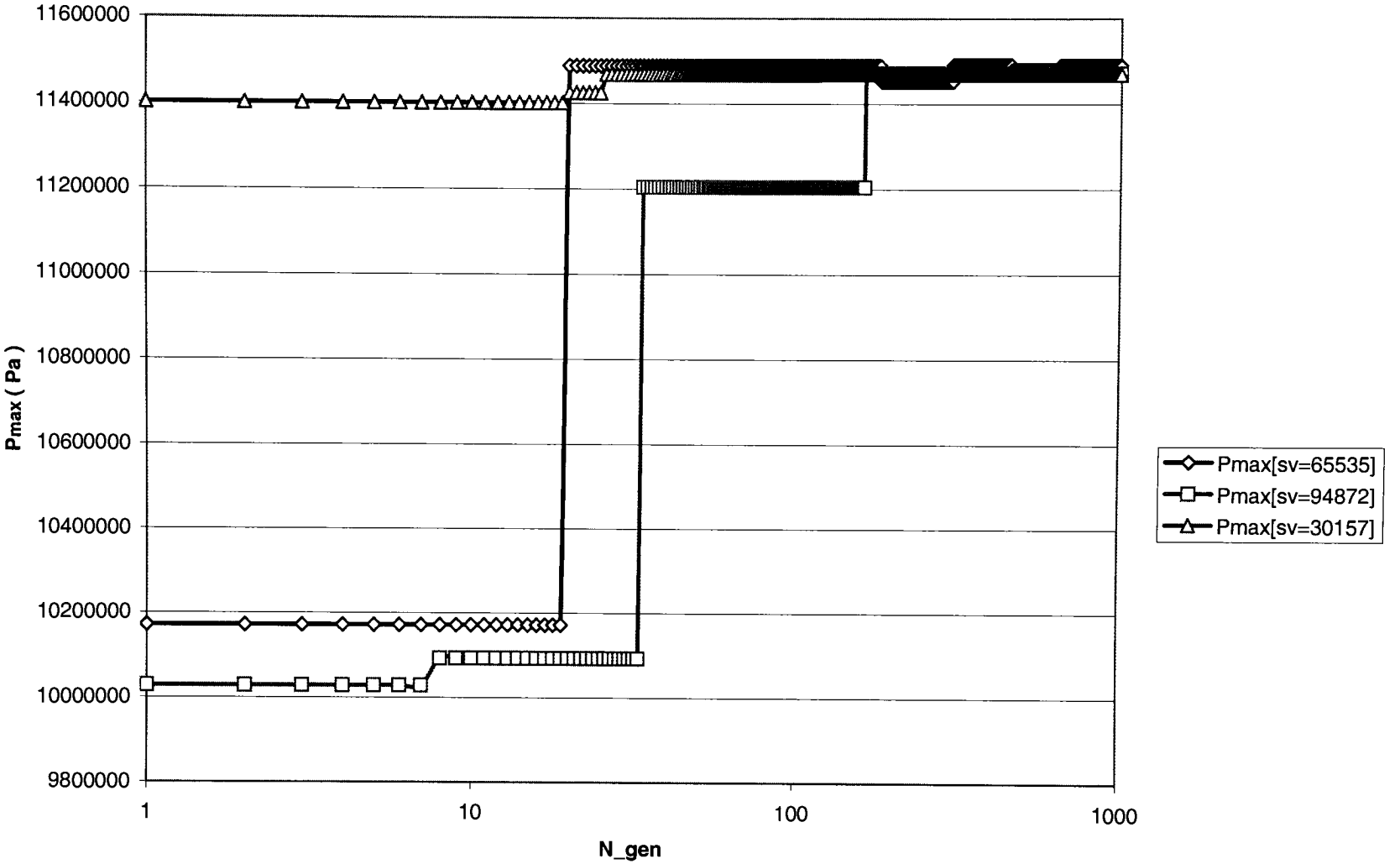

Figure 3.3.11. Plot of P_{max} with three randomly selected sets (D=10.0mm, N_chrom=40)
C A S E # 2.

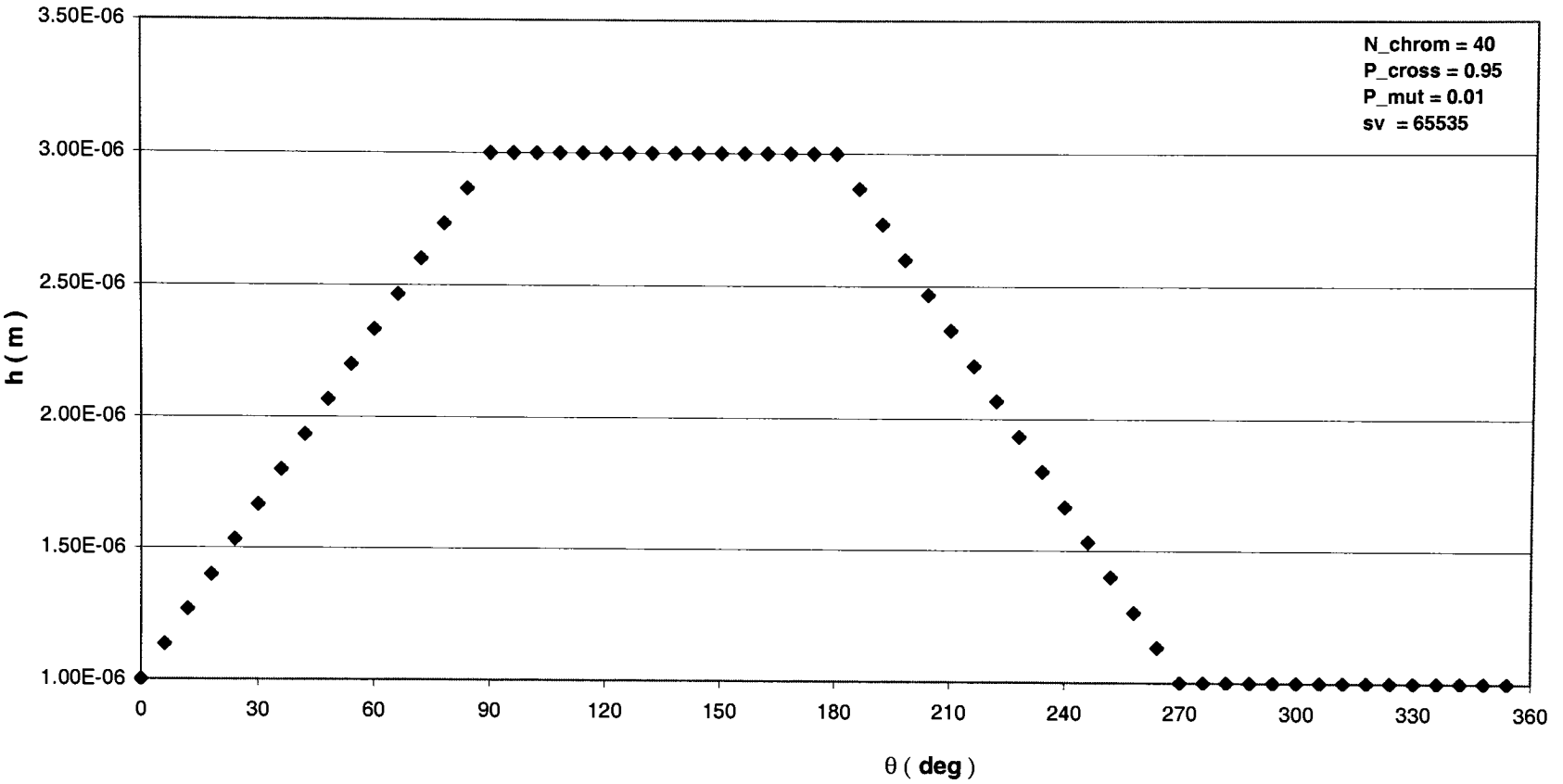

Figure 3.3.12, a. Film thickness distribution with first random set of chromosomes (sv=65535) after 1000 generations
Case # 2. N_chrom=40

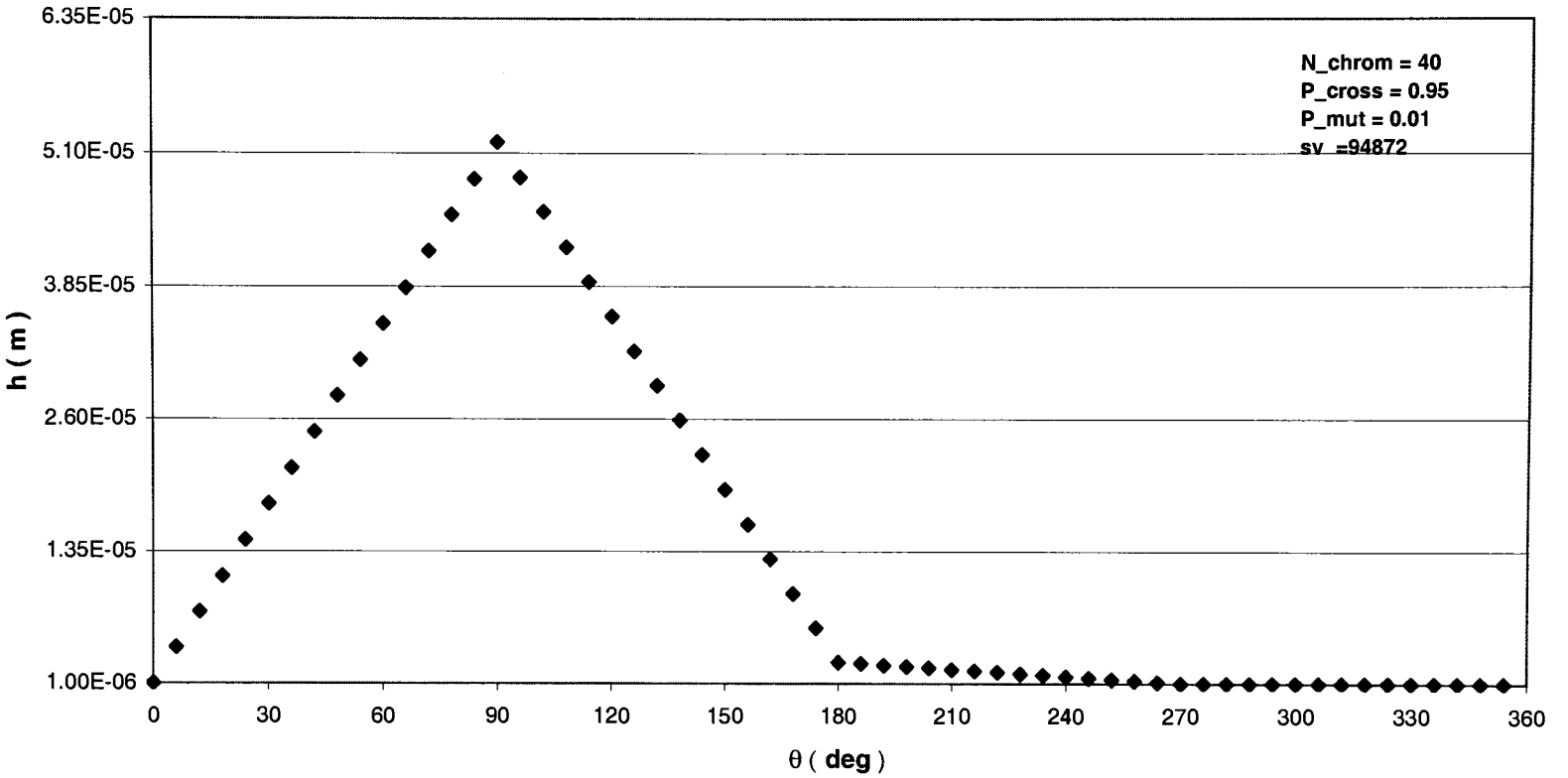

Figure 3.3.12, b. Film thickness distribution with second random set of chromosomes (sv=94872) after 1000 generations
Case # 2. N_chrom=40

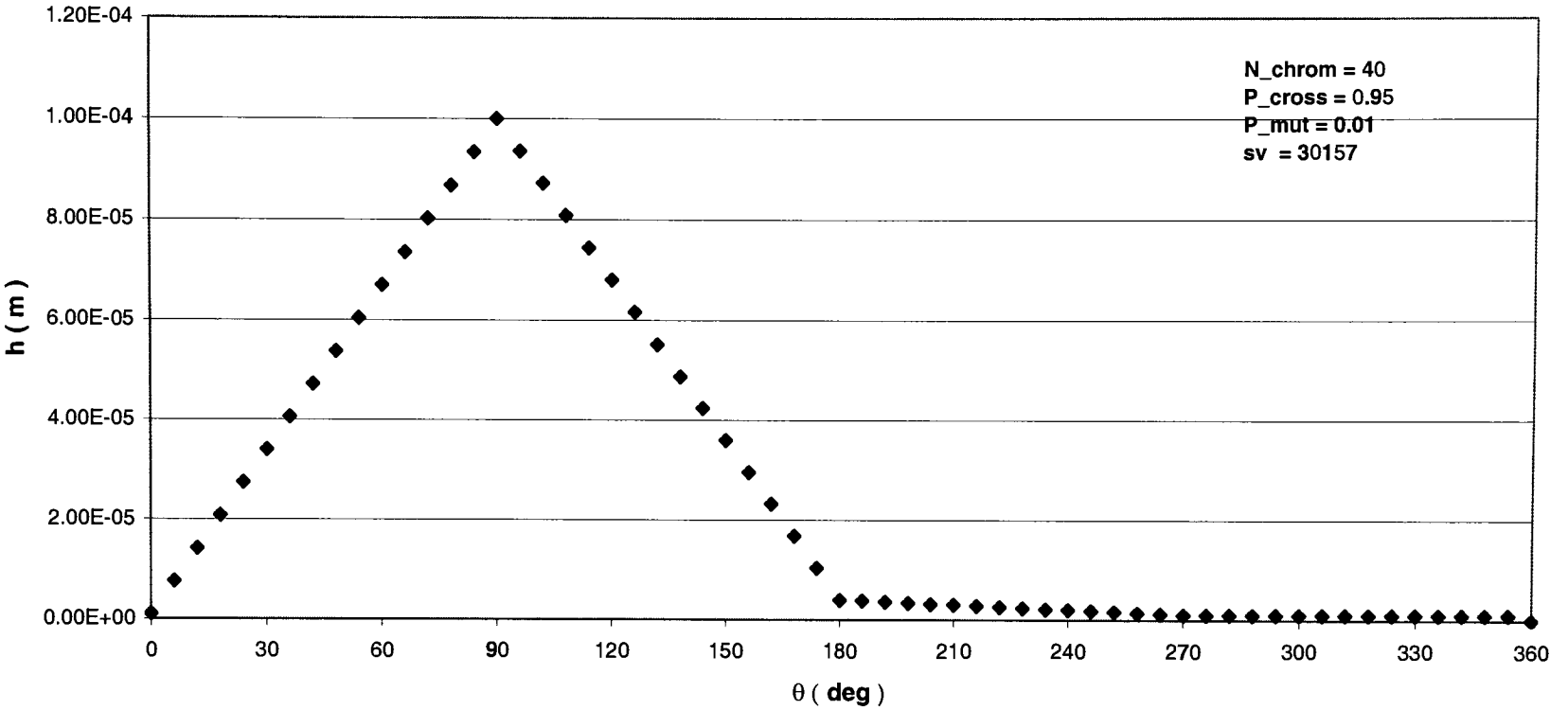

Figure 3.3.12, c. Film thickness distribution with third random set of chromosomes (sv = 30157) after 1000 generations
Case # 2. N_chrom =40

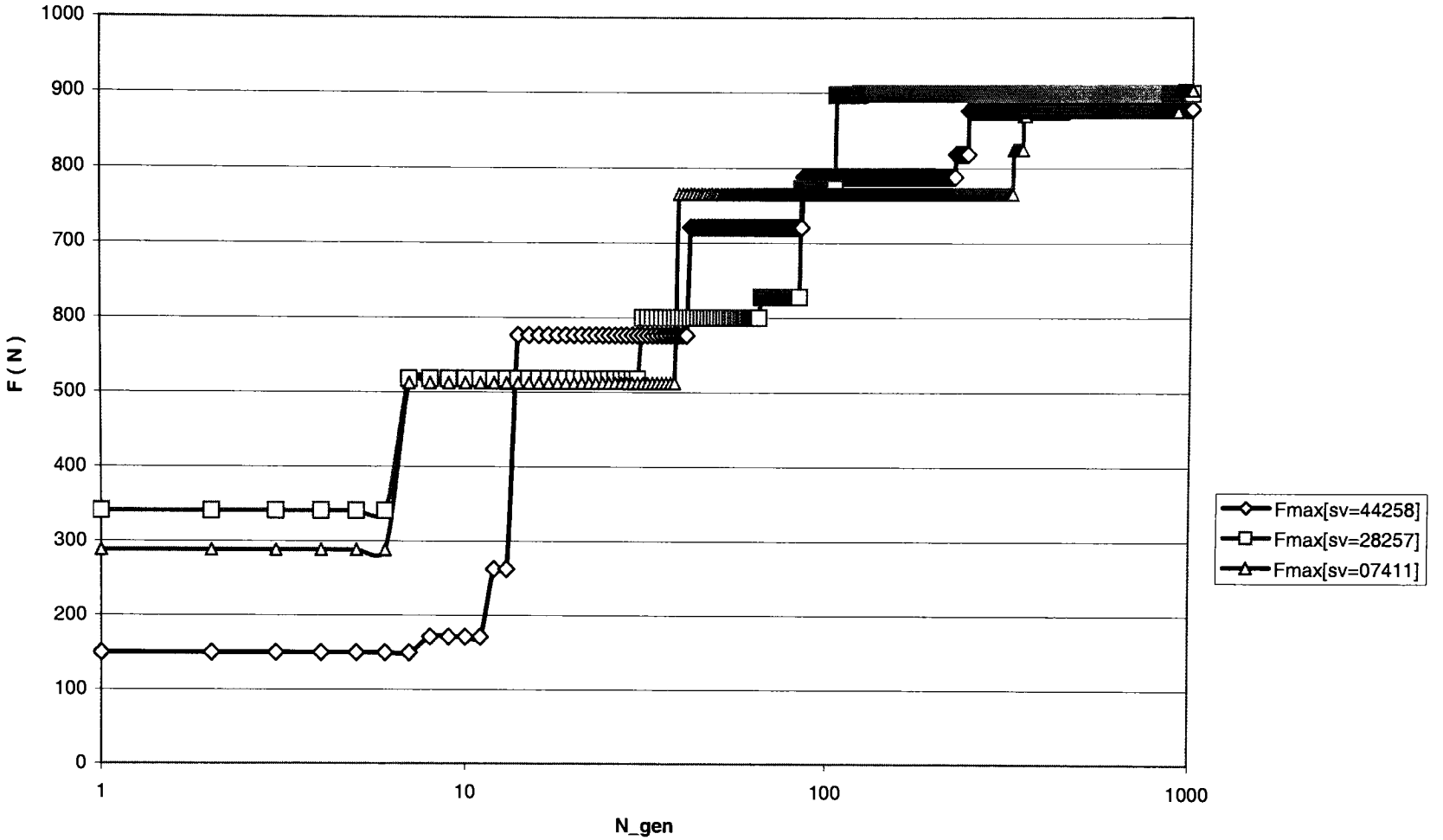

Figure 3.4.1. Bearing load evolutions for each of three randomly selected sets (D=20.omm, N_chrom=20) CASE # 3.

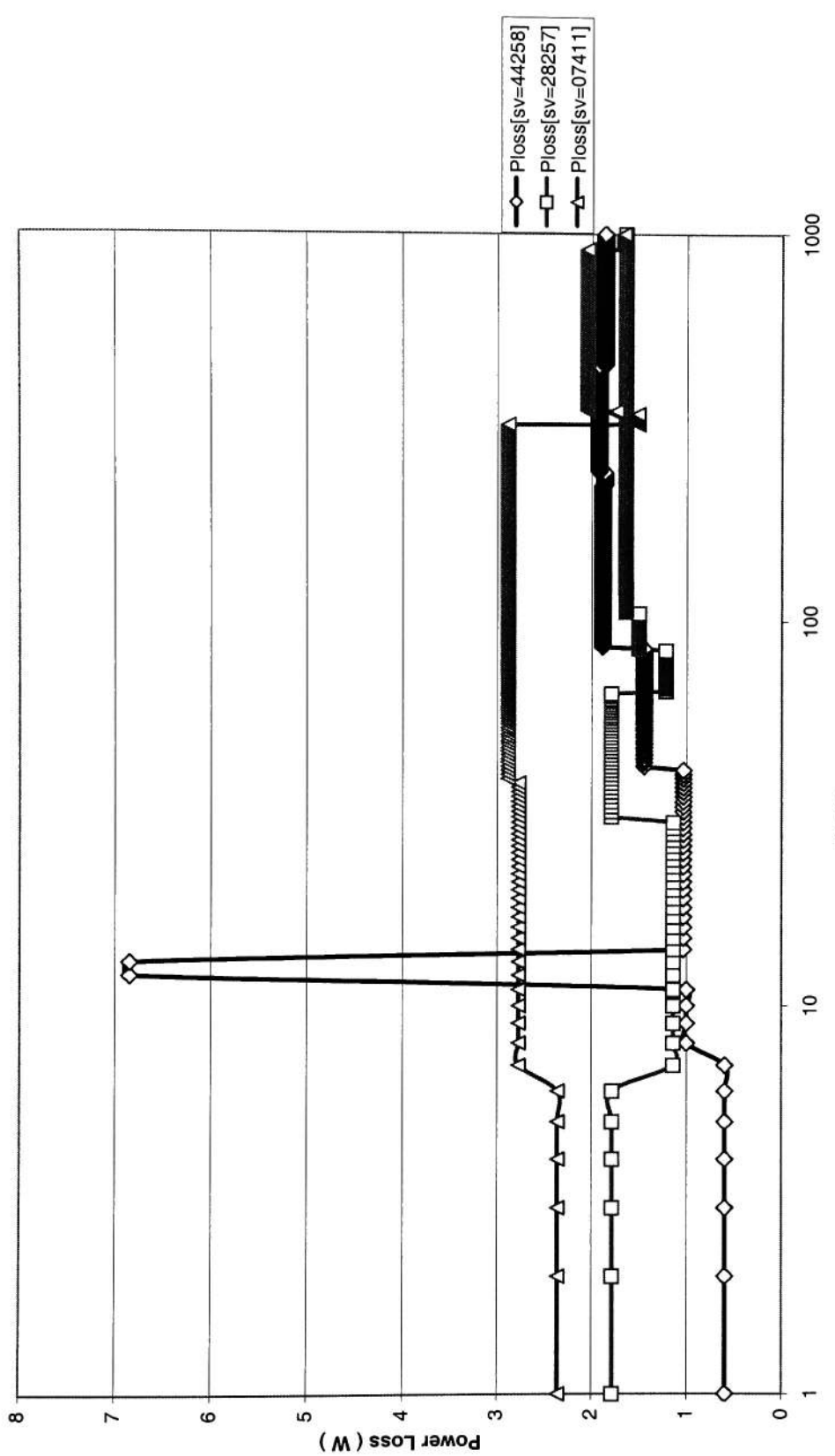

Figure 3.4.3. Plot of Power Loss with three randomly selected sets (D=20.0mm, N_chrom=20)
CASE # 3.

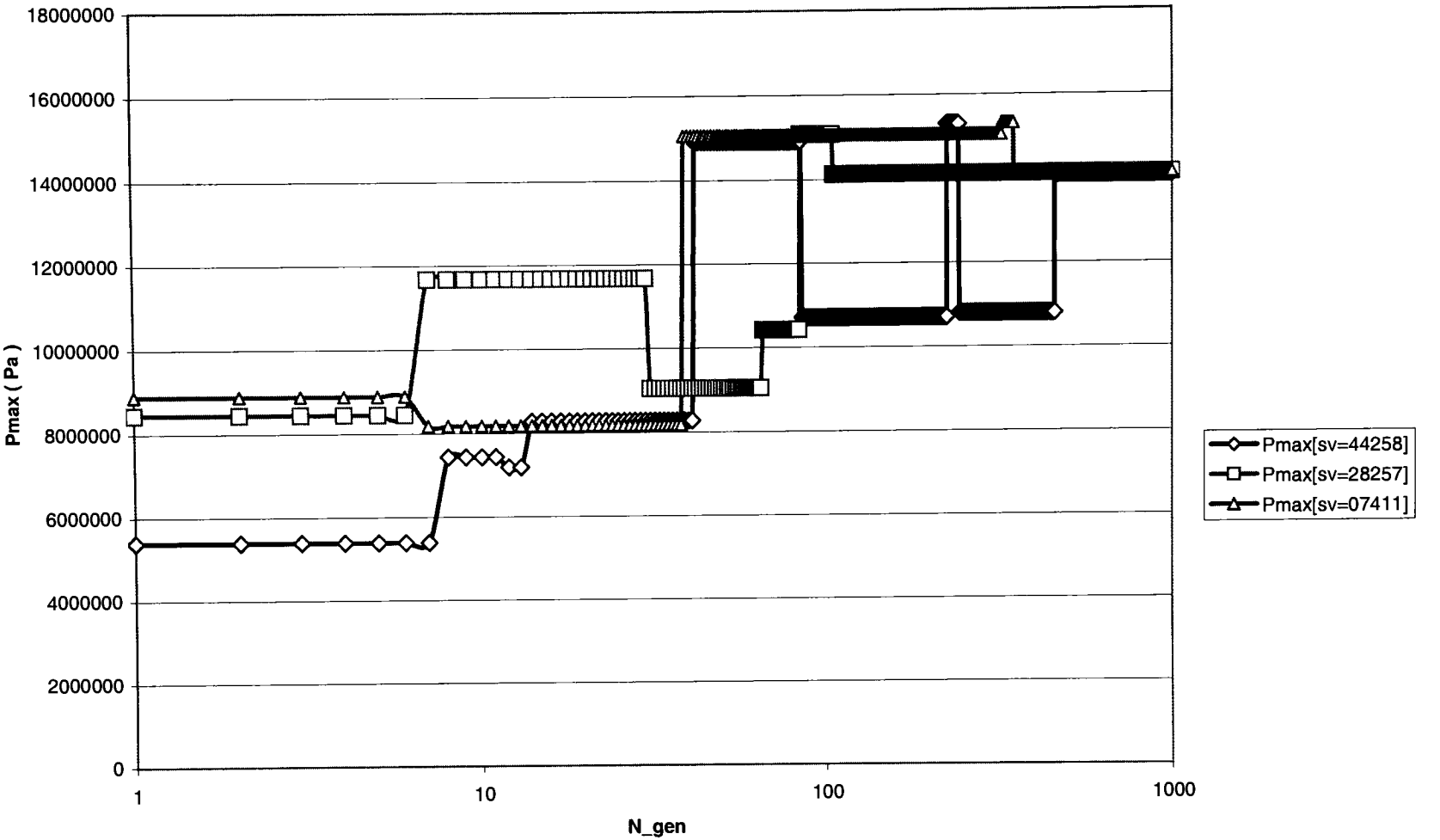

Figure 3.4.2. Plot of Pmax with three randomly selected sets (D=20.0mm, N_chrom=20) CASE # 3.

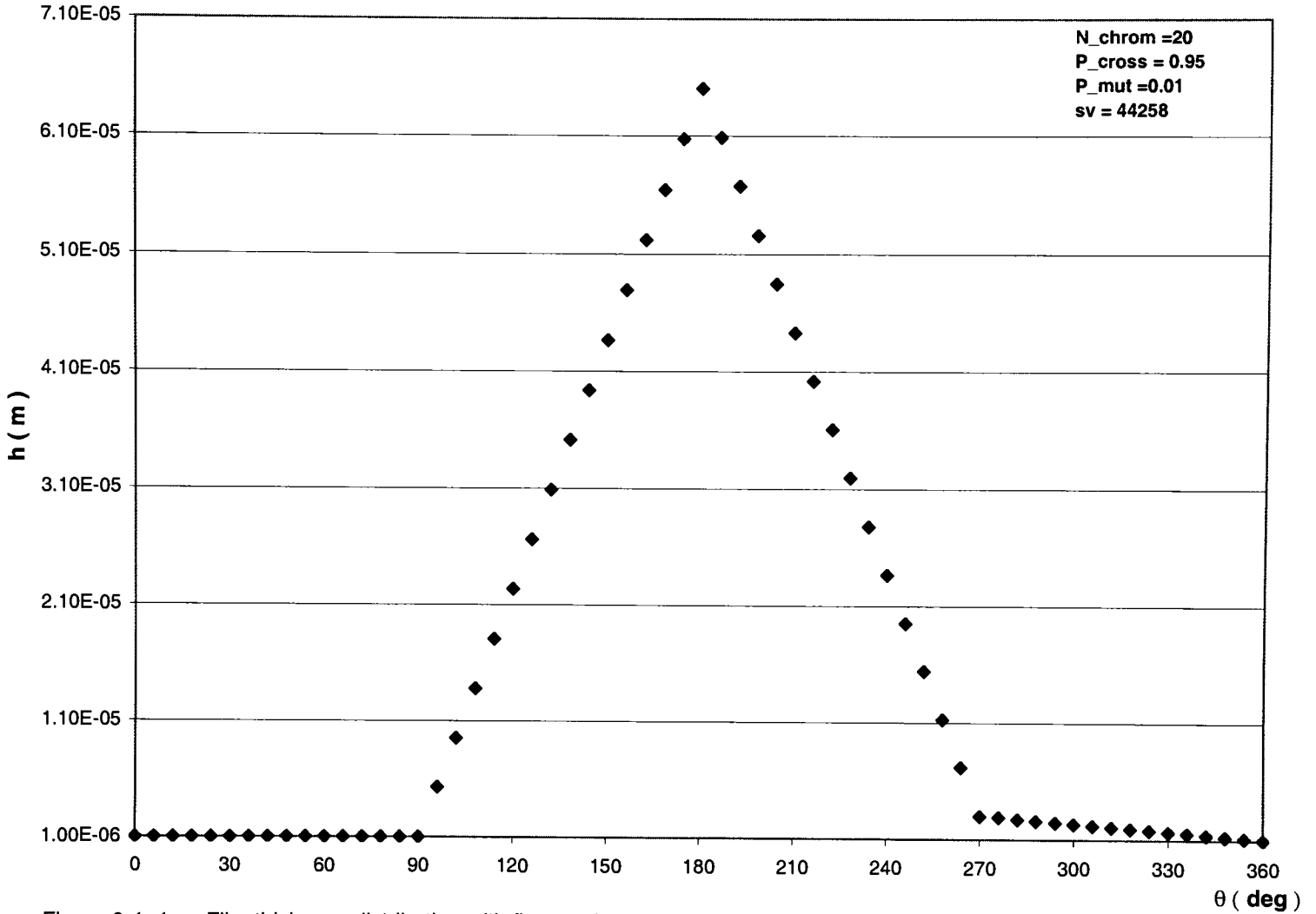

Figure 3.4. 4, a. Film thickness distribution with first random set of chromosomes (sv = 44258) after 1000 generations
Case # 3. N_chrom = 20

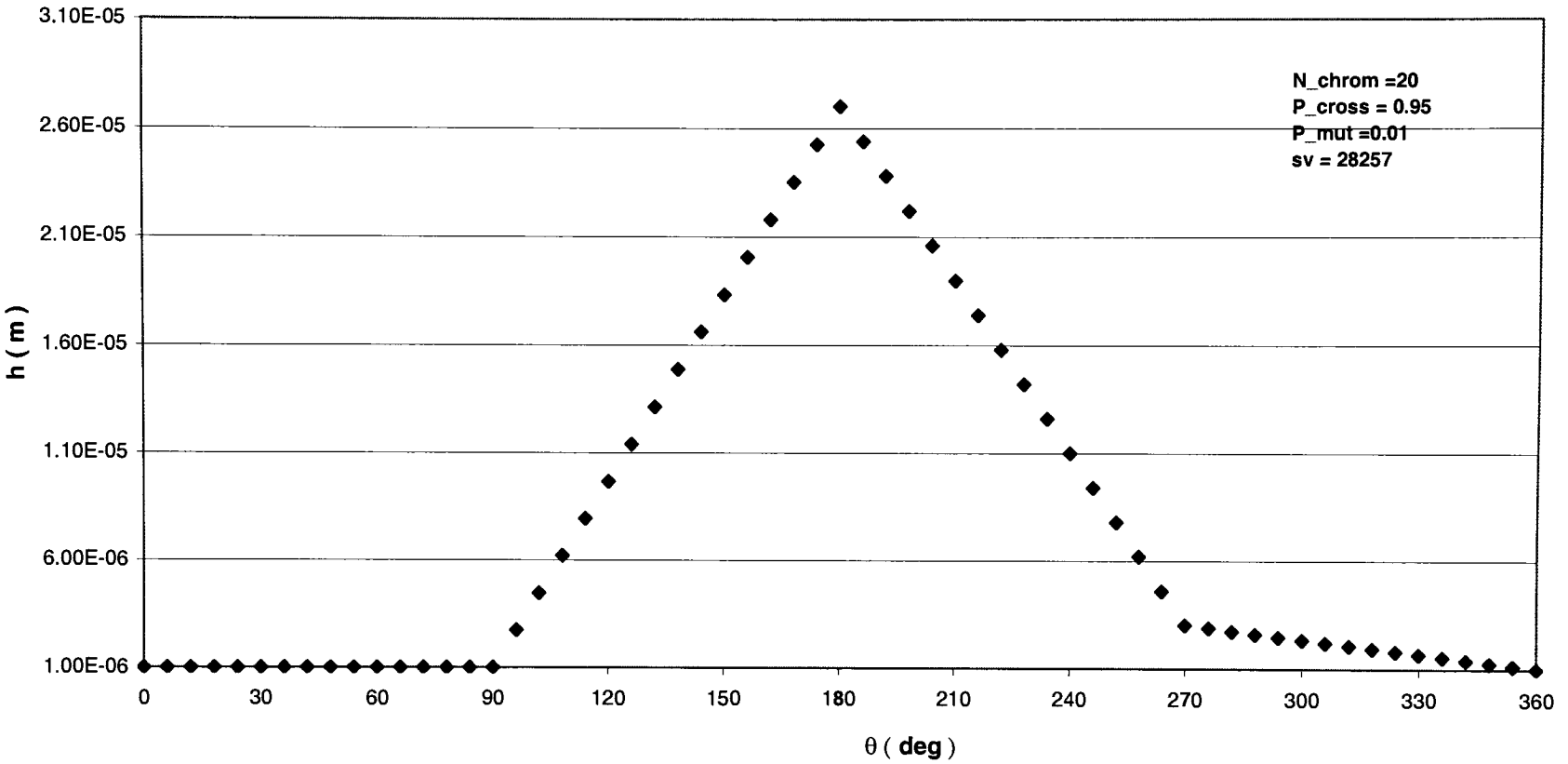

Figure 3.4.4, b. Film thickness distribution with second random set of chromosomes (sv = 28257) after 1000 generations
Case # 3. N_chrom = 20

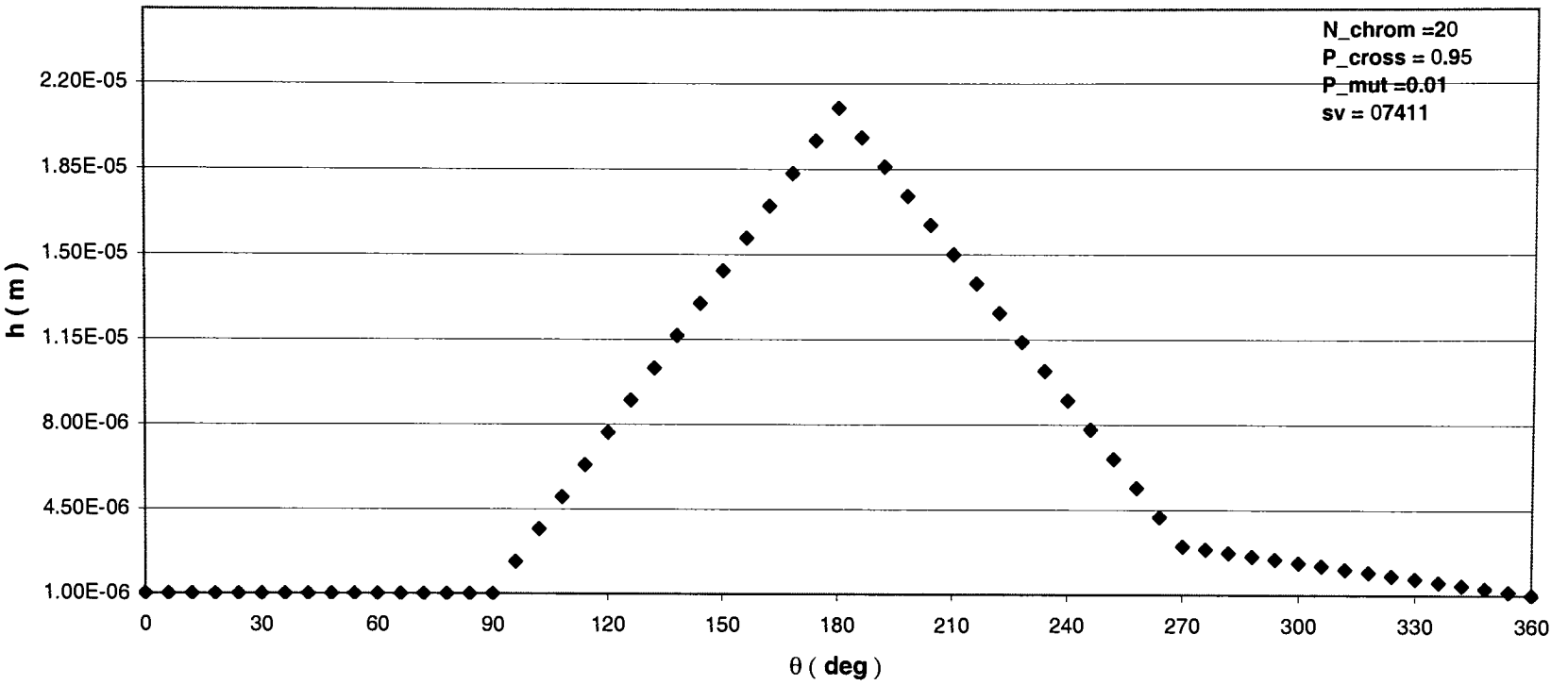

Figure 3.4.4, c. Film thickness distribution with first random set of chromosomes (sv = 07411) after 1000 generations
Case # 3. N_chrom = 20

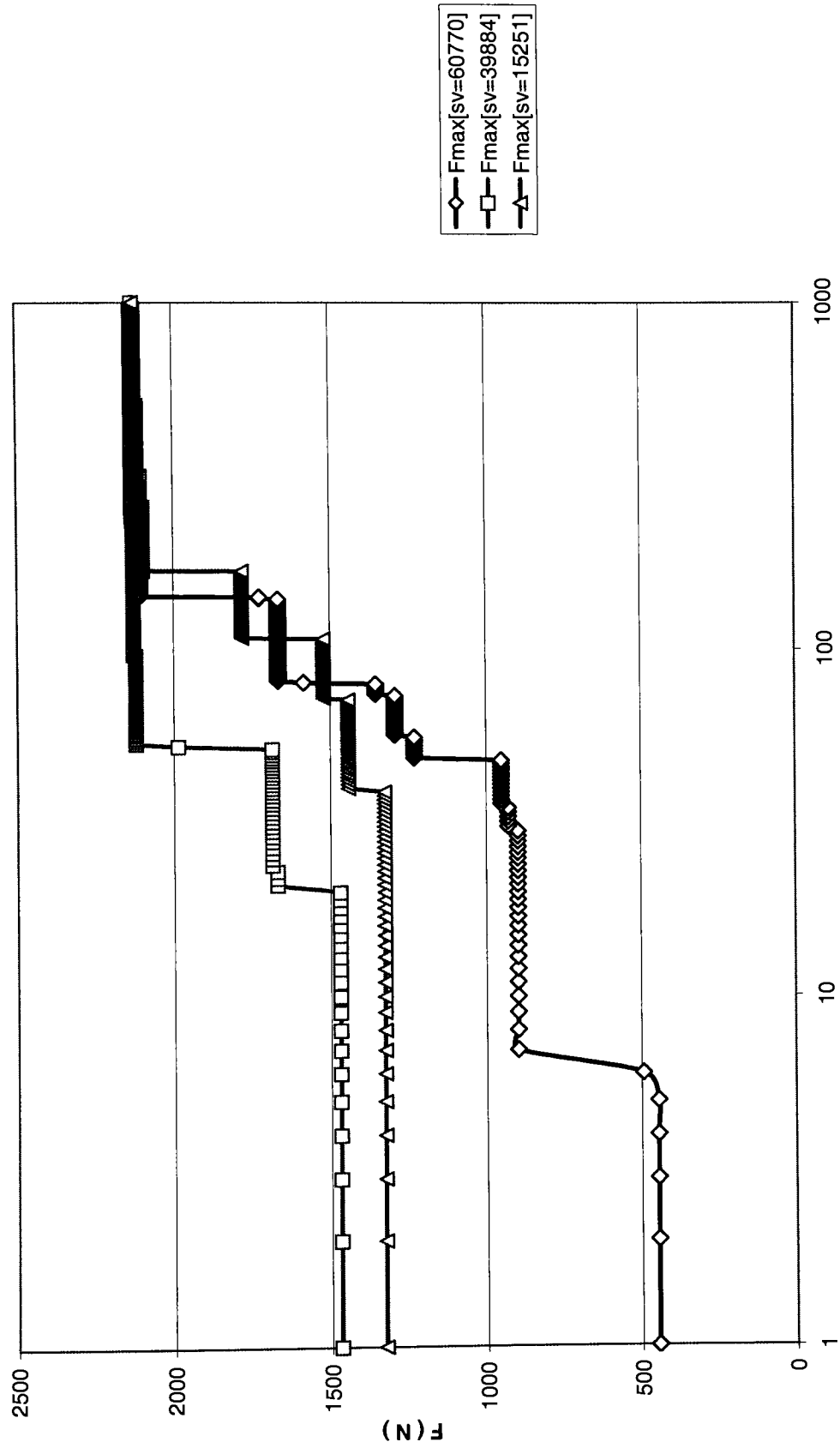

Figure 3.5.1. Bearing load evolutions for each of three randomly selected sets (D=40.0mm, N_chrom=20)
C A S E # 4

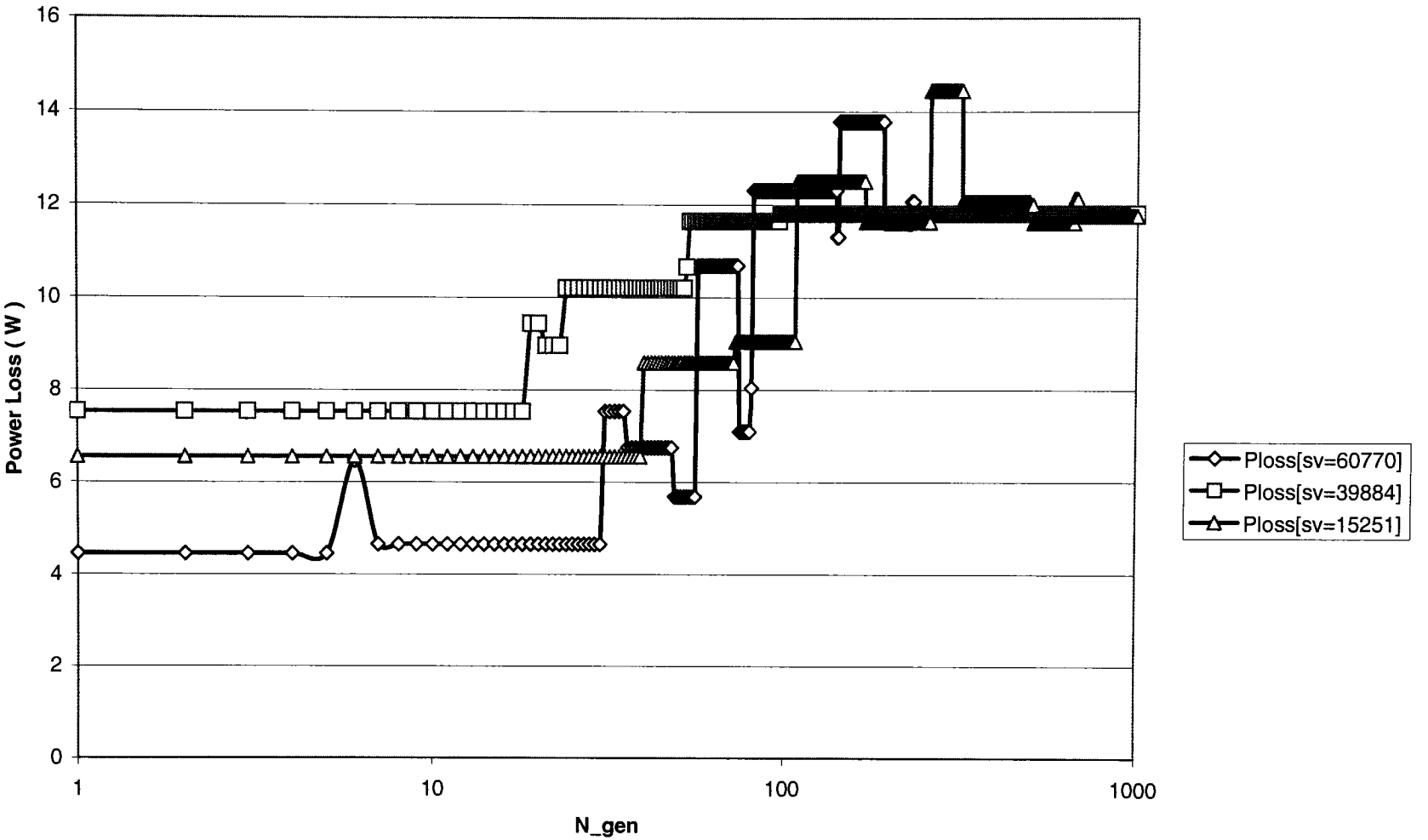

Figure 3.5.2. Plot of Power Loss with three randomly selected sets (D=40.0mm, N_chrom=20)
C A S E # 4

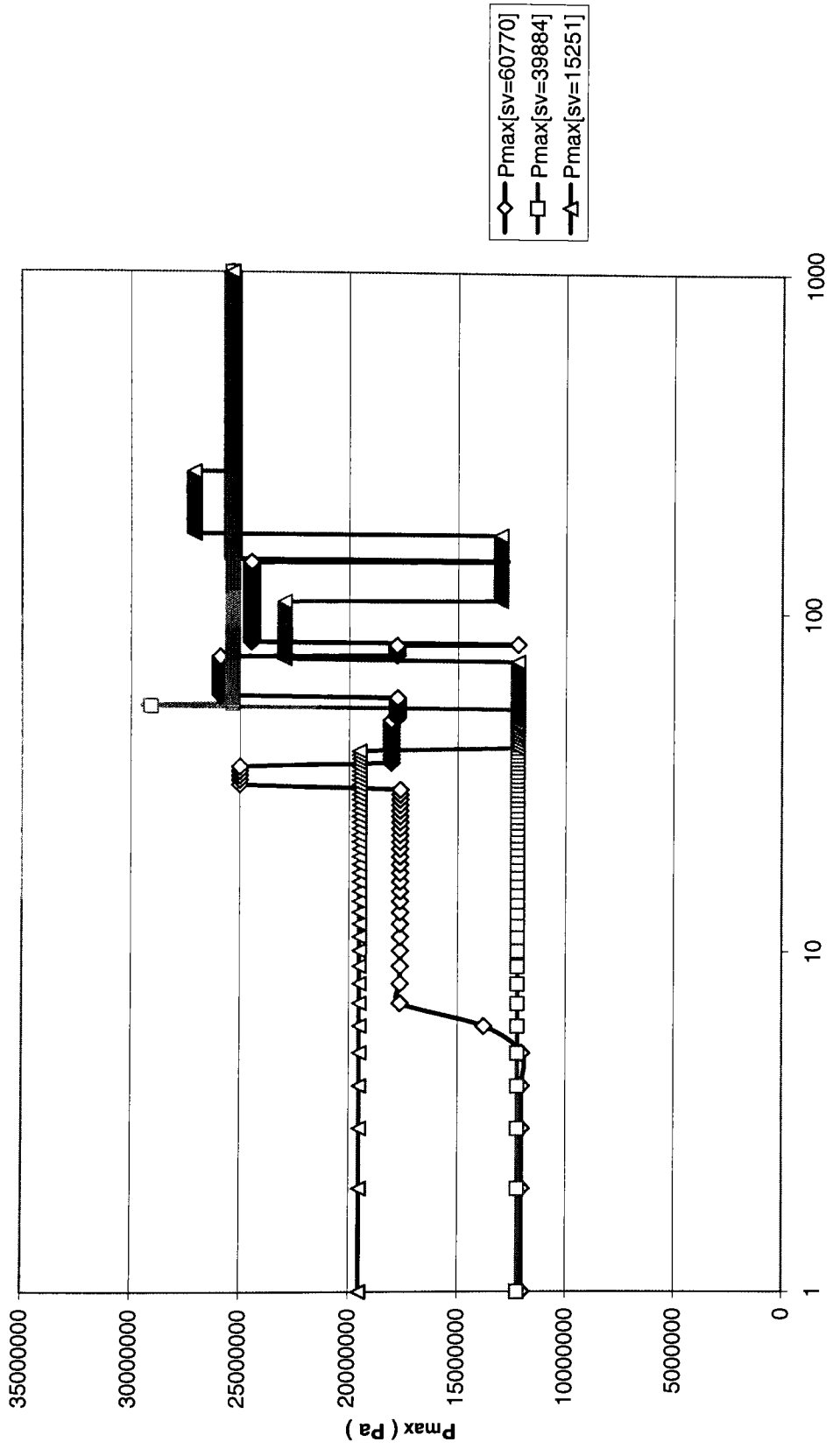

Figure 3. 5.3. Plot of Pmax with three randomly selected sets (D=40.0mm, N_chrom=20)
C A S E # 4

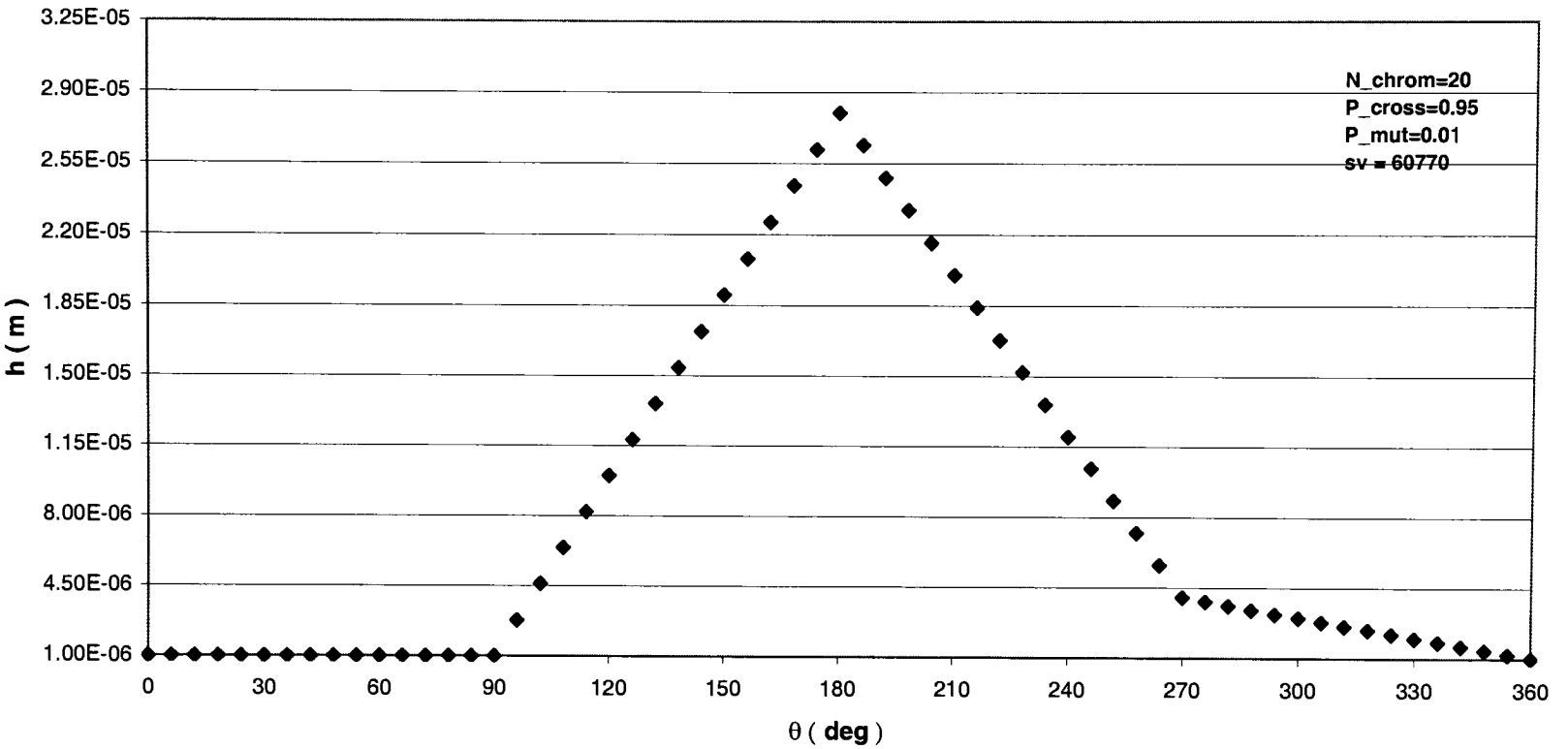

Figure 3.5. 4, a. Film thickness distribution with first random set of chromosomes (sv=60770) after 1000 generations
Case # 4. N_chrom=20

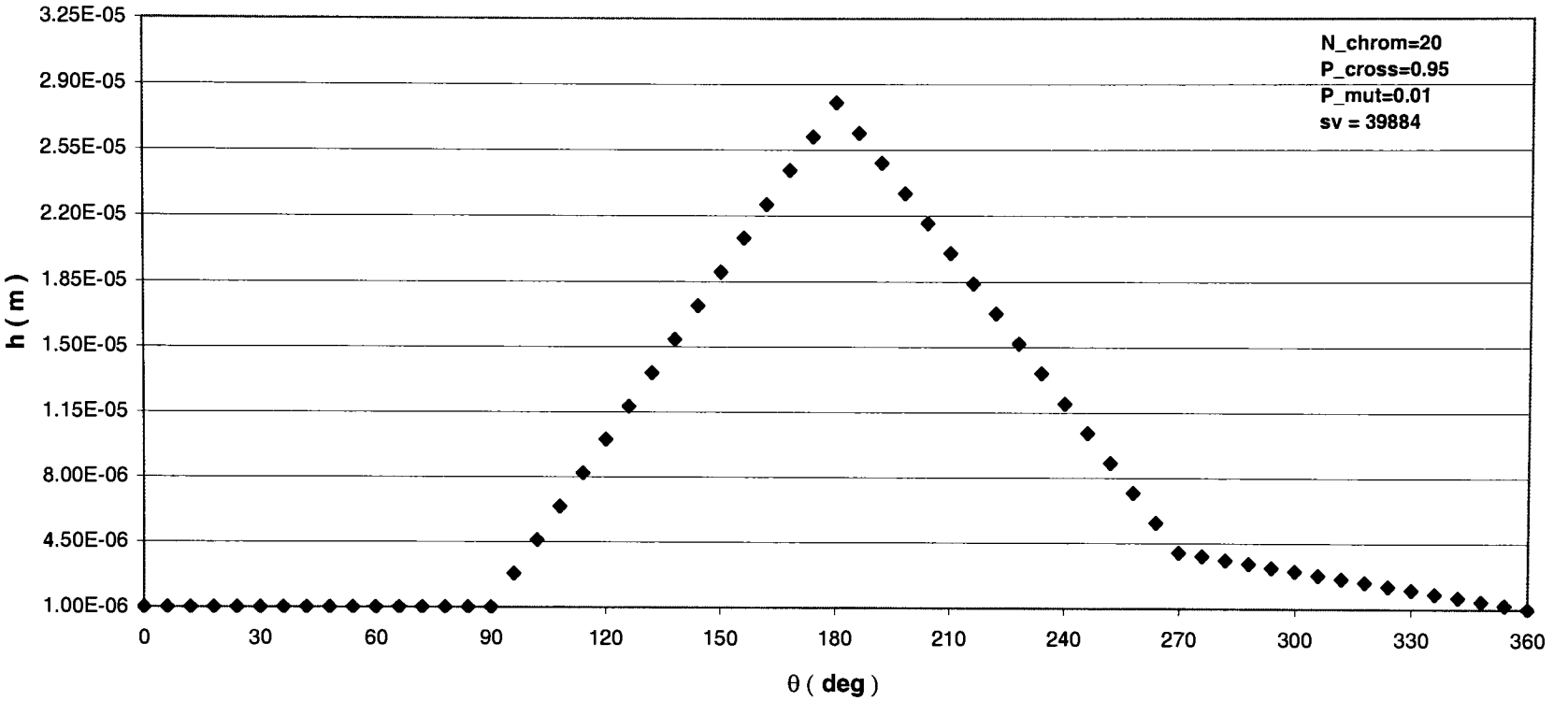

Figure 3.5.4, b. Film thickness distribution with second random set of chromosomes (sv=39884) after 1000 generations
Case # 4. N_chrom=20

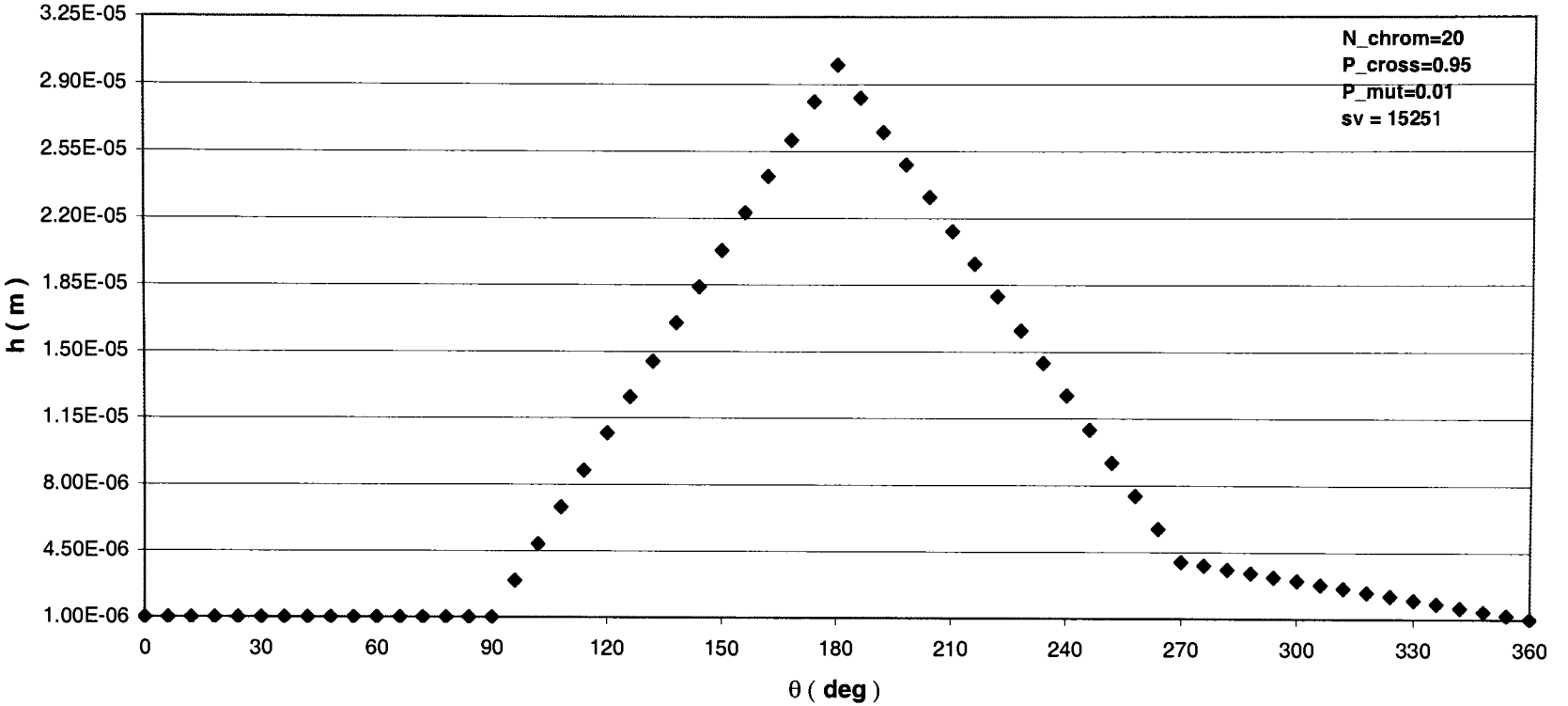

Figure 3.5.4, c. Film thickness distribution with second random set of chromosomes (sv=15251) after 1000 generations
Case # 4. N_chrom=20

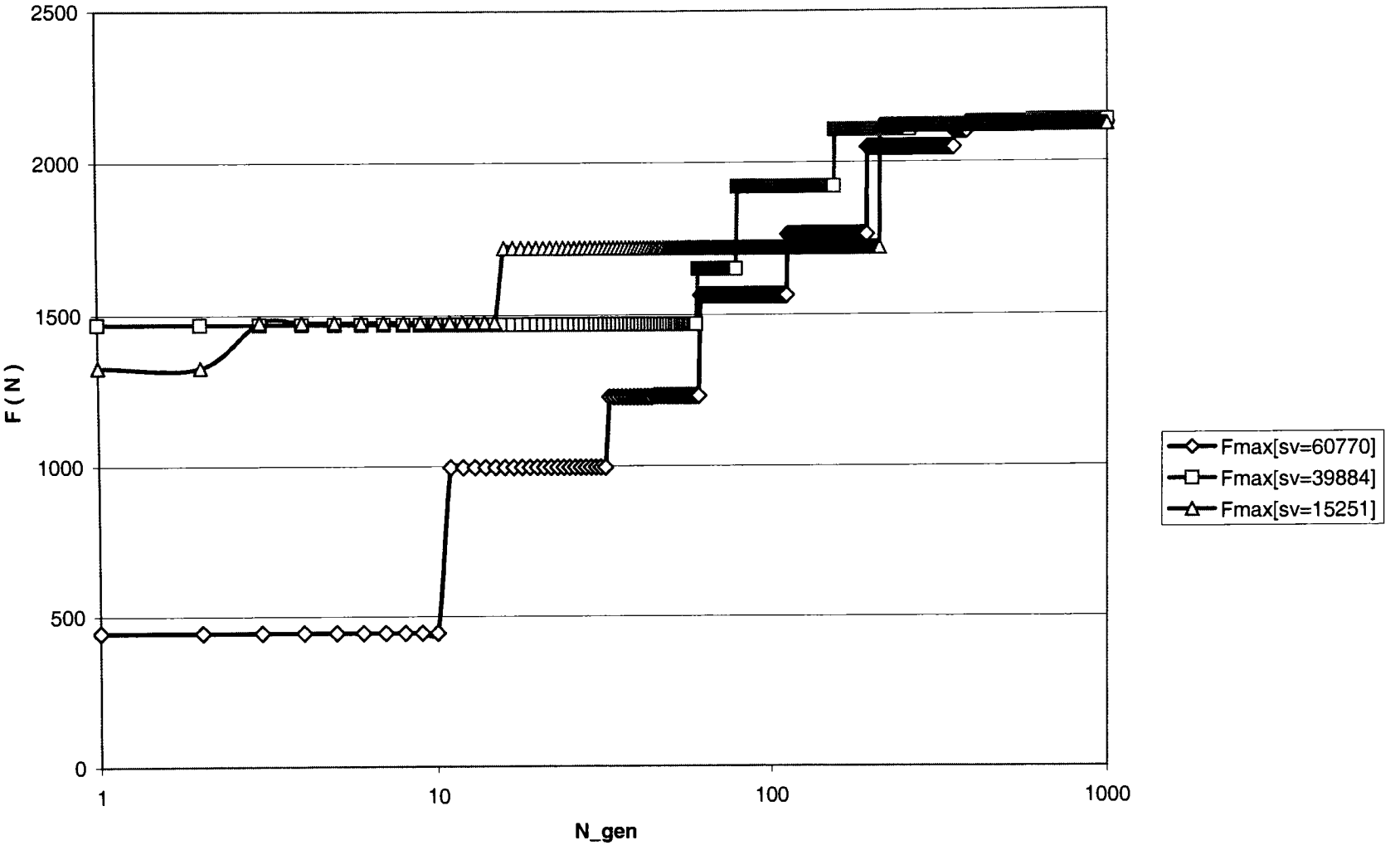

Figure 3.5.5. Bearing load evolutions for each of three randomly selected sets (D=40.0mm, N_{chrom}=20)
Sensitivity studies (P_cross = 0.65, P_mut = 0.01).

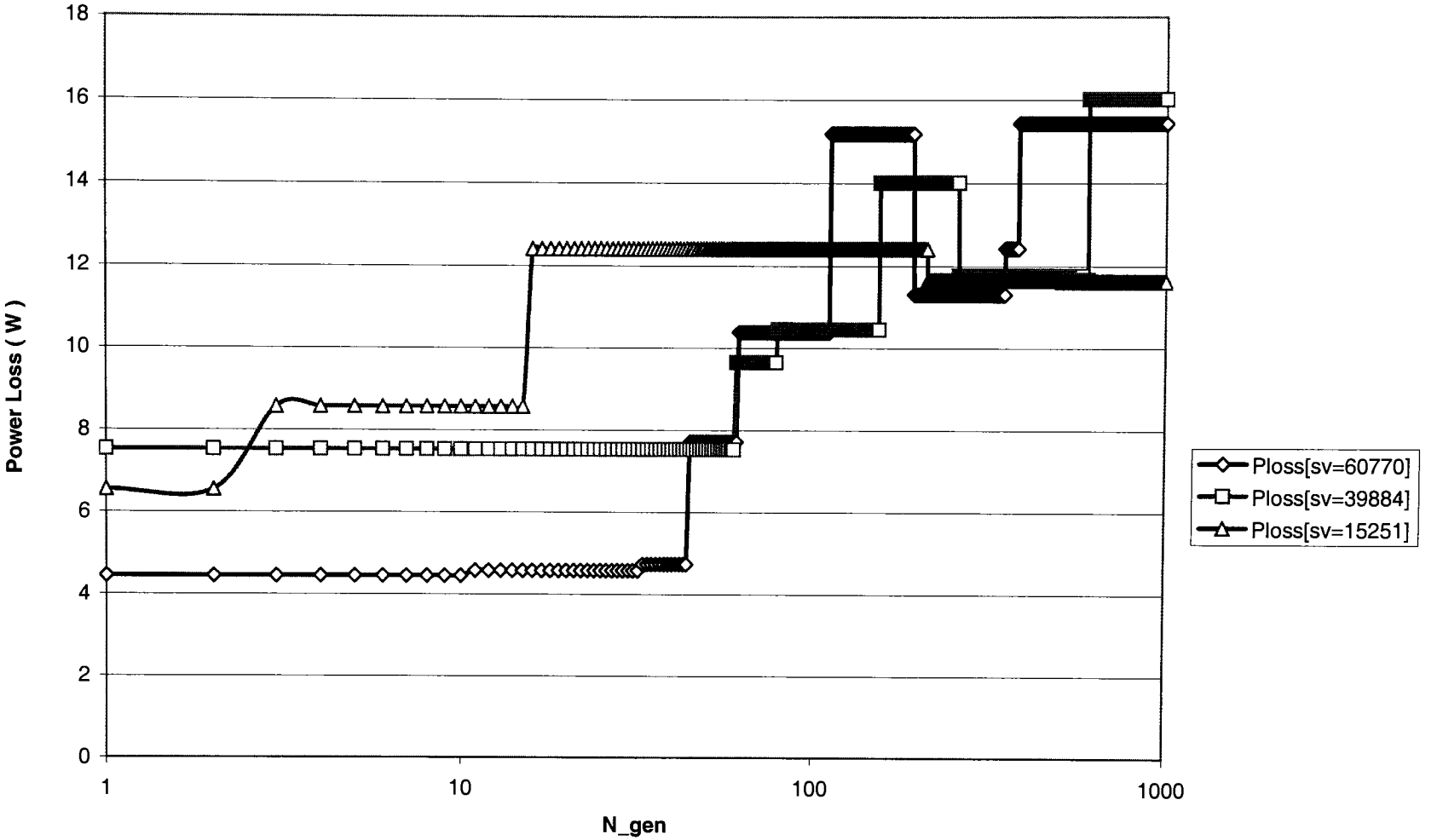

Figure 3.5.6. Plot of Power Loss with three randomly selected sets (D=40.0mm, N_{chrom}=20) Sensitivity studies (P_cross = 0.65, P_mut = 0.01).

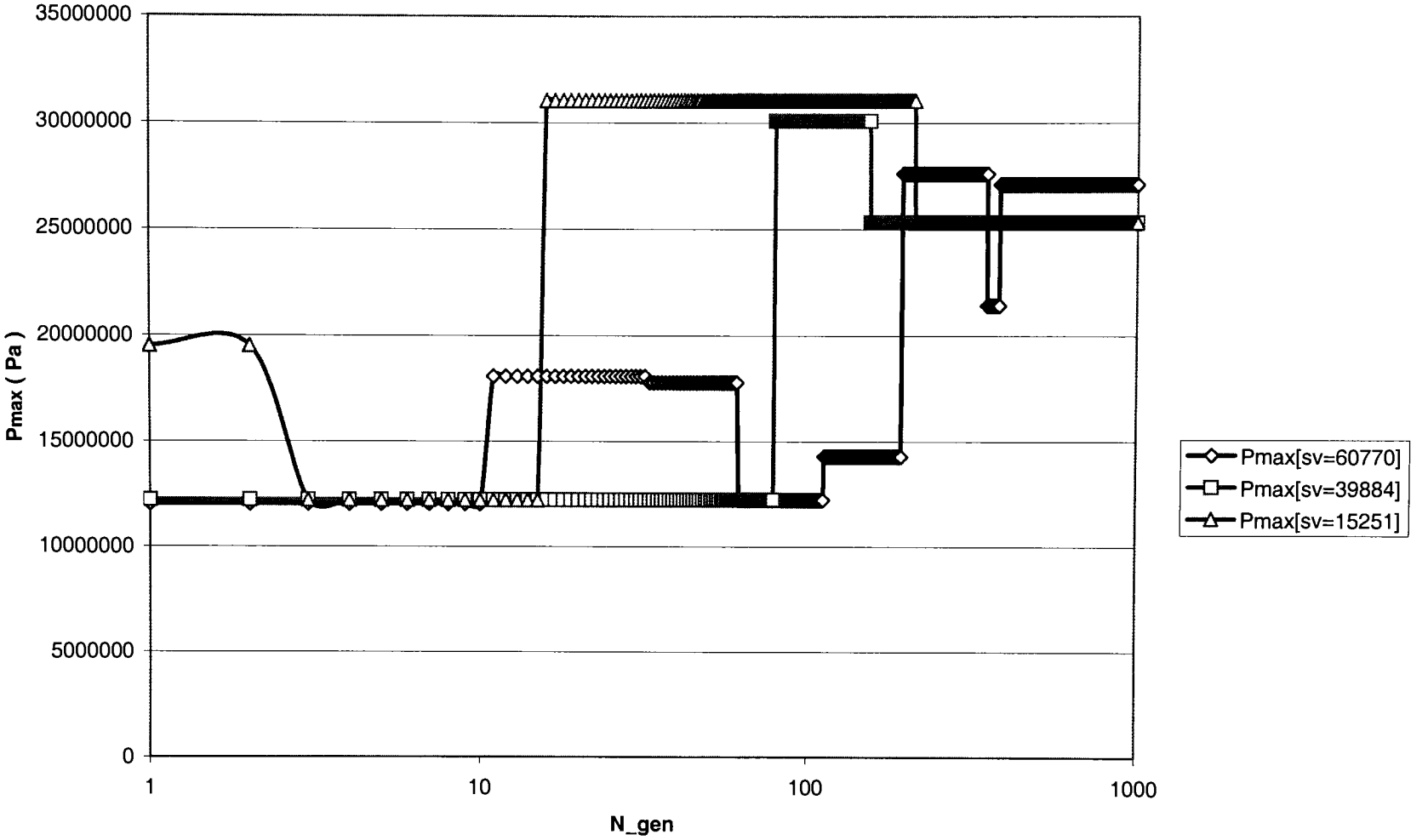

Figure 3.5.7. Plot of P_{max} with three randomly selected sets (D=40.0mm, N_{chrom}=20) Sensitivity studies (P_cross = 0.65, P_mut = 0.01).

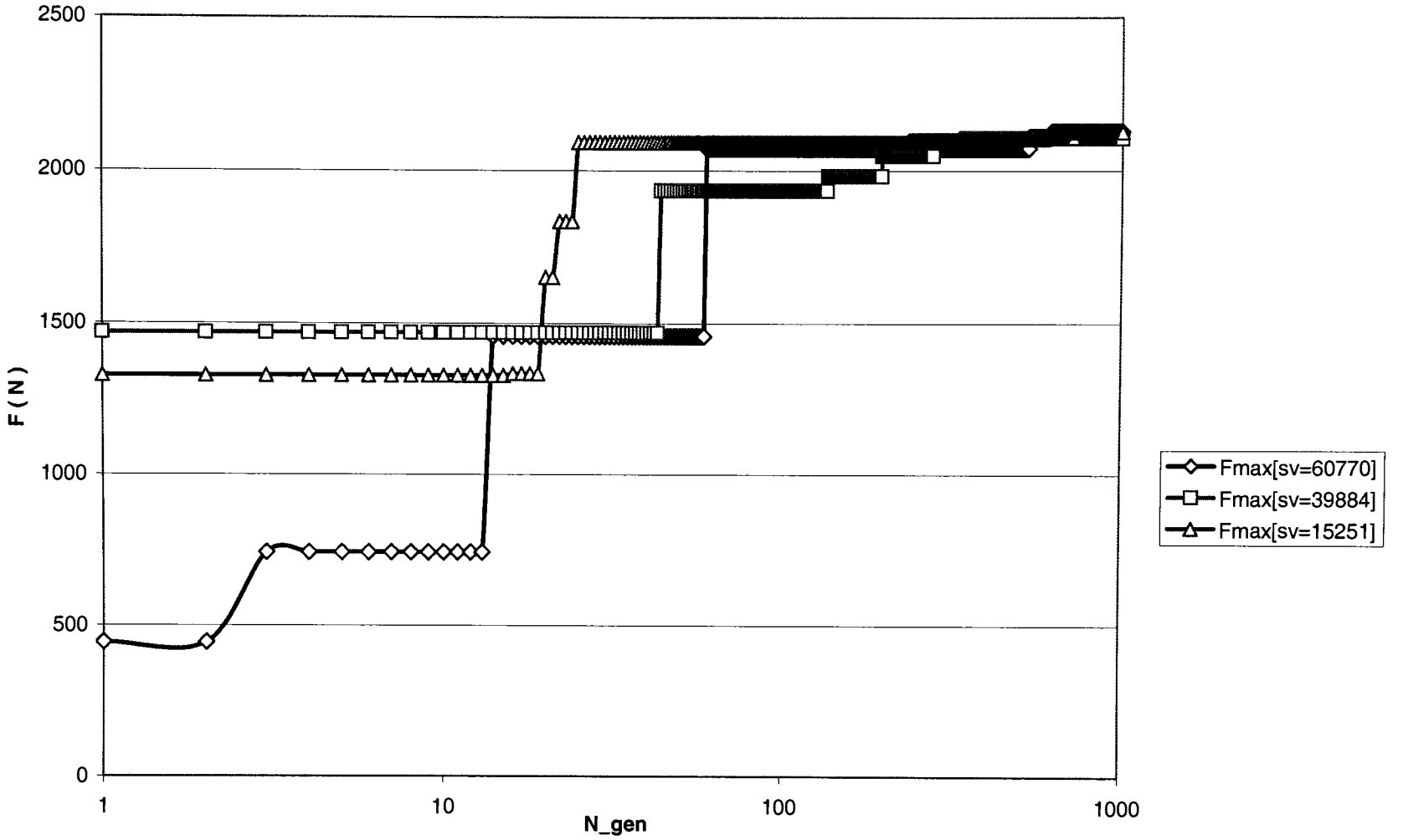

Figure 3.5.8. Bearing load evolutions for each of three randomly selected sets (D=40.0mm, N_{chrom}=20)
Sensitivity studies (P_cross = 0.78, P_mut = 0.01)

Figure 3.5.9. Plot of Power Loss with three randomly selected sets (D=40.0mm, N_{chrom}=20)
Sensitivity studies (P_cross = 0.78, P_mut = 0.01)

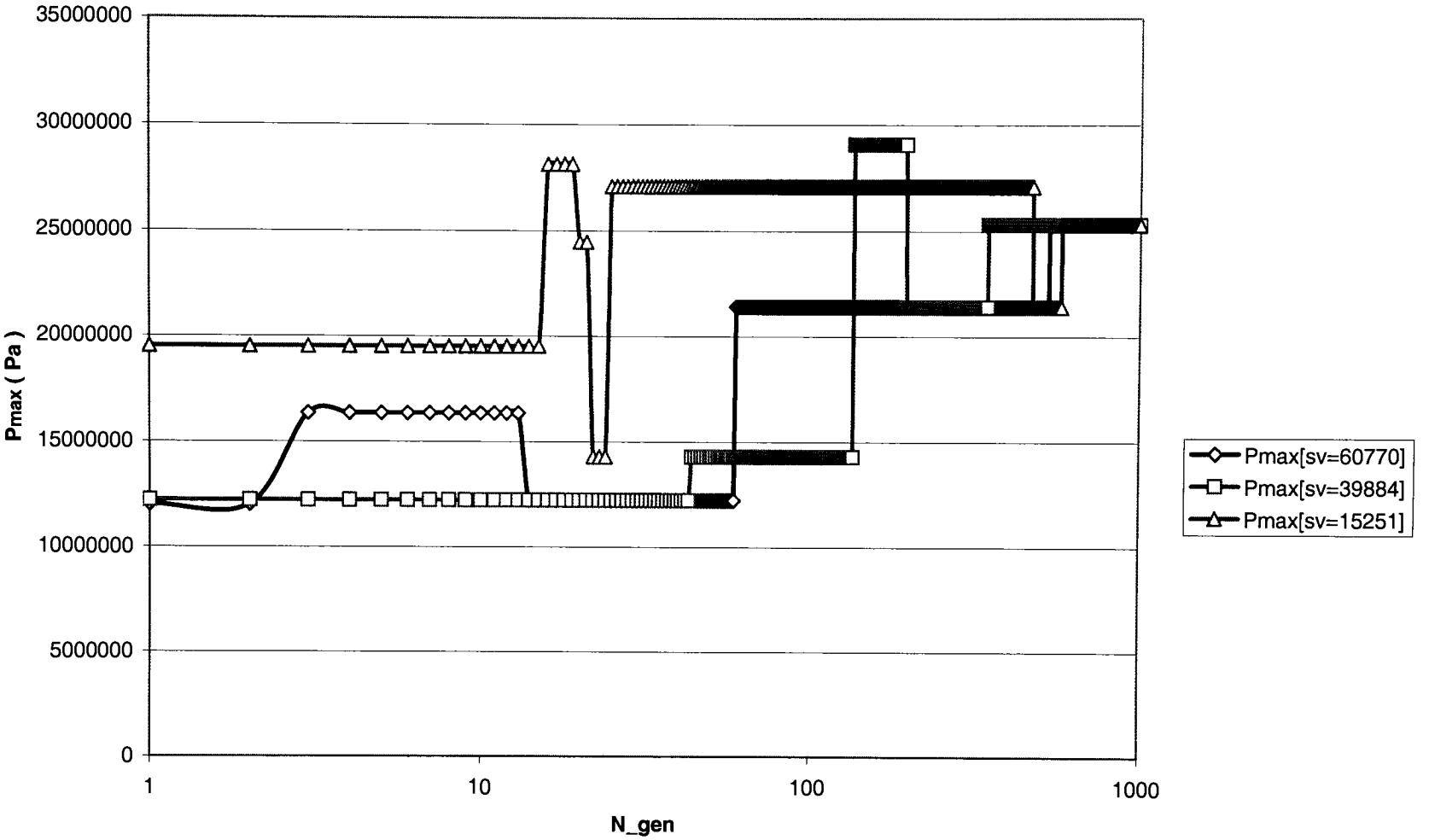

Figure 3.5.10. Plot of P_{max} with three randomly selected sets (D=40.0mm, N_{chrom}=20)
Sensitivity studies (P_cross = 0.78, P_mut = 0.01)

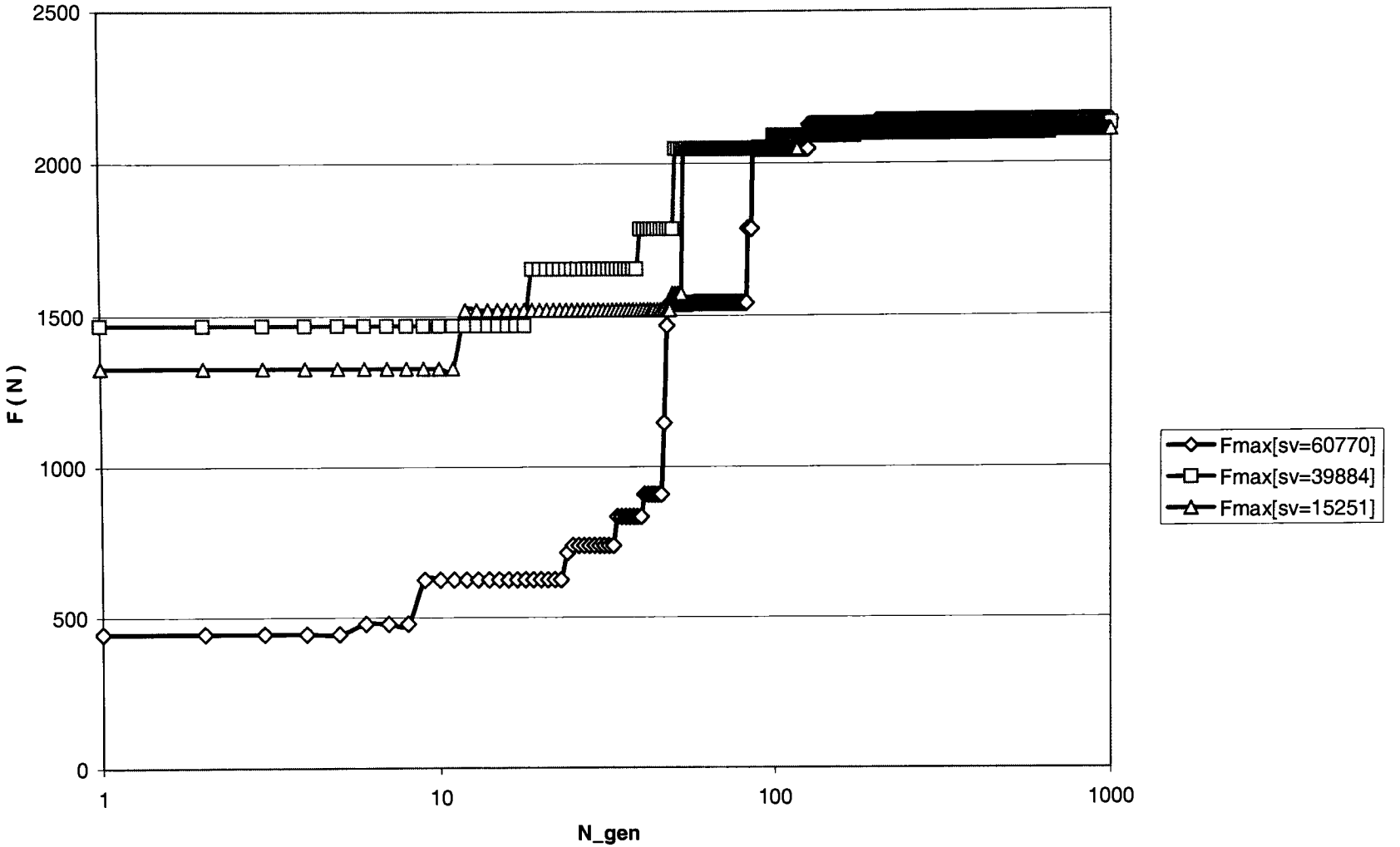

Figure 3.5.11. Bearing load evolutions for each of three randomly selected sets (D=40.0mm, N_{chrom}=20)
Sensitivity studies (P_mut = 0.001, P_cross = 0.95)

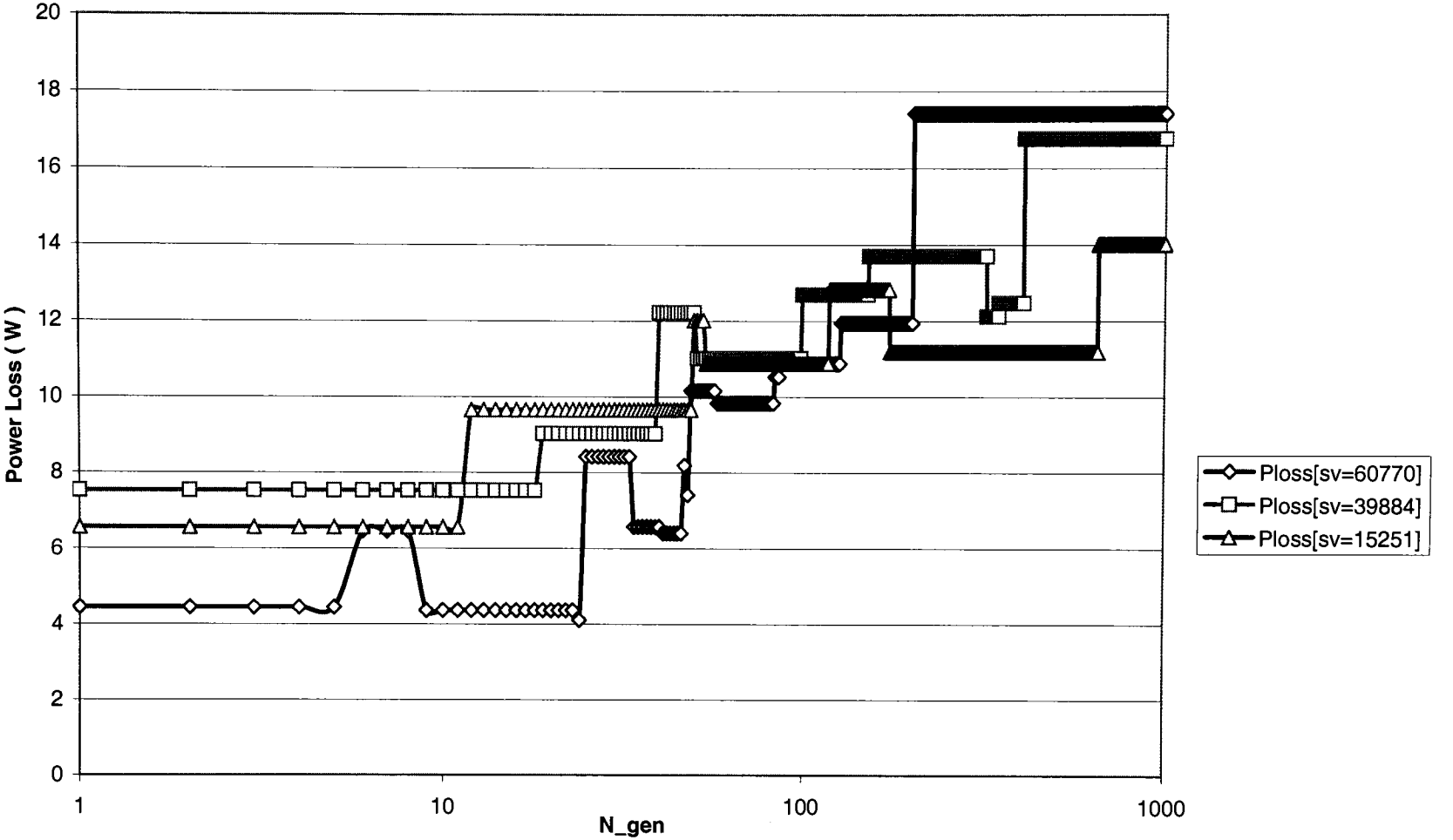

Figure 3.5.12. Plot of Power Loss with three randomly selected sets (D=40.0mm, N_{chrom}=20) Sensitivity studies (P_mut = 0.001, P_cross = 0.95).

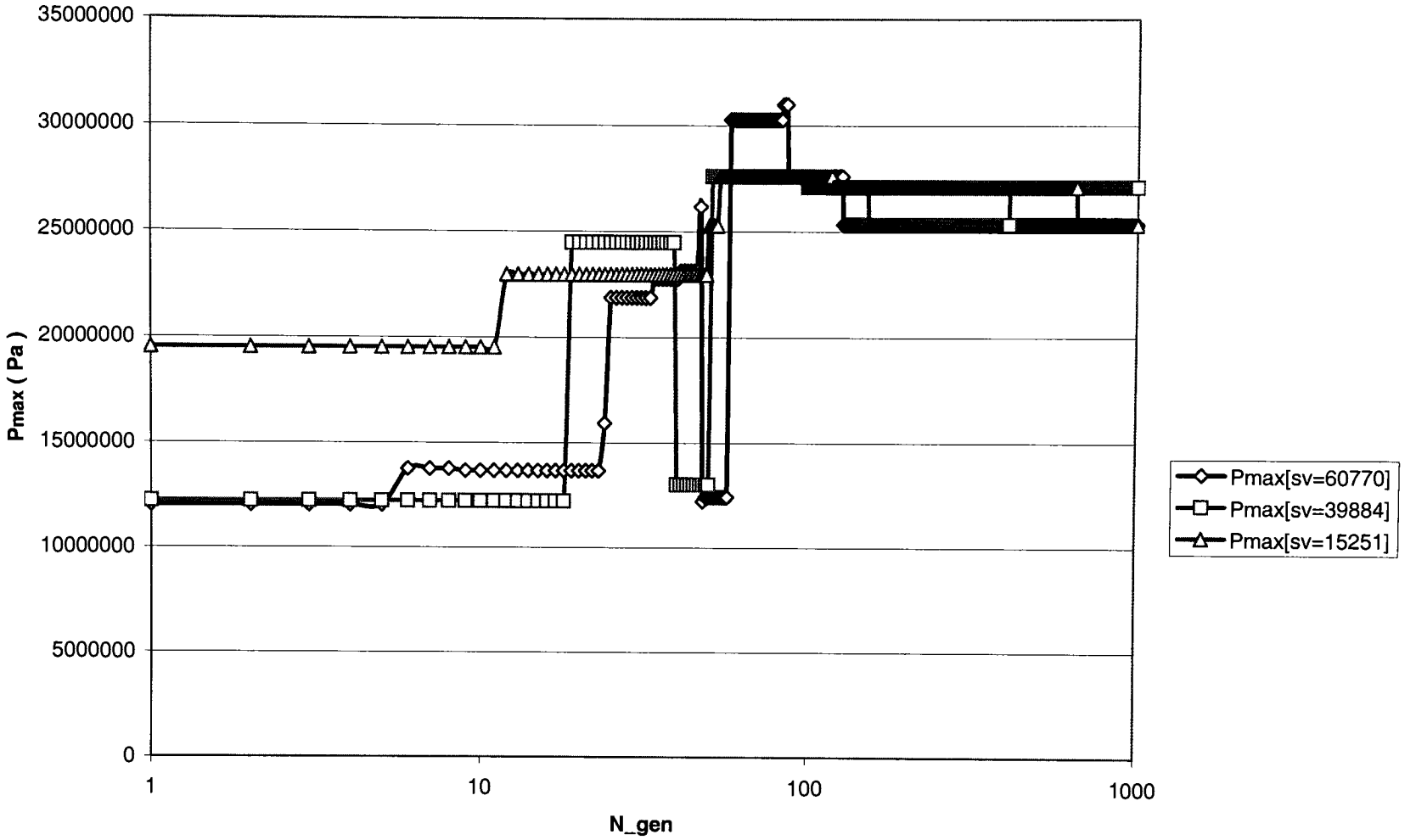

Figure 3.5.13. Plot of P_{max} with three randomly selected sets (D=40.0mm, N_{chrom}=20) Sensitivity studies (P_mut = 0.001, P_cross = 0.95).

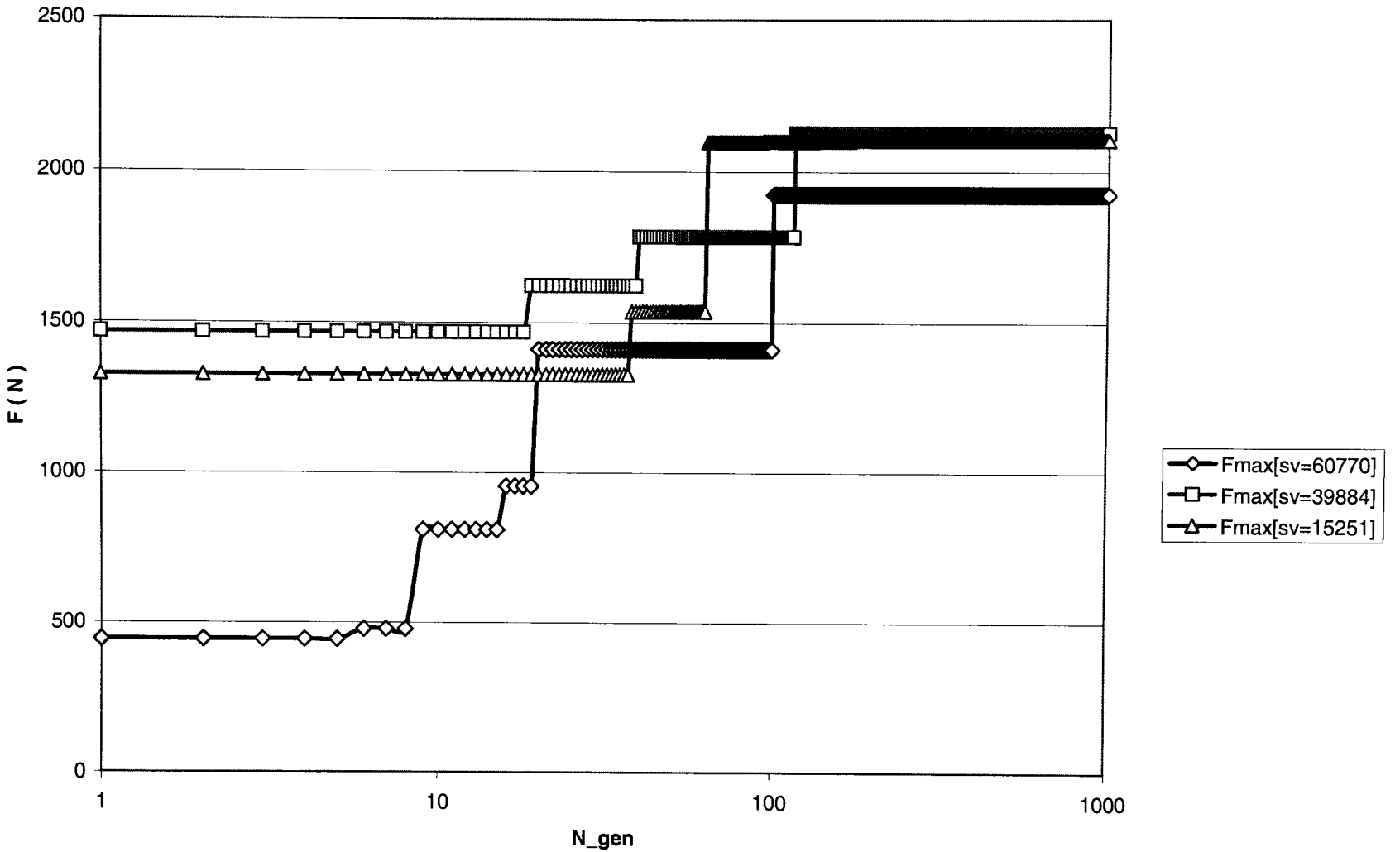

Figure 3.5.14. Bearing load evolutions for each of three randomly selected sets(D=40.0mm, N_chrom=20).
Sensitivity studies (P_cross = 0.95, P_mut = 0).

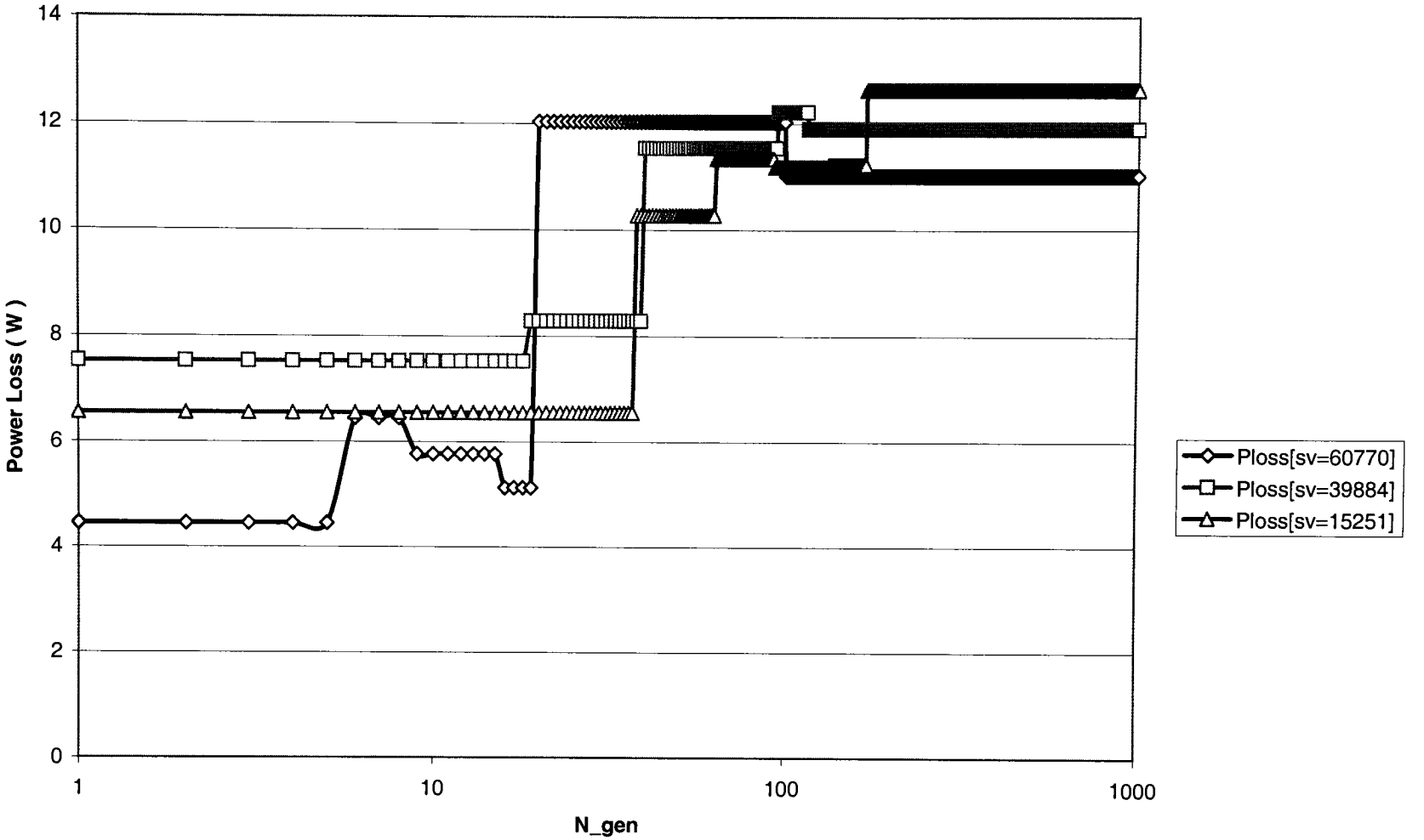

Figure 3.5.15. Plot of Power Loss with three randomly selected sets (D=40.0mm, N_{chrom}=20)
Sensitivity studies (P_cross = 0.95, P_mut = 0)

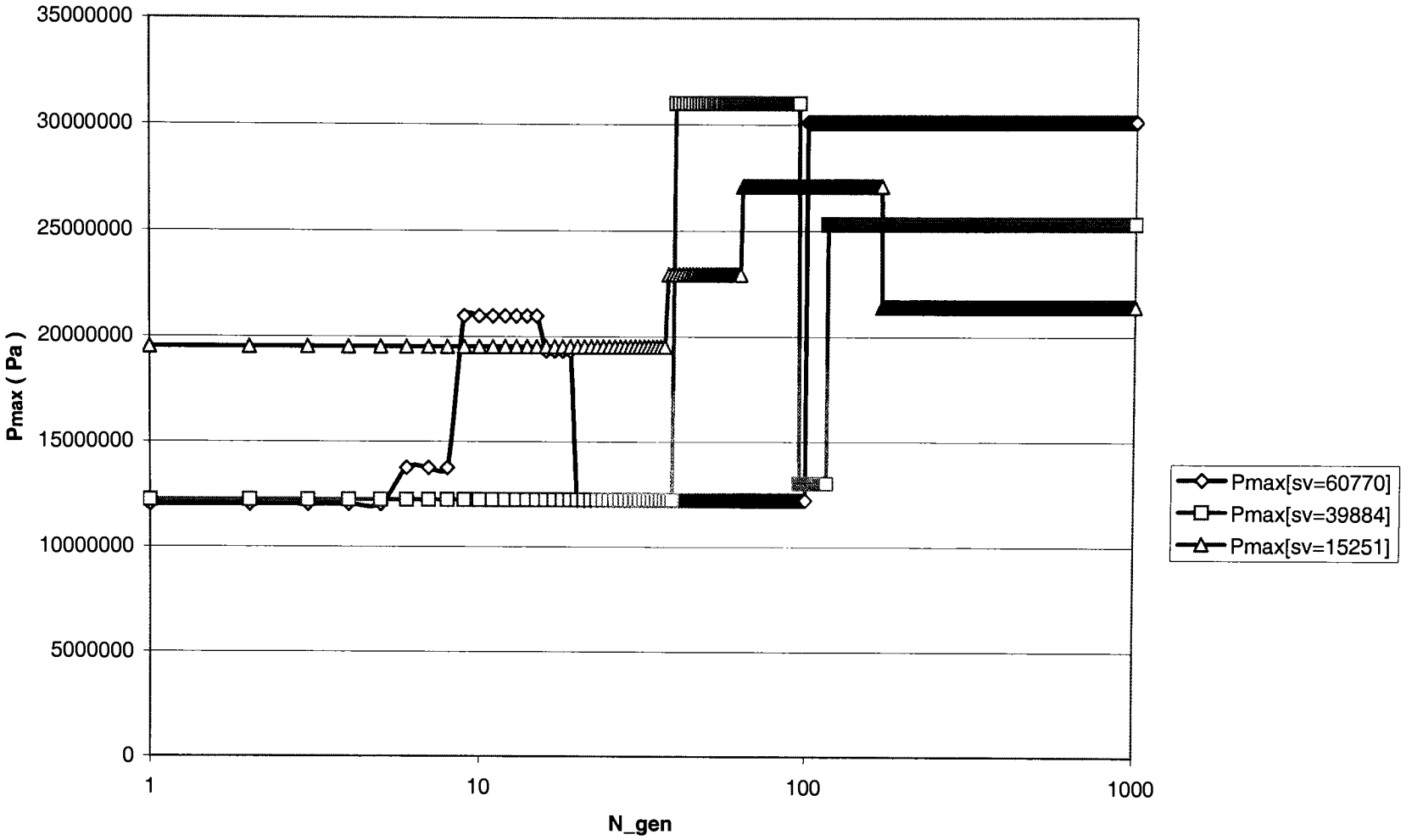

Figure 3.5.16. Plot of P_{max} with three randomly selected sets (D=40.0mm, N_{chrom}=20). Sensitivity studies (P_cross = 0.95, P_mut = 0).

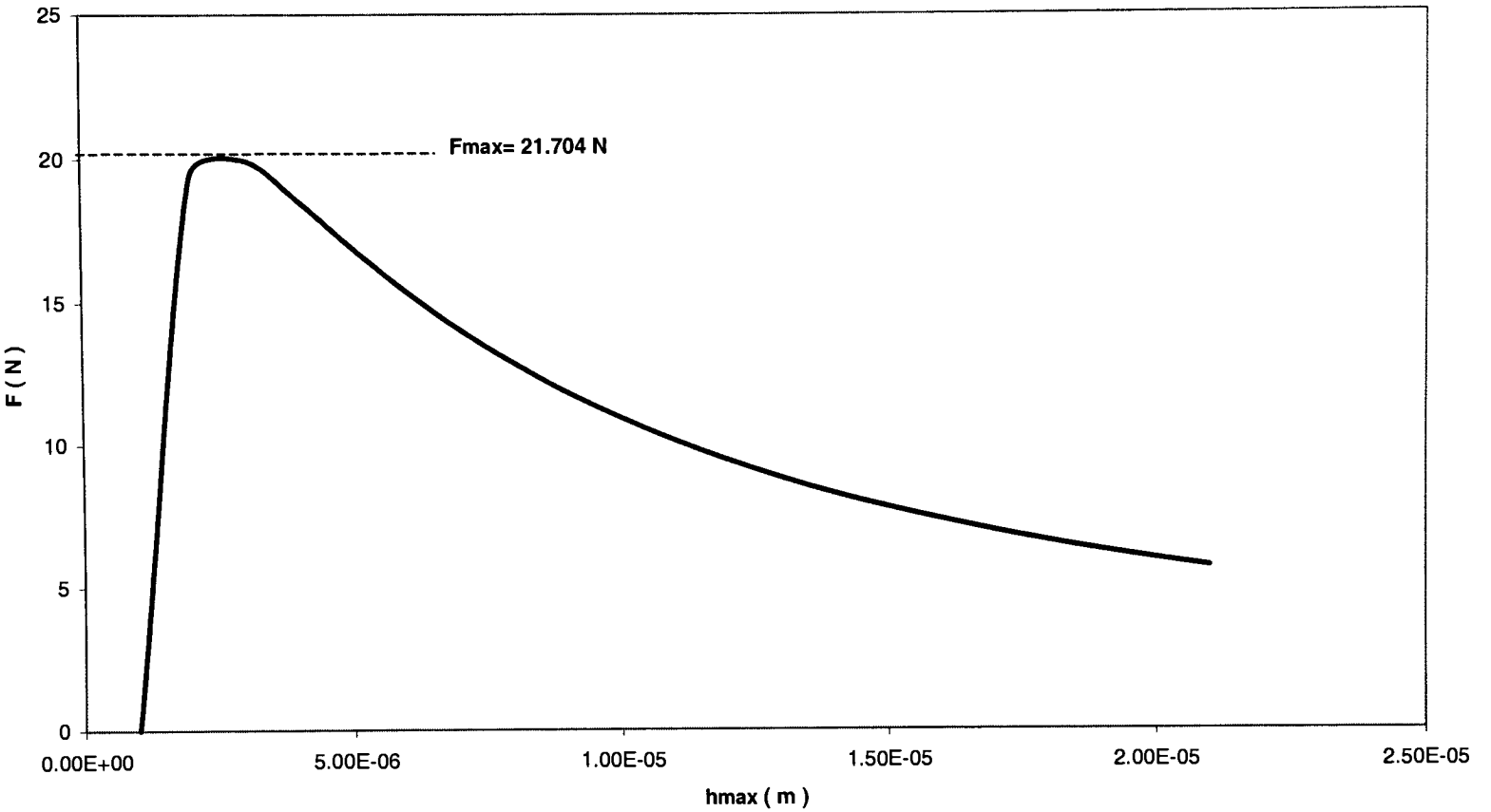

Figure 3.6.2. Plot of best cylindrical journal bearing - F vs. h_{max}
(D=5 mm and L =5 mm), CASE # 1.

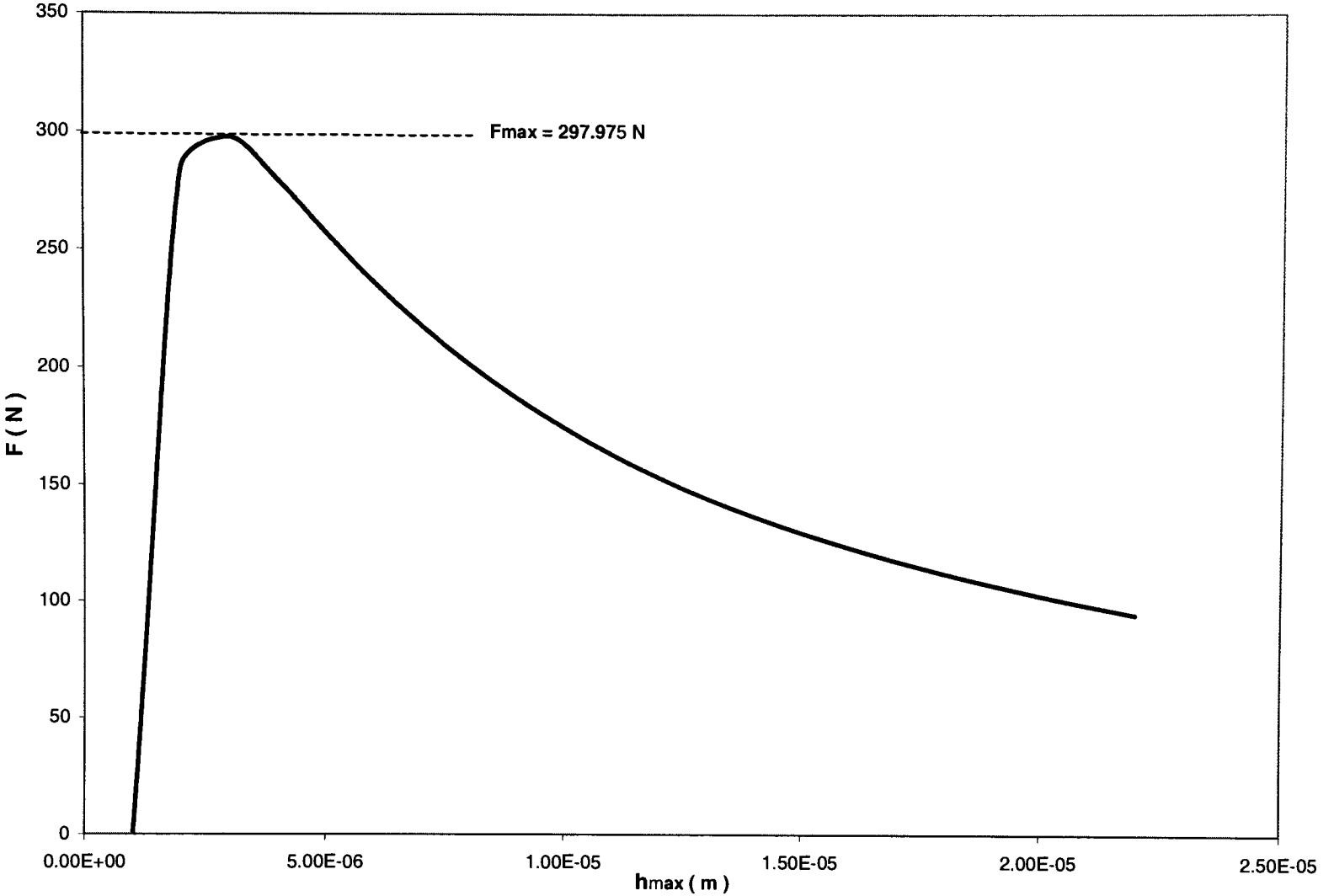

Figure 3.6.3. Plot of best cylindrical journal bearing - F vs. h_{max}
(D=10 mm and L =10 mm), CASE # 2.

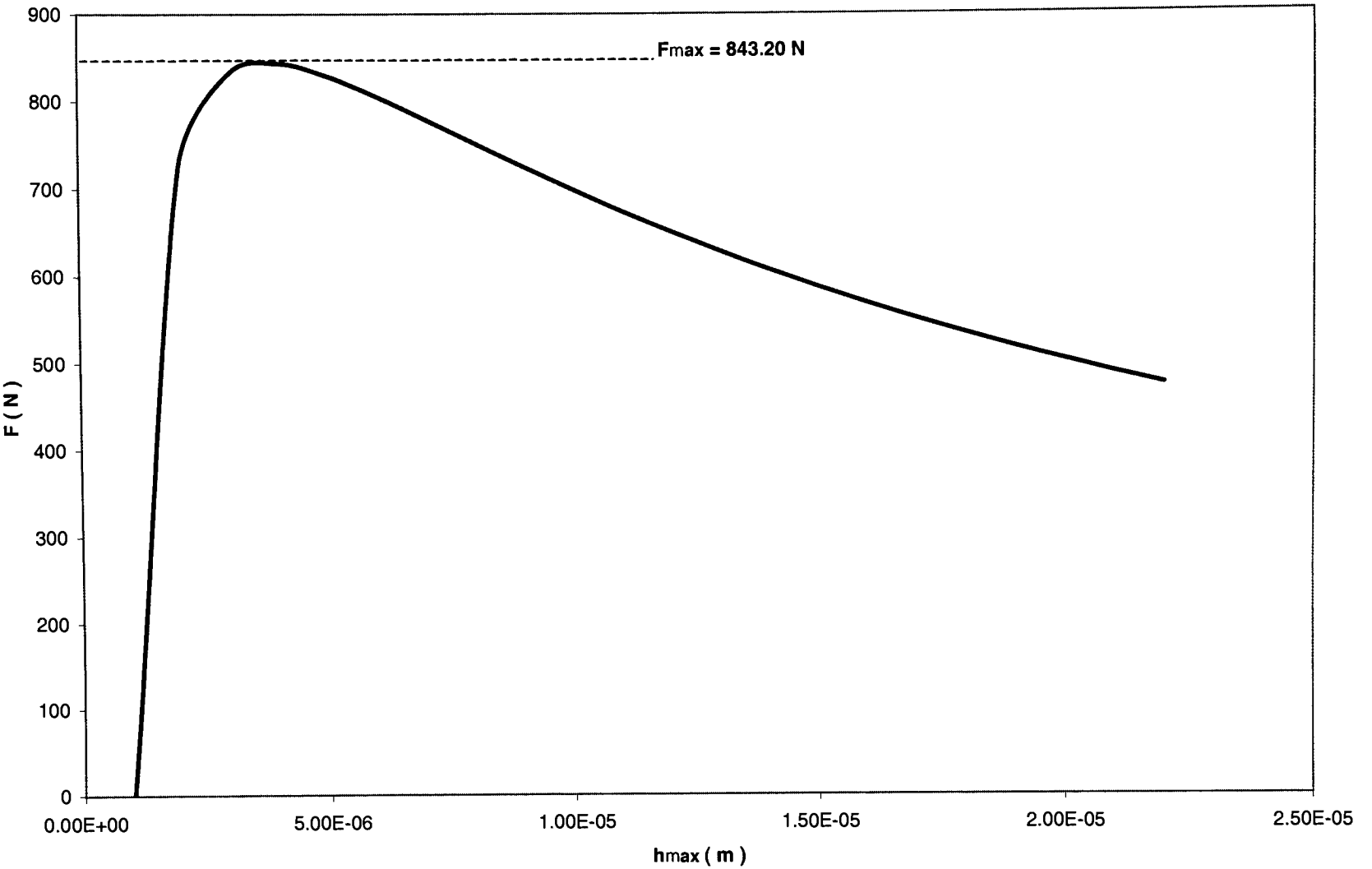

Figure 3.6.4 Plot of best cylindrical journal bearing - F vs. h_{max}
(D=40 mm and L =10 mm), CASE # 3.

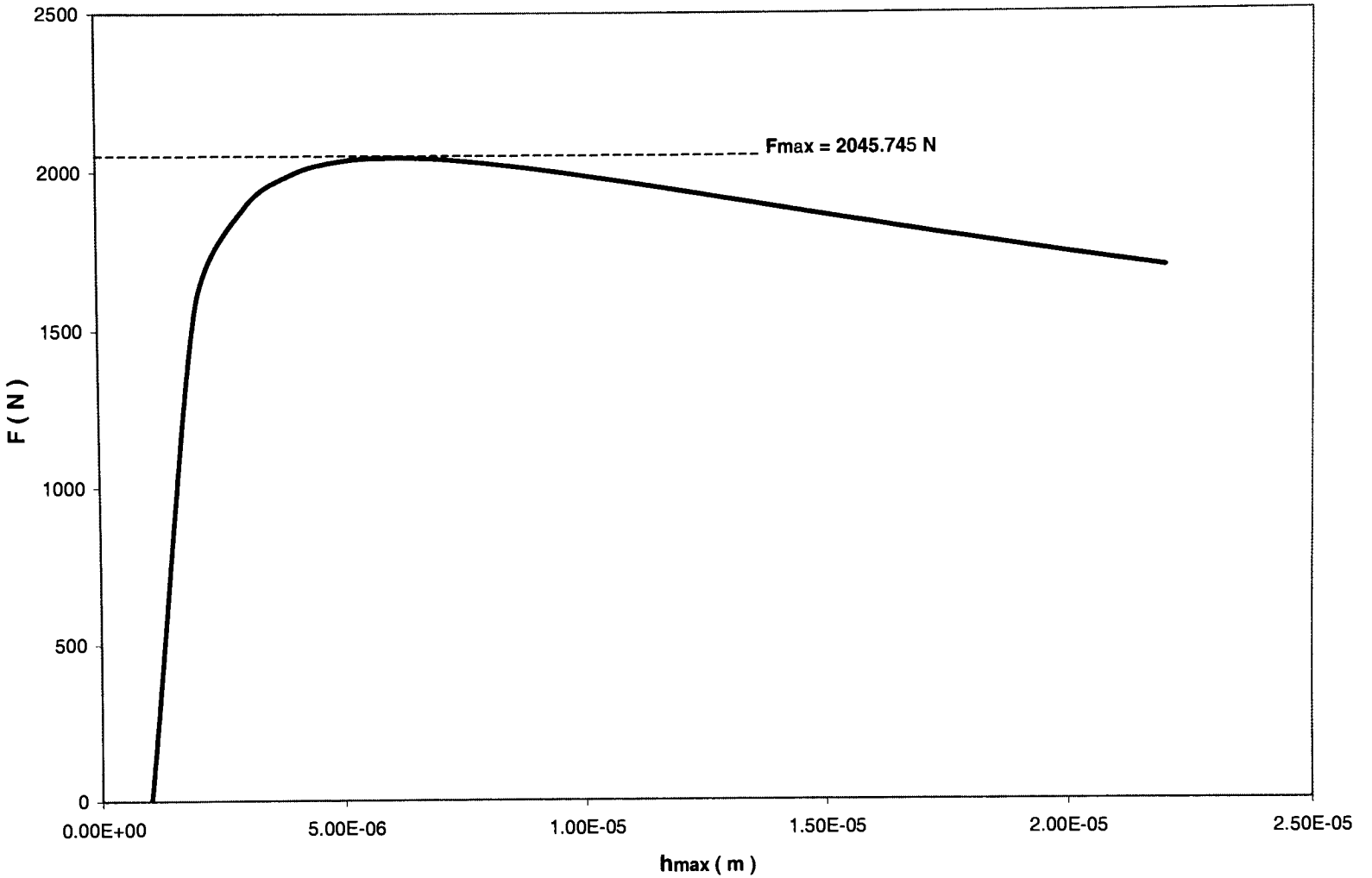

Figure 3.6.5. Plot of best cylindrical journal bearing - F vs. h_{max}
(D=40 mm and L =10 mm), CASE # 4.

Chapter 4

Summary

This thesis has shown that genetic algorithms offer a most promising computational technique for the optimal design of fluid film journal bearings. The algorithm is simple to implement and is relatively fast in finding an optimal shape.

The case studies presented in this thesis have shown that the number of chromosomes per generation and the number of generations to run are two of the key parameters of the genetic algorithms. When running the algorithm with three randomly generated initial sets of 10 chromosomes per generation, three different solutions are typically obtained after 1000 generations. If the number of chromosomes per generation is increased to 20, randomly generated initial sets converge to nearly identical answers after 1000 generations.

The case studies run with 10, 20, and 40 chromosomes per generation take approximately 2.25 hours, 4.5 hours, and 8 hours, respectively, with a 553 MHz Pentium III processor and 256 MB memory. This computational cost trend is expected, as most of the OPTJBG program computations involve computation of bearing load. With 10, 20, and 40 chromosomes per generation, running each to 1000 generations require 10,000, 20,000 and 40,000 bearing load calculations, respectively.

Most noteworthy, the case studies show that running the algorithm with 40 chromosomes per generation yields only a 5% improvement in load capacity when compared with results obtained 20 chromosomes per generation. Even though the 40 chromosomes per generation

size gives a somewhat better answer, from the computing time perspective, it is nearly twice as slow as than 20 chromosome size.

As a final computing cost assessment, an exhaustive search over the design space would require 2^{21} = 2,097,152 bearing calculations. Assuming 40,000 calculations take 8 hours, an exhaustive search for each case study would take approximately 419 hours, or 17.5 days using the same computer configuration; hence, this study was not performed.

The importance of the mutation operator can be observed in case # 4 of mutation sensitivity studies, which differs from case # 4 only with its zero mutation probability. The final results of the case show that the lack of the mutation operator produces a load which is approximately 20-30% lower than the optimal.

Further work will investigate the sensitivity of small perturbations of load and shape deviations from the optimal, along with investigations of dynamic loads and speeds.

References

Abramowitz, M., and Stegun, I.A., eds., 1965, *Handbook of Mathematical Functions*, Dover Publications, New York, NY.

Baricelli, N. A., 1957, " Symbiogenetic Evolution Processes Realized by Artificial Methods, " *Methods 9*, no. 35-36, pp. 143-182.

Baricelli, N. A., 1962, " Numerical Testing of Evolution Theories, " *ACTA Biotheoretica*, no. 16, pp. 69-126.

Bledsoe, W.W., 1961, " The Use of Biological Concepts in the Analytical Study of Systems, " Paper presented at ORSA-TIMS National Meeting, San Francisco, CA.

Boedo, S., 2000, " Program OPTJBG Version 1.3," FORTRAN Computer Program, " November 6, 2000.

Boedo, S., and Booker, J.F., 2000, " CUIMPD Version 1.1 User's Manual," Report TA-2000-01, Tribology Associates, Ithaca, New York, February 7, 2000.

Booker, J. F., and Huebner, K.H., 1972, " Application of Finite Element Methods to Lubrication: An Engineering Approach, " *ASME Journal of Lubrication Technology*, vol. 94, pp. 313-320.

Booker, J.F., 1965, " Dynamically loaded Journal Bearings: Mobility Method of Solution, " *ASME Journal of Lubrication Tribology*, vol.87, n. 3, p. 537.

Box, G. E. P., 1957, " Evolutionary operation: A method for Increasing Industrial Productivity, " *Journal of the Royal Statistical Society C*, vol. 6, n. 2, pp. 81-101.

Bremermann, H. J., 1962, "Optimization through Evolution and Recombination," In *Self-Organizing Systems,* M. C. Yovits, G.T. Jacobi, and G. D. Goldstein, eds., Spartan Books.

Burr, A.H., 1982, *Mechanical Analysis and Design*, 2nd ed, Elsevier.

Chapman, C.D., Saitou, K., and Jakiela, M.J., 1994, " Genetic Algorithm as an Approach to Configuration and Topology Design, " *ASME Journal of Mechanical Design*, vol. 116, pp.1005-1011.

Chen, T.Y., Wei, W. J., and Tsai, J. C., 1999, " Optimum Design of Headstocks of Precision Lathes, " *International Journal of Machine Tools and Manufacture*, vol. 39, pp. 1961-1977.

Davies, R., ed., 1964, *Cavitation in Real Liquids*, Elsevier Publishing Company, New York.

Elsharkawy, A., and Guedouar, L.H., 2000, " An Inverse for Steady-State Elasto-hydrodynamic Lubrication of One-Layered Journal Bearings, " *ASME Journal of Tribology*, vol. 122, pp. 524-533.

Friedman, G. J., 1959, " Digital Simulation of Evolutionary Process, " *General Systems Yearbook,* vol.4, pp. 171-184.

Hajela, P., and Lee, E., 1995, " Genetic Algorithms in Truss Topological Optimization, " *International Journal of Solids and Structures*, vol. 32, n. 22, pp. 3341-3357.

Haraldsson, A., Han, C.S., Tschope, H., and Wriggers, P., 1997, " Shape Optimization of a Lubricated Journal Bearing with Regard to the Distribution of Pressure in the Fluid, " *Engineering Optimization*, vol. 29, pp. 259-275.

Hashimoto, H., 1997, " Optimum Design of High-Speed, Short Journal Bearings by Mathematical Programming, " *STLE Tribology Transactions*, vol. 40, n. 2, pp. 283-293.

Hillis, W.D., 1992, " Co-evolving Parasites Improve Simulated Evolution as an Optimization Procedure, " In *Artificial Life II*, C. G. Langton, C. Taylor, J.D.Farmer, and S. Rasmussen, eds., Addison-Wesley.

Keane, A.J., 1995, " Passive Vibration Control via Unusual Geometries: the Application of Genetic Algorithm Optimization to Structural Design, " *Journal of Sound and Vibration*, vol. 185, 3, pp. 441-453.

Kicinski, J., and Haller, R., 1994, " Computer Optimization of External Fixation and Initial Clamping of a Bushing with respect to Static and Dynamic Properties and Journal Bearings, " *ASME Journal of Tribology*, vol. 116, pp. 690-697.

Kotera, H., Hirasawa, T., Senga, S., and Shima, S., 2000," A Study on the Effect of Air on the Dynamic Motion of a MEMS Device and Its Shape Optimization, " *STLE Tribology Transactions*, vol. 43, n. 4, pp. 842-846.

Kotera, H., and Shima, S., 2000, " Shape Optimization to Perform Prescribed Air Lubrication using Genetic Algorithm, " *STLE Tribology Transactions*, vol. 43, n. 4, pp. 837-841.

Martin, F.G., and Cockerham, C.C., 1960, " High Speed Selection Studies, " In *Biometrical Genetics*, O. Kempthorne, ed., Pergamon.

Matsumoto, M., and Nishimura, T., 1997, "Mersenne Twister: a 623-dimensionally equidistributed uniform pseudorandom number generator ", To appear in *ACM Transactions on Computer and Simulations*. Software implementation of algorithm in

subroutine *sgrnd* taken from freeware GNU Library General Public License as published by the Free Foundation, Inc., 59 Temple Place, Suite 330, Boston, MA 02111.

Mitchell, M., 1999, *An Introduction to Genetic Algorithms*, MIT Press, Cambridge, Massachusetts.

Montusiewicz, J., and Osyczka, A., 1997, " Computer Aided Optimum Design of Machine Tool Spindle Systems with Hydrostatic Bearings, " *Proc. Instn. Mech. Engnrs.*, vol. 211 Part B, ASME, pp. 43-51.

Rechenberg, I., 1965, " Cybernetic Solution Path of an Experimental Problem, " Ministry of Aviation, Royal Aircraft Establishment (U.K.).

Rechenberg, I., 1973, *Evolutionstrategie: Optimierung Technischher Systeme nach Prinzipien der Biologischen Evolution.* Frommann-Holzboog (Stuttgart).

Reed, J., Toombs, R., and Barricelli, N.A., 1967, " Simulation of Biological Evolution and Machine Learning, " *Journal of Theoretical Biology,* vol. 17, pp. 319 – 342.

Robert, M.P., 1990, " Optimization of Self-Acting Gas Bearing for Maximum Static Stiffness, " *ASME Journal of Applied Mechanics*, vol. 57, pp. 758-761.

Robert, M.P., 1995, " New Class Class of Sliders Numerically Designed for Maximum Stiffness, " *ASME Journal of Tribology*, vol. 117, pp. 456-460.

Schwefel, H. –P., 1975, *Evolutionstrategie und numerische Optimierung*. Ph. D. thesis, Technische Universität Berlin.

Schwefel, H. – P., 1977, *Numerische Optimierung von Computer-Modellen mittels der Evolutionstrategie*. Basel: Birkhäuser.

Wang, N., Ho, C.L., and Cha, K.C., 2000, " Engineering Optimum Design of Fluid-Film Lubricated Bearings, " *STLE Tribology Transactions*, vol. 43, n. 3, pp. 377-386.

Wang, Q., Shi, F., and Lee, S.C., 1997, " A Mixed –Lubrication Study of Journal Bearing Conformal Contacts, " *ASME Journal of Tribology*, vol. 119, pp. 459-461.

Appendix I.

Pseudocode Algorithm for Program OPTJBG.

The following described pseudocode algorithm is used as a computation technique in our research. The program works in the following pattern; first takes all necessary data for the computation, in the input step, and then creates a number of output files for the output data. Consequently, the program starts computation by creating random number sets with binary numbers:

```
while (1 ≤ i ≤ nchrom) do
    while (1 ≤ j ≤ nchrom) do
        z ← grnd( )
        if ( 0<z <0.5 ) then
            num ← 0
        else
            num ← 1
```

Then Genetic Algorithm starts working in the loop. It decodes each of the chromosomes into their design variables and stores in arrays H1, H2, and H3. For each generation one separated set of design variables is created. On the following step, it calculates load for each set of design variables – H1, H2, and H3.

while (1 ≤ k ≤ numgen) **do**

while (1 ≤ i ≤ nchrom) **do**

$h_1\ (i) \leftarrow 0$

$icount \leftarrow 0$

while (1 ≤ j ≤ 7) **do**

$h_1\ (i) \leftarrow h_1\ (i) + (2^{icount})*\ icount(i, j)$

$icount \leftarrow icount + 1$

while (8 ≤ j ≤ 14) **do**

$h_2\ (i) \leftarrow h_2\ (i) + (2^{icount})*\ icount(i, j)$

$icount \leftarrow icount + 1$

while (15 ≤ j ≤ 21) **do**

$h_3\ (i) \leftarrow h_3\ (i) + (2^{icount})*\ icount(i, j)$

$icount \leftarrow icount + 1$

write k

format

while (1 ≤ i ≤ nchrom) **do**

$h_{1des} \leftarrow 1.0d-06 + h_1(i) * 1.0d\text{-}06$

$h_{2des} \leftarrow 1.0d-06 + h_2\ (i) * 1.0d\text{-}06$

$h_{3des} \leftarrow 1.0d-06 + h_3\ (i) * 1.0d\text{-}06$

write ichrom(i, j), h_{1des}, h_{2des}, h_{3des}

format

After that the algorithm calculates load for each set of design variables and computes the radial clearance at each mesh node based on values of the design variables using linear interpolation. Also, in this step, the algorithm calculates the force magnitude, which will be the basis for sorting chromosomes in the next step;

while (1 ≤ i ≤ nchrom) **do**

$h_{1des} \leftarrow 1.0d-06 + h_1(i) * 1.0d\text{-}06$

$h_{2des} \leftarrow 1.0d-06 + h_2\ (i) * 1.0d\text{-}06$

$h_{3des} \leftarrow 1.0d-06 + h_3\ (i) * 1.0d\text{-}06$

call interp (h_{1des}, h_{2des}, h_{3des} , *d, x, numnod, rclr*)

while (1 ≤ l ≤ nchrom) **do**

$clrtbl\ (l, i) \leftarrow rclr\ (l)$

call mesh file

$fmag\ (i) \leftarrow \sqrt{f^2(x) + f^2(y)}$

$pmaxtbl\ (i) \leftarrow pmax$

$plosstbl\ (i) \leftarrow power$

write ichrom(i, j), h_{1des}, h_{2des}, h_{3des}

format

The following step sorts out chromosomes based on maximum load values to get corresponding values of power loss, maximal pressure and nodal clearance. The coming algorithm stores the chromosomes as parents in sorted order, that is, from the highest load to the lowest load. Each time the algorithm carries the two highest load – carrying chromosomes over the next generation without any modification or mutation at all. It performs crossover operation on the remaining pairs of chromosomes picking the crossover point randomly, and coping into the temporary storage, parents. Then it performs crossover operation over the children at randomly selected points and stores in the storage of children. Consequently, it starts hitting the children with mutation at random points in chromosomes and leaving retained the first two chromosomes again without doing any operation over them. It sets children for the next generation. A single crossover scheme is utilized in this program. All these steps are repeated over and over the number of generation times;

call piksk2 (nchrom, fmag, fsort, index)

while (1 ≤ i ≤ numnod) **do**

clrmax (i) = clrtbl (i, index(nchrom))

press ← *pmaxtbl (index(nchrom))*

ploss ← *plosstbl (index(nchrom))*

while (1 ≤ i ≤ nchrom) **do**

while (1 ≤ j ≤ 21) **do**

iparent (i, j) ← *ichrom (index(nchrom + 1 − i), j)*

while (1 ≤ j ≤ 21) **do**

ichild (1, j) ← *iparent (1, j)*

ichild (2, j) ← *iparent (2, j)*

```
while (3 ≤ j ≤ nchrom) do
    while (1 ≤ j ≤ 21) do
        ipar1 ( j)   ←   iparent (1, j)
        ipar2 (2, j) ←   iparent (I+1, j)
    z  ←  grnd ( )
    if ( z ≤ pcross ) then
        z       ←  grnd ( )
        icross  ←  z * 21 + 0.5
    else
        icross  ←  0
    while (1 ≤ j ≤ icross) do
        ichild ( i, j)     ←  ipar1 ( j )
        ichild ( i + 1, j) ←  ipar2 ( j )
    while (icross + 1 ≤ j ≤ 21) do
        ichild ( i, j)     ←  ipar2 ( j )
        ichild ( i + 1, j) ←  ipar1 ( j )
```

```
while (3 ≤ i ≤ nchrom) do
    while (1 ≤ j ≤ 21) do
        z      ←  grnd ( )
        if ( z ≤ pmutat ) then
            if ( ichild =1 ) then
                ichild (i, j)  ←  0
            else
                ichild (i, j)  ←  1

while (3 ≤ i ≤ nchrom) do
    while (1 ≤ j ≤ 21) do
        ichrom (i, j)  ←  ichild(i, j)

stop

end
```

In the previous algorithms, there are two subroutines, **"piksk2"** for sorting of chromosomes based on maximal load and **"interp"** for supplying of interpolation data points. These subroutines of the algorithm function in the following order:

```
subroutine piksr2 ( n, b, arr, index )
implicit double precision (a-n, o-z )
dimension arr (n), b(n), index(n)
while (1 ≤ i ≤ n) do
    arr (i)   ←   b (i)
    index (i) ←   i
* pick out each  element in turn
while (2 ≤ j ≤ n) do
    a         ←   arr (j)
    indval    ←   index (j)
   * look for the place to insert it
    while (j-1 ≤ i ≤ 1) do
        if (arr(i) ≤ a ) goto  while (j-1 ≤ i ≤ 1) do
        arr (i+1)    ←   arr (i)
        index (i+1)  ←   index (i)
    i  ← 0
   * insert it
    arr (i+1)   ←   a
    index (i+1) ←   indval
return
end
```

subroutine interp (h_{1des} , h_{2des} , h_{3des} , d, χ, numnod, rclr)

implicit double precision (a-n, o-z)

parameter (kn = 1200)

dimension xtable (5), ytable (5), χ (kn), rclr (kn)

* design variable h_{1des} *at* $\chi = (d/2)*(\pi/2)$

* design variable h_{2des} *at* $\chi = (d/2)*\pi$

* design variable h_{3des} *at* $\chi = (d/2)*(3*\pi/2)$

* 1 μm clearance at $\chi = 0$ and at $\chi = (d/2)*(2*\pi)$

π = 4 * atan (1.0d + 0)

Xtable (1) = 0.

Xtable (2) = (d/2)*(π/2)

Xtable (3) = (d/2)*π

Xtable (4) = (d/2)*(3*π/2)

Xtable (5) = (d/2)*(2*π)

*

Ytable (1) = 1.0d-06

Ytable (2) = h_{1des}

Ytable (3) = h_{2des}

Ytable (4) = h_{3des}

Ytable (5) = 1.0d-06

while $(1 \leq i \leq \text{numnod})$ **do**

$\chi node \leftarrow \chi(i)$

* find xnode intable

* find rclr by linear interpolation

$k \leftarrow 1$

if $(\chi node \geq Xtable(k))$ *and* $(\chi node \leq Xtable(k+1))$ **then**

$slope \leftarrow \dfrac{Ytable(k+1) - Ytable(k)}{Xtable(k+1) - Xtable(k)}$

$rclr \leftarrow (Ytable(k) + slope * (\chi node - Xtable(k)))$

goto **while** $(1 \leq i \leq \text{numnod})$ **do**

else

$k \leftarrow k + 1$

goto **while** $(1 \leq j \leq 21)$ **do**

stop

return

end

As a final note, the random number generator *grnd* (Matsumoto and Nishimura, 1997) is used to create the initial set of chromosomes and perform crossover and mutation operations.